MEMBRANE COATINGS FOR CATALYTIC WET-AIR OXIDATION, MEMBRANE DISTILLATION, AND OIL-WATER SEPARATIONS

By

Seth R. Hogg

A Dissertation

Submitted to
Michigan State University
in partial fulfillment of the requirements
for the degree of

Chemistry – Doctor of Philosophy

2013

ABSTRACT

MEMBRANE COATINGS FOR CATALYTIC WET-AIR OXIDATION, MEMBRANE DISTILLATION, AND OIL-WATER SEPARATIONS

By

Seth R. Hogg

Thin polymeric films often impart attractive properties to a substrate without substantially altering the performance of the bulk material. This dissertation demonstrates three potential applications of polymeric films to enhance the functionality of membranes for water production and wastewater remediation, which are becoming increasingly important for combatting water scarcity.

Layer-by-layer adsorption of polyelectrolytes and citrate-stabilized nanoparticles creates a catalytically active film for wet-air oxidation of pollutants in water. Incorporation of these catalytic films in membranes allows for improved oxygen availability at the catalyst surface in a three phase reaction. In this work, the use of tubular catalytic membranes with small inner diameters (< 1 mm) reduces diffusion limitations relative to similar systems based on larger ceramic membranes. The reduction in the diffusion distance required for aqueous pollutants to reach the catalyst surface leads to a 5- to 10-fold increase in the single-pass pollutant oxidation compared to previous work with ceramic membranes.

Deposition of thin, rough polypropylene (PP) coatings rapidly produces superhydrophobic surfaces. Remarkably, addition of such a PP coating to a poly(vinylidene

difluoride) (PVDF) membrane increases the advancing water contact angle from 124° to 155°. These superhydrophobic membranes are well suited for membrane distillation (MD), where a nonwetted membrane allows water vapor to transfer from a warm feed solution to a chilled permeate phase. During MD with highly fouling humic acid, membranes coated with porous PP show three-fold higher salt rejections than unmodified PVDF membranes. Moreover, the PP-coated membranes resist pore wetting for at least 20 hours during MD of a solution containing dairy whey. In contrast, bare PVDF membranes show pore wetting within 3.5 h of MD with dairy why solutions.

Finally, adsorption of charged polyelectrolyte multilayers (PEMs) on membranes increases their hydrophilicity. This increase in hydrophilicity decreases fouling when filtering aqueous solutions with hydrophobic foulants, such as oil and grease. During cross-flow microfiltration of a 0.2% hexadecane-in-water emulsion, flux declines 80% after two hours for a PEM-modified membrane compared to a >90% flux decrease for an untreated membrane. Fouling resistance should be especially high if the foulant and the polyelectrolyte coating have the same charge. Exploiting electrostatic repulsions, the addition of anionic surfactants to oil emulsions causes a nearly two-fold increase in oil droplet rejection by anionically modified membranes.

To Shana, my teammate in life and love

ACKNOWLEDGEMENTS

I want to express my sincerest gratitude to the many people who assisted me in completing this degree. I appreciate the countless hours, plentiful advice, and encouragement to think on my own provided to me by my advisor, Dr. Merlin Bruening. Dr. Volodymr Tarabara was also instrumental in this project assisting with membrane knowledge and engineering advice while serving on my committee along with Dr. Gary Blanchard and Dr. Tom Hamann. I also wish to thank Dr. Baokang Bi for training and assistance with use of the SEM-EDS system. Without the kind encouragement of Dr. Lynn Melton I would never have known the thrill which was graduate school.

Likewise, I wish to thank Dr. David Dotzauer, Dr. Lu Ouyang, Dr. Sebastian Grajales, and Jason Armstrong for their guidance and friendship as well as the rest of the members of the Bruening Research Group, both past and present, for their suggestions and encouragement.

Finally, I would be remiss if I failed to thank the people who assisted me most in my studies, my family. I thank my parents for raising me in a nurturing home where I was encouraged to explore my interests and pursue my dreams as well as for their continuing support and encouragement. I also am forever grateful to Shana Santos for her help on many late nights, constant encouragement, and her open mind to always listen to my ideas, no matter how farfetched. Without her strength and perseverance, this project would not be feasible.

TABLE OF CONTENTS

LIST OF TABLES

LIST OF FIGURES

LIST OF ABBREVIATIONS

RO	Reverse osmosis
WAO	Wet air oxidation
CWAO	Catalytic wet air oxidation
MD	Membrane distillation
LbL	Layer-by-layer
PSS	Poly(styrene sulfonate)
PAA	Poly(acrylic acid)
PAH	Poly(allylamine hydrochloride)
PP	Polypropylene
PS	Polysulfone
PEI	Poly(ethyleneimine)
SEM	Scanning electron microscope
ICP-OES	Inductively coupled plasma optical emission spectroscopy
RSD	Relative standard deviation
DCMD	Direct contact membrane distillation
PVDF	Poly(vinylidine difluoride)
MEK	Methylethylketone
PEM	Polyelectrolyte multilayer
CTAB	Cetrimonium bromide
SDS	Sodium dodecyl sulfate
Triton	Triton X-100
DCM	Dichloromethane
GC	Gas chromatography

CHAPTER 1: Introduction

1.1 Water concerns

Few resources on earth play as important a role to the sustenance of life as water. No known species remain viable with prolonged isolation from water.[1,2] Despite the major scientific and technological advancements of the past two centuries, 780 million individuals still lack access to clean water.[3] This value represents over 10% of the world's population relying on unimproved sources of water, and areas within developing countries and regions of high poverty disproportionately suffer from water scarcity issues. The absence of reliably clean water results in 3.4 million deaths each year with more than 99% occurring in developing nations.[4]

Recognizing the global importance of water issues, the United Nations assembled in September 2000 to adopt the Millennium Declaration committing participating nations to a new global partnership aimed at reducing extreme poverty and improving world health. As part of this declaration, Goal 7 focuses on improving worldwide environmental sustainability. By 2015, the United Nations desires to halve the proportion of the population without sustainable access to safe drinking water and basic sanitation.[5] Despite achieving the targeted increase in safe drinking water availability five years ahead of schedule in 2010, current estimates project an inability to reach the desired sanitation goals, and millions still lack drinking water primarily in sub-Saharan Africa and Oceana.[3] Thus, a great need remains for advances in wastewater sanitation along with improved clean water access.

While the United States and other highly developed nations generally do not suffer from widespread sanitation or water safety issues, increasing worldwide water demand is creating higher incidences of water scarcity. Such scarcity occurs when the local total demand for water exceeds either the quantity available or the achievable production rate. Agriculture accounts for 90% of global freshwater use and plays a large role in economies around the world.[6] The United States produces the most corn in the world while also growing soybeans and wheat at levels exceeding 50 and 10% of world supply, respectively. Altogether, agricultural exports from the United States contribute greater than 290 billion dollars to the economy while providing food products to the world.[7] Clearly, reduction of water stress through improved water production or agriculturally appropriate treatment methods requires further study.

This dissertation focuses on three different membrane-based water treatment options to assess growing water contamination concerns. Specifically the use of catalytic membranes provides an attractive solution to the treatment of industrial waste water, whereas the use of thin, polymeric films supported on membranes should reduce fouling in both membrane distillation and oil filtration. The remainder of this chapter discusses recent developments in membrane applications for water production and treatment. First, I review four common membrane water treatment procedures related to the work presented in this dissertation. Next, I give relevant information on catalytic nanoparticle incorporation into membranes along with a discussion on polyelectrolyte and thin polymer film deposition procedures. Finally, the introduction concludes with a brief overview of the dissertation research.

1.2 Membrane applications for water production and treatment

Membrane-based processes are probably the most promising paradigm for water treatment and production. Membranes allow transport of specific components in a mixture, with selectivity based on size, charge, and/or chemical solubility.[8] Feed solutions approach membranes in either a dead-end or cross-flow mode (Figure 1.1). In dead-end filtration, the feed solution reaches the membrane surface, and components either pass through the membrane into a permeate stream or remain in the feed solution and give rise to increased concentrations. To help avoid the accumulation of rejected feed components at the membrane surface, in cross-flow filtration the feed stream continuously passes tangentially along the membrane surface. Components of the mixture still pass through the membrane into a permeate stream, but the continual replenishment of feed solution at the membrane surface limits the accumulation of rejected components. The availability of membranes with a wide range of pore sizes allows for tunable rejection and product flow rates suitable for many applications (Table 1.1). Industrial applications typically utilize membranes due to their low material costs, low energy requirements, absence of additional adsorbents or solvents, and easy scale up ability for increased production capacity.

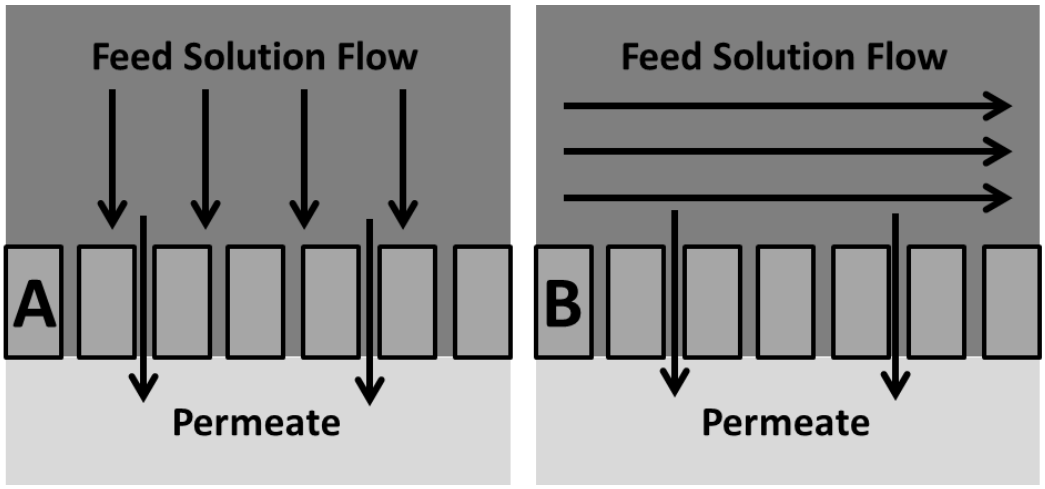

Figure 1.1: Membrane feed flow modes in dead-end (**A**) and cross-flow (**B**) filtration.

Table 1.1: Properties and applications of commercially available membranes. Table adapted from Mulder.[8]

Membrane Type	Pore Size (nm)	Pressure Range (bar)	Flux Range (L/m^2 h bar)	Filtration Size Equivalent
Microfiltration	100 - 5000	0.1 - 2	>50	Bacteria, yeast cells
Ultrafiltration	10 - 100	1 - 5	10 - 50	Colloidal silica, virus, proteins
Nanofiltration	1 - 10	5 - 20	1.4 - 12	Dye, multivalent ions, antibiotics
Reverse Osmosis	0.1 - 1	10 - 100	0.05 - 1.4	Aqueous salts

1.2.1 Reverse osmosis

Desalinated sea water is the largest sustainable source of water for addressing the growing needs from agriculture, human consumption, and industry.[9] Of the wide range of available technologies, reverse osmosis (RO) is the most economical process for desalination of

seawater to potable water and accounts for 44% of the world's desalination capacity.[10,11] Additionally, the Desalination Market 2010 report from the Global Water Intelligence organization predicts exponential growth of RO over the next four years, whereas the utilization of traditional thermal desalination will likely remain stagnant.[12] This projected exponential growth assumes that fossil fuel costs will limit the feasibility of thermal processes, and membrane separations will continue to improve.

RO provides fresh water fluxes exceeding 40 L/m^2h with more than 99% removal of salt but requires feed pressures above 5.5 MPa for treating seawater.[12] Although the high pressure requirements contribute substantially to the cost of RO desalination, water production prices fell from \$1-2.00/m^3 of seawater in 1998 to \$0.50-0.70/m^3 in 2005, slightly below the price of the most common thermal processes.[13,14]

In RO operation, pressure applied to the salty feed solution drives water through the semi-permeable polyamide film on the membrane surface and into the permeate. The applied pressure must be greater than the osmotic pressure of the seawater feed solution to reverse the thermodynamically favored flow of water from low to high solute concentration. The Morse equation provides an estimate for the osmotic pressure, Π, of ideal solutions (equation 1.1).

$$\Pi = iMRT \qquad (1.1)$$

The osmotic pressure depends on the sum of the molarity, M, of all dissolved solutes, the dimensionless van't Hoff factor, i, which accounts for solute dissociation, the universal gas

constant R, and the temperature of the solution in Kelvin, T.[15] As solute concentrations increase in contaminated water, osmotic pressure also increases necessitating higher feed pressure to continue permeate flow. The osmotic pressure dependence on solute concentration traditionally limits single-stage RO processes to only 35-40% water recovery, although new advances incorporating a second stage high pressure membrane system allow for up to 60% water recovery.[16]

While RO provides a promising method to efficiently produce fresh water, the technique still suffers from membrane fouling and instability to chlorine, as well as insufficient boron rejection.[12] Fouling affects the performance of all membrane processes, and biofouling in particular remains the largest limitation of seawater RO desalination.[17] Microorganism attachment to RO membrane surfaces leads to growth of biofilms containing extra-cellular polymers, and these films reduce membrane water permeability and increase concentration polarization.[18,19] Additionally, biological microorganisms release acidic byproducts that may degrade membrane polymers and reduce RO operational lifetimes.[18,20]

Currently, there are three main procedures to reduce biofouling.[21] First, biocides, such as ozone, chlorine, or ultraviolet light can reduce biological activity in the feed solution. Second, pretreatment of RO feed solutions using microfiltration membranes removes common biological contaminants before they reach the RO membranes. Finally, work continues on

developing RO membranes and coatings with biofouling resistant surfaces to decrease the need for feed pretreatment.[22-24]

The polyamide film responsible for the high salt rejection of RO membranes suffers from chlorine addition at the amide linkages, limiting chlorine's application in water pretreatment. Chlorine replaces the hydrogen on the amide nitrogen to form n-chlorinated amides that undergo an irreversible Orton rearrangement.[25] Addition of chlorine to the polyamide films alters their morphology from a crystalline to an amorphous state to decrease salt rejection.[26] The presence of chlorine under high pressures also promotes Orton rearrangement and causes maximum polyamide restructuring. Therefore membrane cleaning should occur under passive conditions to minimize damage.[27]

Boric acid and borates find use in many industrial products including glass, soaps, flame retardants, antiseptics, cosmetics, pharmaceuticals, pesticides, and fertilizers. Surface runoff and industrial effluents may increase groundwater concentrations of boron, and some borates and borosilicates naturally leach from rocks and soils into water reservoirs. However, the majority of the Earth's boron accumulates in oceans, which contain on average 4.5 mg of boron per L.[28] Groundwater boron levels vary from 0.3 to >100 mg/L depending on geographic location. The highest levels of boron occur in regions with highly mineralized, carbonated groundwater such as Turkey and deserts in the United States southwest region. Current World Health Organization standards call for a maximum boron concentration of 2.4 mg/L in drinking water to avoid undesired health effects.[29] As this targeted safe maximum concentration is less

than the average boron concentration in ocean water, the production of safe drinking water requires efficient boron removal. Unfortunately, uncharged boric acid easily permeates through RO membranes due to its small size and diffusion through the polyamide film using hydrogen bridges within membrane active groups.[30-32] Currently, the best method for boron rejection relies on feed solutions with pH values >11 to dissociate boric acids into polynuclear ions that do not pass through RO membranes.[33,34] However, high pH solutions also promote salt scaling on membrane surfaces and increased hydraulic resistance.[35] To achieve necessary reductions in boron concentrations, blending with low boron water or multiple passes through RO elements must occur to overcome the limited rejection possible with current RO technologies.

1.2.2 Catalytic wet air oxidation

Many industrial processes produce concentrated waste streams not amenable to RO and thus require other treatment options. Advanced oxidation procedures can potentially provide an effective solution to the removal of organic solutes from wastewater by producing primarily carbon dioxide and water as the final products. Among advanced oxidation procedures, wet air oxidation (WAO) is attractive due to its simplicity and low cost, which results from utilizing air as an oxidant instead of chemicals like peroxide, ozone, or Fenton's reagent. WAO is best suited for treatment of waste streams too concentrated for biological treatment and too dilute to justify the expense of incineration. In a process known as catalytic wet air oxidation (CWAO), most industrial WAO plants currently utilize fixed-bed catalysts to

treat water from chemical, petrochemical, municipal water-treatment, and pharmaceutical industries.[36]

At temperatures and pressures from 180 °C and 20 bar to 315 °C and 150 bar, WAO uses solution residence times between 15-120 minutes to oxidize 75-90% of organic contaminants while producing primarily carbon dioxide and water without generation of dioxins, hydrochloric acid, sulfur dioxide, or other hazardous products.[36] However, although WAO effectively oxidizes hazardous organic and inorganic solutes to benign products, the high temperatures and pressures required limit widespread application. The introduction of heterogeneous catalysts in CWAO reduced the temperatures and pressures required but introduced new challenges to the process. These challenges include diffusion limitations in the transport of gaseous reactants to dispersed catalysts surfaces, the necessity for recovery of catalysts made from precious metals, and catalyst leaching.[37]

Incorporation of catalysts within interfacial membrane contactors allows separation of the product and reactant streams on opposite sides of the membrane while facilitating a gas-liquid interface within the membrane pores (Figure 1.2).[38-42] The interfacial contact within the membrane pores reduces diffusion distances gaseous reactants to reach the catalyst's surface, while the incorporation of catalyst within a membrane eliminates the need for catalyst recovery addressing two concerns of heterogeneous CWAO.

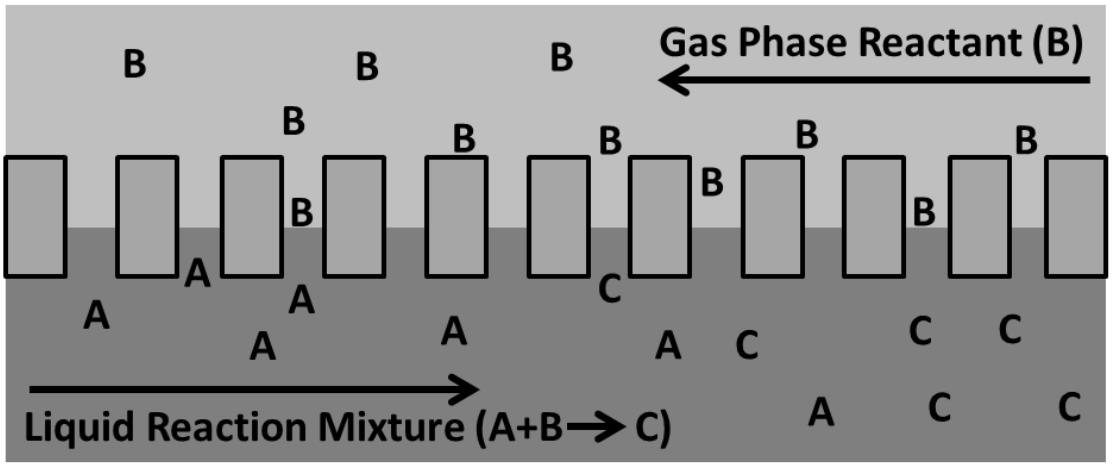

Figure 1.2: Schematic drawing of membrane pores in an interfacial contactor that creates a gas-liquid interface for a reaction occurring between aqueous component A and gaseous component B to produce product C.

Previous work utilizing tubular ceramic membranes loaded with platinum nanoparticle catalysts demonstrated 3-6 times higher conversion in formic acid oxidation when compared to a stirred tank reactor under the same conditions. The membranes also exhibited a five-fold increase in catalyst specific activity compared to the stirred tank reactor.[41] After these encouraging lab-scale tests that suggested potential industrial membrane CWAO applications, pilot-scale testing using single and multi-channel ceramic membranes demonstrated toxic waste treatment on a large scale but also showed that low reaction rates in the system limited the economic benefits of the process. Importantly though, membrane CWAO systems facilitated competitive conversion rates for industrial effluents under mild conditions.[40] While most studies focus on formic acid as a simple model compound, some research assessed the oxidation of phenol, another common industrial water pollutant. Phenol oxidation occurred with the formation of no intermediates when using membrane CWAO over cerium oxide

catalysts.[38] One other study demonstrated oxidation of phenol, oxalic acid, and acetic acid at room temperature and less than 4 bar of pressure indicating the possibility of treating aromatic and aliphatic organic contaminants.[43]

Incorporation of catalysts into membranes most commonly occurred through anionic impregnation or evaporation crystallization, but one study examined the performance of membranes loaded with catalyst using layer-by-layer deposition of polyelectrolytes and charged nanoparticles. Although the reaction rates in membranes treated with layer-by-layer deposition were 33-50% lower than in membranes modified with traditional methods, specific catalyst activity increased five-fold due to precise localization of platinum at the air-liquid interface.[44] Finally, one paper examined the use of polymeric membranes in place of ceramic membranes and found that in mild conditions, high single pass conversions occurred because of small fiber diameters, despite low catalyst specific activity due to delocalization of catalyst from the air-liquid interface.[45] While CWAO treats contaminated industrial waste streams, the resulting water typically is not suitable for human consumption or agricultural use due to the potential presence of hazardous inorganic contaminants. CWAO therefore requires coupling with other treatment options to finish water purification to acceptable levels for consumption.

1.2.3 Membrane distillation

Distillation produces highly pure water from sources contaminated with non-volatile solutes. Unfortunately, most distillation processes require a high-temperature heat source to

drive evaporation of feed water into the product. However, over the last two decades membrane distillation (MD) emerged as a growing technique for desalination or water treatment at milder temperatures. MD utilizes a porous, non-wetted membrane to separate a warm feed solution from a cool permeate stream. The membrane must avoid condensation of permeate vapor within membrane pores, and at least one side of the membrane must directly contact the process liquids in one of the four common orientations in Figure 1.3.[46]

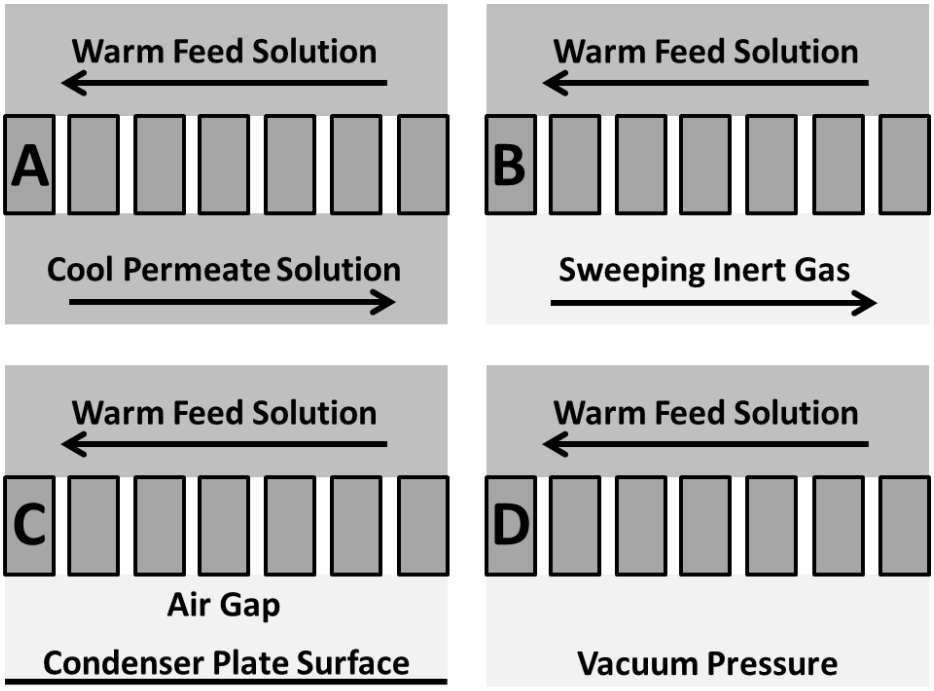

Figure 1.3: Common MD flow configurations showing A) direct contact MD, B) sweeping gas MD, C) air gap MD, and D) vacuum MD.

The original goal in developing MD was to reduce the space requirements of traditional distillation by replacing large distillation columns with smaller membrane modules. Unlike conventional distillation, MD only requires aqueous feed temperatures between 60-90 °C,

which may reduce energy requirements and allow for incorporation of low grade, waste, or alternative energy sources of heat.[47] Coupling of solar energy with MD water production might prove cost competitive with RO in rural areas.[48,49] The low temperatures in MD also allow dehydration of food and pharmaceutical products while avoiding thermal damage to temperature-sensitive components, thereby preserving flavor, aroma, or active ingredient functionality.[34,50-52]

Direct contact MD remains the most common configuration due to its simplicity, with the feed solution on one side of the non-wetted membrane and the permeate solution on the other side (Figure 1.3A). Water vapor from the feed stream diffuses through the hydrophobic membrane pores due to the water partial pressure difference that arises from the temperature gradient across the membrane. The water vapor condenses upon reaching the chilled aqueous stream passing along the permeate side of the membrane. Heat loss through the membrane into the permeate stream reduces the temperature gradient between the feed and permeate streams, however, lowering the driving force and reducing flux. Current studies of direct contact MD focus on applications in food processing or acid manufacturing.[53-58]

Replacing the aqueous permeate stream with an inert sweep gas (sweeping gas MD, Figure 1.3B) leads to increased mass transport through the membrane pores by maintaining a low water vapor pressure on the permeate side of the membrane. The sweep gas also reduces the heat loss through the membrane, increasing efficiency and flux.[59] However, sweeping gas MD requires condensation of the permeate water vapor downstream from the membrane. The

condenser must be large to accommodate the high volume of sweep gas containing relatively small amounts of water vapor permeate.[60] Despite the proposed increases in flux predicted for sweeping gas MD, no industries currently utilize the technique, and less than five percent of published MD papers discuss it.[61]

To avoid the complications associated with condensing permeate vapors downstream from the membrane in sweeping gas MD, air gap MD (Figure 1.3C) employs a condensing surface separated by a small, stationary air gap from the permeate side of the membrane. Water vapor diffuses through the membrane, across the air gap, and subsequently condenses on the chilled surface for collection. This configuration reduces heat loss through the membrane compared to direct contact MD, but mass transfer resistance increases due to the stagnant vapor barrier. Thus air gap MD has low fluxes compared to other MD methods.[47] Nevertheless, air gap MD allows easier recovery of trace volatile contaminants from aqueous streams than direct contact MD.[62] Other uses for air gap MD may include produced water treatment and concentration of non-volatile solutes.[63-65]

Vacuum MD (Figure 1.3D) utilizes reduced pressure at the permeate side of the membrane to increase vapor flux. This is similar to pervaporation, but the membrane plays no active role in the separation other than supporting the liquid-vapor interface. Energy and capital expenses for maintaining the vacuum increase the cost of vacuum MD compared to the other methods but once again, heat loss through the membrane is negligible. Similar to sweeping gas MD, the permeate vapors must also be condensed downstream from the

membrane. Of all the available MD techniques, vacuum MD most effectively removes volatile organic components from aqueous streams.[66] Current studies of vacuum MD focus on desalination or removal of organic contaminants such as benzene, aroma compounds, and polyphenols from water.[67-70]

1.2.4 Filtration of oil-water emulsions

Over the last 15 years, hydraulic fracturing, colloquially referred to as “fracking”, has emerged as an effective method to extract oil and natural gas from non-porous rock formations. After drilling an appropriate well, injection of high pressure fracturing fluids into rock formations creates cracks and channels for oil and natural gas release and capture. Subsequent addition of solutions containing propping agents, including sand or ceramic beads, fixes the fractures in place to allow continued oil and gas release upon removal of the pumping pressure. Traditionally, fracturing fluids contain up to 99% water with various chemical additives, and fracturing coalbed and shale formations requires up to 350,000 gallons or 5,000,000 gallons, respectively. As the water for hydraulic fracturing primarily comes from local surface or groundwater, the process results in water stress in areas with multiple wells. Additionally, wells typically recover only 15-80% of injected volumes, and the recovered water, known as produced water, contains a dangerous mixture of toxic components and needs further treatment.[71]

The composition of the dissolved and dispersed components in produced water varies with geography and even the age of a particular well. Dissolved organic compounds in produced water may include formic and propionic acid, benzene, toluene, ethylbenzene, xylene, and phenols. The latter 4 compounds are relatively toxic. In addition to dissolved compounds, insoluble oil dispersed in the solution primarily contains aliphatic hydrocarbons along with dangerous polyaromatic hydrocarbons and heavy alkyl phenols.[72] Dissolved minerals further complicate produced water. Cations and anions dissolved from the formation include Na^{+}, K^{+}, Ca^{2+}, Mg^{2+}, Ba^{2+}, Sr^{2+}, Fe^{2+}, Cl^{-}, SO_4^{2-}, CO_3^{2-}, and HCO_3^{-}. These ions all increase salinity, and some of them enhance the scaling potential of the solution. Incredibly, salt concentrations in produced water can exceed 300 g/L.[73] Other minerals present even greater danger including heavy metals such as cadmium, chromium, copper, lead, mercury, nickel, silver, and zinc, as well as naturally occurring radioactive materials consisting primarily of radium deposits in scale formation.[74,75] Finally, further complicating treatment procedures, produced water also contains production chemicals such as scale inhibitors, biocides, and emulsion breakers.[76]

In 2009, the average oil and natural gas well in the United States created seven barrels of produced water for every barrel of oil recovered.[77] Each barrel creates a possible environmental hazard due to proximity to natural water sources as well as an economic burden for proper treatment. Recent challenges in treating the Deepwater Horizon oil spill in 2010 only highlight the need for further developments of systems that remove oil from contaminated

waters rapidly without significant economic impact. Membrane filtration provides one of the best methods for large-scale separation of dilute, oily wastewaters. Rapid production of highly purified water can occur with readily deployed pre-built modules.[78]

Membrane-based separations of oil and water generally rely on size exclusion of oil droplets rather than chemical selectivity, but formation of an oil film on the membrane reduces water flux and oil rejection. Frequent cleaning procedures must occur to either flush the oil from the membrane or chemically renew its surface.[79] A number of recent studies explored increasing membrane hydrophilicity to reduce oil fouling. Segregation of hydrophilic groups to the membrane surface and graft polymerization yield extremely hydrophilic membranes that resist oil wetting.[80-82] In an aqueous solution, these extremely hydrophilic surfaces adsorb a layer of water that prevents contact with the high fouling oil components that plague hydrophobic membrane processes. Additionally, the adsorbed water layer creates an entropic barrier to oil droplet passage through membrane pores, allowing for high oil rejections even in membranes with pore sizes larger than the oil droplets.[82]

Despite the gains in oil rejection achieved through creating hydrophilic membrane surfaces, most studies only assess oil rejection using concentrations exceeding 1000 mg/L and droplet diameters greater than 50 µm. Under these conditions, oil exists in an unstable state that is simpler to remove from water than more stable droplets of less than 20 µm in diameter.[83] Traditional oil-treatment methods including gravity separation or chemical emulsion breaking are also inefficient for removal of oil droplets below 10 µm in size.[84,85]

While membranes may promote coalescence of small oil droplets into larger ones that are treatable by conventional technologies, further studies must prove this theory conclusively through addressing rejection of small, stable oil droplets.

1.3 Catalytic nanoparticles

Incorporation of catalytic particles, as earlier discussed for CWAO, represents a promising method for future water treatment advances. Catalysts play important roles in the synthesis of most important industrial products and many vital biological processes. Typically, catalysts lower the activation energy of reactions to increase their rate relative to the non-catalyzed reaction at the same temperature. Unlike the reactants, reactions do not consume catalysts so they participate in multiple reactions.[86]

Enzymatic catalysts participate in biological reactions such as phosphorylation, oxidation, and esterification that are critical in signal transduction and cellular regulation.[87] With the need for high specificity in biological processes, enzymatic catalysts unsurprisingly afford the highest selectivity of all catalysts. Alternatively, homogeneous small-molecule catalysts provide tunable chemoselectivty, regioselectivity, or enantioselectivity while residing in the same phase as the reactants. However, applications of homogeneous catalysts are mostly limited to the synthesis of fine chemicals because of the difficulty of recovering the expensive catalyst from the final products.[88] On the other hand, solid catalysts containing transition metals facilitate a wide range of industrial reactions in gases and liquids. Reaction on

these heterogeneous catalysts takes place at solid-gas or solid-liquid interfaces. However, the variability in the active sites present on heterogeneous catalysts results in relatively low specificity compared to enzymes and homogeneous catalysts.[86] Despite the lack of selectivity, heterogeneous catalysts dominate the global market and find use in many industrial synthetic processes.

Although nanoparticles have facilitated various processes for many years, only in the last 30-40 years did the scientific community focus on controlled design of nanoparticles for catalysis.[89-92] Interest in imparting unique properties to nanoparticle catalysts arose from the discovery of gold nanoparticles with high catalytic activity despite the relative inactivity of bulk gold.[93,94] Further studies revealed that the optimal size for catalytically active nanoparticles falls between 1 and 10 nm.[95,96] At this small diameter, the particles maintain a high surface area to volume ratio, allowing efficient use of precious noble metal catalysts while affording unique electronic and catalytic properties.[96-98] However, the small particle diameters also lead to high particle surface energies that cause rapid aggregation and loss of activity unless a ligand or support stabilizes the particles.[99-101]

1.4 Functional nanoparticles on porous membranes

Incorporation of nanoparticles within membranes prevents particle aggregation and avoids time-consuming catalyst recovery steps. Additionally, immobilization of nanoparticles in

membranes allows for continuous operation of the reactor unlike what is possible for traditional batch or stirred-tank reactors.[102] Compared to other supports such as porous beads, membranes have the potential to improve heterogeneous catalysis by reducing the distance reactants must diffuse before adsorbing to the catalyst surface. Diffusion limitations commonly challenge the efficiency of reactions involving heterogeneous catalysts in liquids, so catalytic membranes may lead to gains in observed reaction rates.

Another potential advantage of catalytically active membranes is the possibility of separating reactant from newly formed products. Continuous removal of product may eliminate further post-reaction separations. More importantly, removal of products from the reaction mixture shifts the equilibrium towards products to increase the possible degree of conversion.[102]

Highly porous membranes with small pore diameters contain a large surface area for incorporation of catalysts, and high catalyst concentrations allow increased conversion or the use of high reactant concentrations. Along with porosity and pore size, the selection of the membrane composition for a specific application allows a balance of performance and cost. Current membrane materials include both hydrophilic and hydrophobic polymers as well as temperature- and solvent-resistant ceramic membranes. For reactions at temperatures below 100 °C in mild conditions, polymeric hollow fiber membranes are likely the best choice due to their inexpensive production, small diameter, and high packing density. However, for more extreme catalytic environments, ceramic membranes provide the necessary durability despite

increased costs. Potential applications for catalytic nanoparticles immobilized in membranes include the reduction of nitroaromatic compounds in water, hydrogenation of organic compounds, and the synthesis of hydrogen peroxide from methanol.[103-106] In order for nanoparticles to function on membrane surfaces, effective incorporation through covalent or electrostatic attachment must occur.

1.5 Layer-by-layer assembly of polyelectrolyte multilayer films

Despite the strength of covalent attachment of nanoparticles to surfaces, electrostatic interactions also provide a suitable immobilization method without as many limitations from chemical reactivity. The layer-by-layer (LbL) method is the preeminent choice for electrostatic film attachment to surfaces. LbL assembly techniques employ alternating adsorption of complementary species to form thin films one "layer" at a time. The most common LbL technique exploits alternating electrostatic adsorption of polyanions and polycations as Figure 1.4 illustrates. Nearly any surface which allows adsorption of an initial polymer either through hydrophobic or electrostatic interactions may support the LbL approach.[107-109] Surface geometries previously modified include flat surfaces, membrane pores, cylindrical particles, and carbon nanotubes.[44,105,110-113] Adsorption of each polyelectrolyte chain typically overcompensates the charge of the modified surface so the final surface charge depends on the composition of the terminating polyelectrolyte layer. In addition to typical synthetic

polyelectrolytes, LbL adsorption can employ other charged species such as catalytic nanoparticles, dendrimers, enzymes, and carbon nanotubes.[114-120]

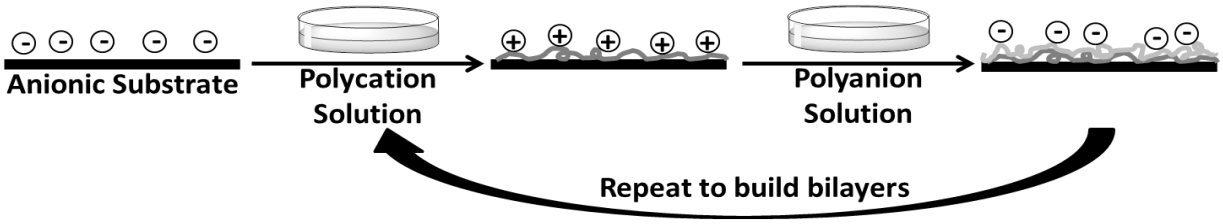

Figure 1.4: LbL deposition via alternating adsorption of polycations and polyanions.

Along with the versatility in choosing constituents for LbL deposition, the properties of the polymer films vary with deposition conditions including pH, salt concentration, polyelectrolyte concentration, or solvent composition. While some polymers, such as poly(styrene sulfonate) (PSS), are strong electrolytes with high charge at nearly all pH conditions, others are weak electrolytes and pH strongly affects their deposition. Rubner demonstrated that the thicknesses of films comprised of poly(acrylic acid) (PAA) and poly(allylamine hydrochloride) (PAH) depends on the pH of deposition solutions. At a pH of 7 where both the carboxylic acid groups of PAA (pKa ~ 4.5) and the amine groups in PAH (pKa ~ 9.5) are ionized, a single bilayer produces a compact, ~5 Å-thick film. However, at a pH of 5, partial protonation of the carboxylic groups of PAA causes deposition of a less extended polymer and a 14-fold increase in thickness.[121] Related effects occur upon increases in the ionic strength of the polyelectrolyte deposition solutions because higher salt concentrations screen the charge within the polyelectrolyte chains to create more coiled polymers and thicker

films.[121,122] In summary, tailoring of LbL polyelectrolyte adsorption affords control over surface charge, swelling, and thickness. Thus, the LbL technique offers a versatile platform for immobilizing catalytic nanoparticles in membranes and modifying membrane surface to create low-fouling membranes that reject oil.

1.6 Superhydrophobic coatings

In addition to varying charge and chemical functionality, surface scientists also seek to control surface wetting. For instance, water repellency plays a vital role in the operation of common products such as self-cleaning traffic indicators, self-cleaning windows, frictional drag reducing coatings for naval vessel hulls, and stain resistant textiles.[123,124] Similar coatings are also attractive in the emerging field of biomedical fluid handling without adsorption of blood or other biological materials.[125]

Quantitative exploration of surface wettability typically involves determining the contact angle a droplet of a liquid, either water or oil, makes when in contact with the surface. The equilibrium contact angle, θ, results from a balance of interfacial energies that give rise to the Young Equation (equation 1.2),[126]

$$\cos\theta = \frac{\gamma_{sv} - \gamma_{sl}}{\gamma_{lv}} \qquad (1.2)$$

where γ_{SV} is the solid-vapor interfacial energy, γ_{Sl} is the solid-liquid interfacial energy, and γ_{lV} is the liquid-air interfacial energy. For a smooth surface, the maximum known water contact angle is 120° on a Teflon coating.[127] However, the incorporation of rough features on hydrophobic surfaces allows water contact angles to exceed this value. When the water contact angle on a surface exceeds 150° and does not suffer from large hysteresis (differences >10° between advance and receding contact angles), the surface is considered superhydrophobic. There are two wetting modes possible with rough, hydrophobic surfaces (Figure 1.5).[128,129] In the Wenzel model, the apparent contact angle, θ^*, of a surface increases with the increased surface area available due to the surface roughness, r (equation 1.3). In this equation, r is the ratio of total surface area to the apparent area.

$$cos\theta^* = rcos\theta \quad (1.3)$$

As the Wenzel surface becomes increasingly rough, the apparent contact angle continues to increase.

The Cassie-Baxter model assumes that small air pockets remain trapped within surface roughness features to reduce the liquid-solid interfacial area. Thus, this model calculates the apparent contact angle using equation 1.4 based on the fraction of solid in contact with the liquid, ϕ_S, and the fraction in contact with air (1-ϕ_S).

$$cos\theta^* = -1 + \phi_S(1 + cos\theta) \quad (1.4)$$

As the numbers or size of air traps within the roughness features increases, the fraction of solid contacting the liquid decreases to give a net increase in the contact angle. The incorporation of air in the substrate topology to reduce the surface-liquid contact within the Cassie-Baxter state provides intriguing antifouling possibilities. In many areas, fouling components of solutions never contact surfaces due to trapped air.

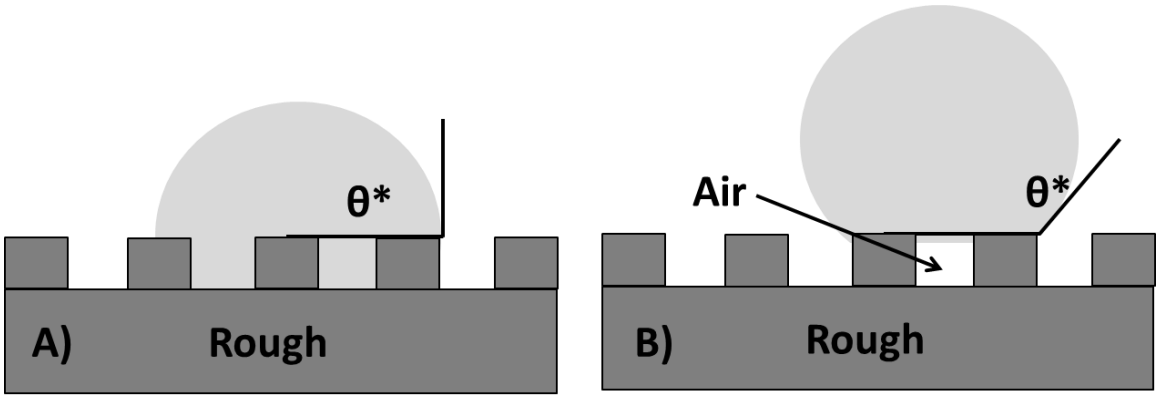

Figure 1.5: Rough surface wetting behavior in A) Wenzel and B) Cassie-Baxter models.

Current methods for creating superhydrophobic surfaces include hydrophobic polymer recrystallization, LbL assembly with incorporation of hydrophobic nanoparticles, deposition of fluorinated silsesquioxane films, and adsorption of lubricating omniphobic fluids within roughness features.[125,130-132] These unique surfaces may find applications in oil-water separation membranes, stain resistant surfaces, optically transparent self-cleaning glass, low-fouling microfluidic surfaces, and marine bio-fouling resistant coatings.[125,133-135]

1.7 Scope of this work

This dissertation discusses the development of new membrane coatings that may enhance water production or pollution remediation. The next three chapters each present a specific thrust within the overlying goal of developing new water-treatment membranes. Chapter 2 discusses the incorporation of platinum nanoparticles within polymeric hollow fibers for low temperature CWAO of dilute formic acid waste streams. Studies of the effect of oxygen overpressure, solution residence time, and catalyst loading on CWAO conversion rates explore the performance of the polymeric membranes in comparison to previously utilized ceramic membranes. Chapter 3 covers the development of superhydrophobic, porous polypropylene (PP) membrane coatings for membrane distillation. When compared to unmodified membranes, despite a slight decline in flux resulting from the additional mass transfer resistance of the porous PP, these coatings decrease the rate of fouling by humic acid and other foulants to give longer operational stability with less frequent mandatory cleaning. Chapter 4 introduces the concept and initial results of oil-water separations with membranes whose surface charge matches the charge naturally present on small, emulsified oil droplets. The electrostatic repulsion of droplets provided by the charged membranes leads to higher oil rejection and presumably less membrane fouling from oil adsorption. Finally, chapter 5 discusses conclusions from the sum of the work and attempts to predict future challenges and areas for this work to expand. Overall, this dissertation shows the promise of thin, polymeric films for enhancing fresh-water production capabilities.

REFERENCES

REFERENCES

(1) Rothschild, L. J.; Mancinelli, R. L. *Nature* **2001**, *409*, 1092.

(2) Alpert, P. *Integrative & Comparative Biology* **2005**, *45*, 683.

(3) UNICEF; WHO *Progress on Drinking Water and Sanitation: 2012 Update*; WHO Press: New York, NY, 2012.

(4) Prüss-Üstün, A.; Bos, R.; Gore, F.; Bartram, J. *Safer Water, Better Health: Costs, Benefits and Sustainability of Interventions to Protect and Promote Health*; WHO Press: Geneva, Switzerland, 2008.

(5) United Nations. Millenium Development Goals: Environmental Sustainability. http://www.un.org/millenniumgoals/environ.shtml (accessed 03/09/2013).

(6) Food and Agriculture Organization of the United Nations, *Coping with Water Scarcity: An Action Framework for Agriculture and Food Security*, Rome, Italy, 2012, http://www.fao.org (accessed 03/09/2013).

(7) United States Environmental Protection Agency. Major Crops Grown in the United States. http://www.epa.gov/agriculture/ag101/cropmajor.html (accessed 03/09/2013).

(8) Mulder, M. *Basic Principles of Membrane Technology*; Second ed.; Springer: New York, NY, 1996.

(9) Uemura, T.; Henmi, M. *Thin-film Composite Membranes for Reverse Osmosis*; John Wiley & Sons, Inc.: Hoboken, NJ, 2008.

(10) Greenlee, L. F.; Lawler, D. F.; Freeman, B. D.; Marron, B.; Moulin, P. *Water Research* **2009**, *43*, 2317.

(11) Gupta, V. K.; Ali, I.; Saleh, T. A.; Nayak, A.; Agarwal, S. *RSC Advances* **2012**, *2*, 6380.

(12) Misdan, N.; Lau, W. J.; Ismail, A. F. *Desalination* **2012**, *287*, 228.

(13) Dore, M. H. I. *Desalination* **2005**, *172*, 207.

(14) Wilf, M.; Bartels, C. *Desalination* **2005**, *173*, 1.

(15) Amiji, M. M.; Sandmann, B. J. *Applied Physical Pharmacy*; McGraw-Hill Professional, 2002.

(16) von Gottberg, A.; Pang, A.; Talavera, J. L. *Optimizing Water Recovery and Energy Consumption for Seawater RO Systems*, GE Water & Process Technologies, 2005.

(17) Flemming, H. C.; Schaule, G.; Griebe, T.; Schmitt, J.; Tamachkiarowa, A. *Desalination* **1997**, *113*, 215.

(18) Abd El Aleem, F. A.; Al-Sugair, K. A.; Alahmad, M. I. *International Biodeterioration & Biodegredation* **1998**, *41*, 19.

(19) Kim, D.; Jung, S.; Sohn, J.; Kim, H.; Lee, S. *Desalination* **2009**, *238*, 43.

(20) Flemming, H. C. *Experimental Thermal and Fluid Science* **1997**, *14*, 382.

(21) Vrouwenvelder, J. S.; Van Loosdrecht, M. C. M.; Kruithof, J. C. *Water Research* **2011**, *45*, 3890.

(22) Worthley, C. H.; Constantopoulos, K. T.; Ginic-Markovic, M.; Pillar, R. J.; Matisons, J. G.; Clarke, S. *Journal of Membrane Science* **2011**, *385-386*, 30.

(23) Matin, A.; Ozaydin-Ince, G.; Khan, Z.; Zaidia, S. M. J.; Gleason, K.; Eggenspiler, D. *Desalination and Water Treatment* **2011**, *34*, 100.

(24) Zhang, Z.; Wang, Z.; Wang, J.; Wang, S. *Desalination* **2013**, *309*, 187.

(25) Glater, J.; Hong, S.-K.; Elimelech, M. *Desalination* **1994**, *95*, 325.

(26) Avlonitis, S.; Hanbury, W. T.; Hodgkiss, T. *Desalination* **1992**, *85*, 321.

(27) Antony, A.; Fudianto, R.; Cox, S.; Leslie, G. *Journal of Membrane Science* **2010**, *347*, 159.

(28) *CRC Handbook of Chemistry and Physics*; 69th ed.; Weast, R. C.; Astle, M. J.; Beyer, W. H., Eds.; CRC Press, Inc.: Boca Raton, FL, 1985.

(29) World Health Organization Press, *Boron in Drinking-water*, Geneva, Switzerland, 2009, http://whqlibdoc.who.int/hq/2009/WHO_HSE_WSH_09.01_2_eng.pdf (accessed 03/09/2013).

(30) Cengeloglu, Y.; Arslan, G.; Tor, A.; Kocak, I.; Dursun, N. *Separation and Purification Technology* **2008**, *64*, 141.

(31) Tu, K. L.; Nghiem, L. D.; Chivas, A. R. *Separation and Purification Technology* **2010**, *75*, 87.

(32) Rodriguez Pastor, M.; Ferrándiz Ruiz, A.; Chillón, M. F.; Prats Rico, D. *Desalination* **2001**, *140*, 145.

(33) Glueckstem, P.; Priel, M. *Desalination* **2003**, *156*, 219.

(34) Hilal, N.; Kim, G. J.; Somerfield, C. *Desalination* **2011**, *273*, 23.

(35) Dominguez-Tagle, C.; Romero-Temero, V. J.; Delgado-Torres, A. M. *Desalination* **2011**, *265*, 43.

(36) Luck, F. *Catalysis Today* **1996**, *27*, 195.

(37) Levec, J.; Pintar, A. *Catalysis Today* **2007**, *124*, 172.

(38) Gutiérrez, M.; Pina, P.; Torres, M.; Cauqui, M. A.; Herguido, J. *Catalysis Today* **2010**, *149*, 326.

(39) Iojoiu, E.; Miachon, S.; Landrivon, E.; Walmsley, J.; Rader, H.; Dalmon, J. *Applied Catalysis B: Environmental* **2007**, *69*, 196.

(40) Iojoiu, E. E.; Landrivon, E.; Raeder, H.; Torp, E. G.; Miachon, S.; Dalmon, J.-A. *Catalysis Today* **2006**, *118*, 246.

(41) Miachon, S.; Perez, V.; Crehan, G.; Torp, E.; Ræder, H.; Bredesen, R.; Dalmon, J. A. *Catalysis Today* **2003**, *82*, 75.

(42) Ræder, H.; Bredesen, R.; Crehan, G.; Miachon, S.; Dalmon, J.-A.; Pintar, A.; Levec, J.; Torp, E. *Separation and Purification Technology* **2003**, *32*, 349.

(43) Alame, M.; Abusaloua, A.; Pera-Titus, M.; Guilhaume, N.; Fiaty, K.; Giroir-Fendler, A. *Catalysis Today* **2010**, *157*, 327.

(44) Dotzauer, D. M.; Abusaloua, A.; Miachon, S.; Dalmon, J.-A.; Bruening, M. L. *Applied Catalysis, B: Environmental* **2009**, *91*, 180.

(45) Hogg, S. R.; Muthu, S.; O'Callaghan, M.; Lahitte, J. F.; Bruening, M. L. *ACS Applied Materials & Interfaces* **2012**, *4*, 1440.

(46) Smolders, C. A.; Franken, A. C. M. *Desalination* **1989**, *72*, 249.

(47) Lawson, K. W.; Lloyd, D. R. *Journal of Membrane Science* **1997**, *124*, 1.

(48) Hogan, P. A.; Sudjito; Fane, A. G.; Morrison, G. L. *Desalination* **1991**, *81*, 81.

(49) Saffarini, R. B.; Summers, E. K.; Arafat, H. A.; Lienhard V, J. H. *Desalination* **2012**, *299*, 55.

(50) Sakai, K.; Ano, T. K.; Muroi, T.; Tamura, M. *The Chemical Engineering Journal* **1988**, *38*, B33.

(51) Calabro, V.; Jiao, B. L.; Drioli, E. *Industrial & Engineering Chemistry Research* **1004**, *33*, 1803.

(52) Ding, Z.; Liu, L.; Yu, J.; Ma, R.; Yang, Z. *Journal of Membrane Science* **2008**, *310*, 539.

(53) Laganà, F.; Barbieri, G.; Drioli, E. *Journal of Membrane Science* **2000**, *166*, 1.

(54) Alves, V. D.; Coelhoso, I. M. *Journal of Food Engineering* **2006**, *74*, 125.

(55) Hsu, S. T.; Cheng, K. T.; Chiou, J. S. *Desalination* **2002**, *143*, 279.

(56) Gunko, S.; Verbych, S.; Bryk, M.; Hilal, N. *Desalination* **2006**, *190*, 117.

(57) Khayet, M.; Mengual, J. I. *Desalination* **2004**, *168*, 373.

(58) Tomaszewska, M.; Gryta, M.; Morawski, A. W. *Journal of Membrane Science* **1995**, *102*, 113.

(59) Charfi, K.; Khayet, M.; Safi, M. J. *Desalination* **2010**, *259*, 84.

(60) Alkhudhiri, A.; Darwish, N.; Hilal, N. *Desalination* **2012**, *287*, 2.

(61) Khayet, M. *Advances in Colloid and Interface Science* **2011**, *164*, 56.

(62) Garcia-Payo, M. C.; Izquierdo-Gil, M. A.; Fernández-Pineda, C. *Journal of Membrane Science* **2000**, *169*, 61.

(63) Izquierdo-Gil, M. A.; García-Payo, M. C.; Fernández-Pineda, C. *Journal of Membrane Science* **1999**, *155*, 291.

(64) Thiruvenkatachari, R.; Manickam, M.; Kwon, T. O.; Moon, I. S.; Kim, J. W. *Separation Science and Technology* **2006**, *41*, 3187.

(65) Alkhudhiri, A.; Darwish, N.; Hilal, N. *Desalination* **2013**, *309*, 46.

(66) Bandini, S.; Saavedra, A.; Sarti, G. C. *AIChE Journal* **1997**, *43*, 398.

(67) Garcia-Castello, E.; Cassano, A.; Criscuoli, A.; Conidi, C.; Drioli, E. *Water Research* **2010**, *44*, 3883.

(68) Li, B.; Sirkar, K. K. *Journal of Membrane Science* **2005**, *257*, 60.

(69) Banat, F. A.; Simandl, J. *Chemical Engineering Science* **1996**, *51*, 1257.

(70) Hasanoglu, A.; Robolledo, F.; Plaza, A.; Torres, A.; Romero, J. *Journal of Food Engineering* **2012**, *111*, 632.

(71) United States Environmental Protection Agency, *Hydraulic Fracturing Research Study Fact Sheet*, Washington, D.C., 2010, http://www.epa.gov/safewater/uic/pdfs/hfresearchstudyfs.pdf (accessed 03/09/2013).

(72) Ekins, P.; Vanner, R.; Firebrace, J. *Journal of Cleaner Production* **2007**, *15*, 1302.

(73) Jacobs, R. P. M. W.; Grant, R. O. H.; Kwant, J.; Marquenie, J. M.; Mentzer, E. In *Produced Water: Technological/Environmental Issues and Solutions*; Ray, J. P., Engelhardt, F. R., Eds.; Plenum Publishing Corp.: New York, 1992, p 13.

(74) Hansen, B. R.; Davies, S. H. *Chemical Engineering Research and Design* **1994**, *72*, 176.

(75) T. Gäfvert; I. Færevik; Rudjord, A. L. *Radioactivity in the Environment* **2006**, *8*, 193.

(76) Stephenson, M. T. In *Produced Water: Technological/Environmental Issues and Solutions*; Ray, J. P., Engelhardt, F. R., Eds.; Plenum Publishing Corp.: New York, 1992, p 1.

(77) Argonne National Laboratory - Environmental Science Division, *Produced Water Volumes and Management Practices in the United States*, 2009, http://www.ead.anl.gov/pub/doc/ANL_EVS__R09_produced_water_volume_report_2437.pdf (accessed 03/09/2013).

(78) Ahmadun, F. l.-R.; Pendashteh, A.; Abdullah, L. C.; Biak, D. R. A.; Madaeni, S. S.; Abidin, Z. Z. *Journal of Hazardous Materials* **2009**, *170*, 530.

(79) Mansouri, J.; harrisson, S.; Chen, V. *Journal of Materials Chemistry* **2010**, *20*, 4567.

(80) Koh, J. K.; Kim, Y. W.; Ahn, S. H.; Min, B. R.; Kim, J. H. *Journal of Polymer Science, Part B: Polymer Physics* **2010**, *48*, 183.

(81) Zhao, Y. H.; Wee, K. H.; Bai, R. *Journal of Membrane Science* **2010**, *362*, 326.

(82) Maguire-Boyle, S. J.; Barron, A. R. *Journal of Membrane Science* **2011**, *382*, 107.

(83) Chakrabarty, B.; Ghoshal, A. K.; Purkait, M. K. *The Chemical Engineering Journal* **2010**, *165*, 447.

(84) Abdessemed, D.; Nezzal, G.; Ben Aim, R. *Desalination* **2000**, *131*, 307.

(85) Benito, J. M.; Rios, G.; Ortea, E.; Fernhdez, E.; Cambiella, A.; Pazos, C.; Coca, J. *Desalination* **2002**, *147*, 5.

(86) Swiegers, G. F. *Mechanical Catalysis: Methods of Heterogeneous, Homogenous, and Enyzmatic Catalysis*; John Wiley & Sons: Hoboken, New Jersey, 2008.

(87) Davis, B. G.; Boyer, V. *Natural Product Reports* **2001**, *18*, 618.

(88) Cole-Hamilton, D. J. *Science* **2003**, *299*, 1702.

(89) Haruta, M.; Tsubota, S.; Kobayashi, T.; Kageyama, H.; Genet, M. J.; Delmon, B. J. *Journal of Catalysis* **1993**, *144*, 175.

(90) Bond, G. C.; Sermon, P. A.; Webb, G.; Buchanan, D. A.; Wells, P. B. *Journal of the Chemical Society, Chemical Communications* **1973**, 444.

(91) Bond, G. C.; Sermon, P. A. *Gold Bulletin* **1973**, *6*, 102.

(92) Haruta, M.; Kobayashi, T.; Sano, H.; Yamada, N. *Chemistry Letters* **1987**, 405.

(93) Hammer, B.; Norskov, J. K. *Nature* **1995**, *376*, 238.

(94) Haruta, M. *Chemical Record* **2003**, *3*, 75.

(95) Valden, M.; Lai, X.; Goodmand, D. W. *Science* **1998**, *281*, 1647.

(96) Astruc, D.; Lu, F.; Aranzaes, J. R. *Angewandte Chemie International Edition* **2005**, *44*, 7852.

(97) Pool, R. *Science* **1990**, *248*, 1186.

(98) Pachón, L. D.; Rothenberg, G. *Applied Organometallic Chemistry* **2008**, *22*, 288.

(99) Mirkin, C. A. *Small* **2005**, *1*, 14.

(100) Doyle, A. M.; Shaikhutdinov, S. K.; Jackson, S. D.; Freund, H. J. *Angewandte Chemie International Edition* **2003**, *42*, 5240.

(101) Schmid, G.; Maihack, V.; Lantermann, F.; Peschel, S. *Journal of the Chemical Society, Dalton Transactions: Inorganic Chemistry* **1996**, 589.

(102) Armor, J. N. *Catalysis Today* **1995**, *25*, 199.

(103) Melada, S.; Pinna, F.; Strukul, G.; Perathoner, S.; Centi, G. *Journal of Catalysis* **2006**, *237*, 213.

(104) Gao, H.; Xu, Y.; Liao, S.; Liu, R.; Liu, J.; Li, D.; Yu, D.; Zhao, Y.; Fan, Y. *Journal of Membrane Science* **1995**, *106*, 213.

(105) Dotzauer, D. M.; Dai, J.; Sun, L.; Bruening, M. L. *Nano Letters* **2006**, *6*, 2268.

(106) Liu, C.; Xu, Y.; Liao, S.; Yu, D. *Applied Catalysis A: General* **1998**, *172*, 23.

(107) Decher, G.; Schlenoff, J. B. *Multilayer Thin Films: Sequential Assembly of Nanocomposite Materials*; Wiley-VCH: Weinheim, Germany, 2003.

(108) Decher, G. *Science* **1997**, *277*, 1232.

(109) Decher, G.; Schmitt, J. *Thin Solid Films* **1992**, *210/211*, 831.

(110) Kidambi, S.; Bruening, M. L. *Chemistry of Materials* **2005**, *17*, 301.

(111) Cho, J.; Caruso, F. *Chemistry of Materials* **2005**, *17*, 4547.

(112) Gheith, M. K.; Sinani, V. A.; Wicksted, J. P.; Matts, R. L.; Kotov, N. A. *Advanced Materials* **2005**, *17*, 2663.

(113) Schönhoff, M. *Journal of Physics: Condensed Matter* **2003**, *15*, R1781.

(114) Tan, Y.-J.; Wang, W.-H.; Zheng, Y.; Dong, J.; Stefano, G.; Brandizzi, F.; Garavito, R. M.; Reid, G. E.; Bruening, M. L. *Analytical Chemistry* **2012**, *84*, 8357.

(115) Srivastava, S.; Kotov, N. A. *Accounts of Chemical Research* **2008**, *41*, 1831.

(116) Bergbreiter, D. E.; Franchina, J. G.; Kabza, K. *Macromolecules* **1999**, *32*, 4993.

(117) Cavalieri, F.; Postma, A.; Lee, L.; Caruso, F. *ACS Nano* **2009**, *3*, 234.

(118) Chirea, M.; Pereira, C. M.; Silva, F. *Journal of Physical Chemistry C* **2007**, *111*, 9255.

(119) Chirea, M.; Garcia-Morales, V.; Manzanares, J. A.; Pereira, C.; Gulaboski, R.; Silva, F. *Journal of Physical Chemistry B* **2005**, *109*, 21808.

(120) Porcel, C. H.; Izquierdo, A.; Ball, V.; Decher, G.; Voegel, J. C.; Schaaf, P. *Langmuir* **2005**, *21*.

(121) Shiratori, S. S.; Rubner, M. F. *Macromolecules* **2000**, *33*, 4213.

(122) Ruths, J.; Essler, F.; Decher, G.; Riegler, H. *Langmuir* **2000**, *16*, 8871.

(123) Nakajima, A.; Hashimoto, K.; Watanabe, T. *Monatshefte fuer Chemie* **2001**, *132*, 31.

(124) Coulson, S. R.; Woodward, I.; Badyal, J. P. S.; Brewer, S. A.; Willis, C. *Journal of Physical Chemistry B* **2000**, *104*, 8836.

(125) Wong, T.-S.; Kang, S. H.; Tang, S. K. Y.; Smythe, E. J.; Hatton, B. D.; Grinthal, A.; Aizenberg, J. *Nature* **2011**, *477*, 443.

(126) Young, T. *Philosophical Transactions of the Royal Society* **1805**, *95*, 65.

(127) Nishino, T.; Meguro, M.; Nakamae, K.; Matsushita, M.; Ueda, Y. *Langmuir* **1999**, *15*, 4321.

(128) Wenzel, R. N. *Industrial & Engineering Chemistry Research* **1936**, *28*, 988.

(129) Cassie, A. B. D.; Baxter, S. *Transactions of the Faraday Society* **1944**, *40*, 546.

(130) Erbil, H. Y.; Demirel, A. L.; Avci, Y.; Mert, O. *Science* **2003**, *299*, 1377.

(131) Zhai, L.; Cebeci, F.; Cohen, R. E.; Rubner, M. F. *Nano Letters* **2004**, *4*, 1349.

(132) Tuteja, A.; Choi, W.; Ma, M.; Mabry, J. M.; Mazzella, S. A.; Rutledge, G. C.; McKinley, G. H.; Cohen, R. E. *Science* **2007**, *318*, 1618.

(133) Kobaku, S. P. R.; Kota, A. K.; Lee, D. H.; Mabry, J. M.; Tuteja, A. *Angewandte Chemie* **2012**, *51*, 10109.

(134) Genzer, J.; Efimenko, K. *Biofouling* **2006**, *22*, 339.

(135) Shirtcliffe, N. J.; Roach, P. *Methods in Molecular Biology* **2013**, *949*, 269.

Some of the text and figures contained in chapter two appeared in the following publication.

Hogg, S.R.; Muthu, S.; O'Callaghan, M.; Lahitte, J.F.; Bruening, M.L. *ACS App. Mater. Interfaces* **2012**, 4, 1440-1448.

Chapter 2: Catalytic wet air oxidation of formic acid using modified polysulfone hollow fibers as membrane contactors

2. 1 Introduction

As discussed in chapter 1, CWAO is potentially attractive for remediating aqueous streams containing organic pollutants that are too dilute for efficient incineration and too concentrated for biological processing.[1,2] Due to the low solubility of O_2 in water, however, CWAO requires high air pressure to achieve appreciable oxidation. Gas-liquid membrane contactors control the introduction of multiple reactants to a fixed catalyst surface[3,4] and can potentially overcome O_2-solubility limitations to provide higher CWAO conversions than conventional batch reactors operating under similar gas pressures.[5] Such contactors utilize membrane pores to create an interface between liquid and gas streams (Figure 2.1), and management of the gas overpressure in these systems can sometimes control the degree of pore wetting to position the gas-liquid interface near an area rich in catalyst.[6] In specific cases, the increased availability of gaseous reactant at the catalyst surface gives conversion rates three to six times higher in membrane contactors than in trickle bed reactors.[2,5] Hollow fiber membranes provide an attractive choice for contactor systems due to their large surface-area-to-volume ratio and high packing density,[4,7-10] and several recent studies employed catalytic hollow fibers as membrane reactors.[11-17] This chapter examines whether immobilization of

nanoparticle catalysts in polymeric hollow fibers enhances the oxidation of a model pollutant compared to oxidation in ceramic fibers with much larger diameters. The small lumen diameter in the polymeric fibers should greatly reduce diffusion distances to increase pollutant conversion relative to typical ceramic fibers with much larger inner diameters.

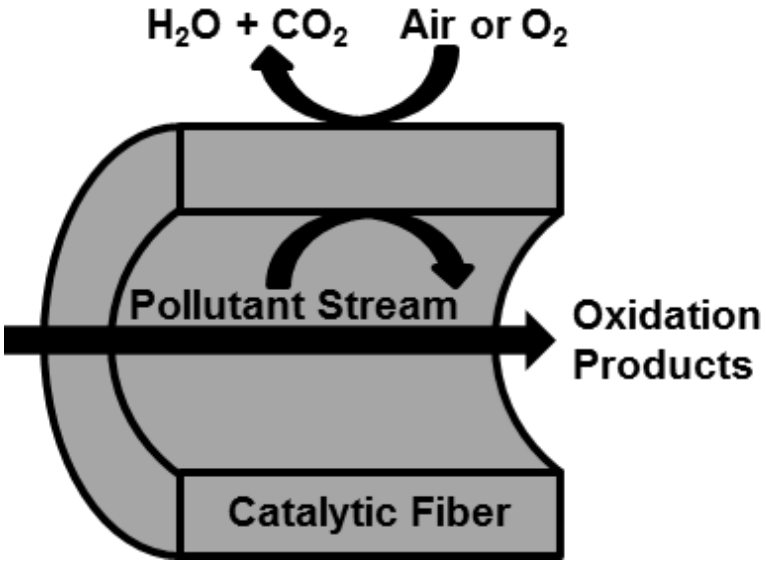

Figure 2.1: Schematic drawing of a cylindrical membrane contactor for CWAO with liquid feed passing through the lumen and gas supplied to the shell side.

Metal nanoparticles are promising catalysts for hollow fiber membrane contactors because of their high surface area to mass ratio.[18-26] Additionally, nanoparticles often possess unusual electronic and catalytic properties that stem from their unique size between the bulk and molecular regimes.[18,19,27] Entrapment of such nanoparticles in a hollow fiber both prevents catalyst aggregation and allows for continuous reactions. Although several methods exist for forming nanoparticles by reduction of metal ions in membranes,[28-30] synthesis of

nanoparticles in solution prior to loading onto supports typically yields more uniform particle shapes and diameters.[21,28,31-38] However, loading of preformed nanoparticles in membranes requires strong adhesion between the nanoparticle and the support.

We employ layer-by-layer (LbL) adsorption of nanoparticles and oppositely charged polyelectrolytes to immobilize preformed catalytic nanoparticles in membrane pores.[39-45] LBL deposition occurs on many substrate materials with geometries that include flat surfaces, membrane pores, cylindrical particles, and carbon nanotubes.[29,35,36,38,39,46,47] Thus, this technique is amenable to hollow-fiber modification. Moreover, the amount of immobilized particles increases with the number of adsorbed layers.

Miachon and coworkers examined tubular ceramic membranes as interfacial contactors for CWAO and found increased activity compared to a stirred tank reactor because of control over the position of the gas-liquid interface within the membrane.[5,48-52] Notably, LBL deposition of polyelectrolyte multilayers and Pt nanoparticles yielded a membrane reactor with the highest Pt activity among those tested.[29] However, the pollutant conversion was relatively low, and the price of the ceramic membranes might limit their potential application.[53] Polymeric hollow fibers may provide a much less expensive option for CWAO of organic pollutants if these membranes are sufficiently stable.

This chapter describes LBL deposition of polyelectrolytes and citrate-stabilized Pt nanoparticles in polysulfone (PS) hollow fibers to create membrane reactors for CWAO of aqueous formic acid. We compare catalytic activities and conversions to previous work with

ceramic hollow fiber membranes and model concentration profiles in membrane reactors to assess the potential benefits of the polymeric hollow fibers. The small diameters of these fibers give rise to higher single-pass conversions compared to previous, larger ceramic membranes, but catalyst activity is more modest in the polymeric hollow fibers.

2.2 Experimental methods

2.2.1 Materials

Poly(sodium 4-styrenesulfonate) (PSS, Mw = 70,000 Da), branched poly(ethyleneimine) (PEI, Mw = 25,000 Da), hexachloroplatinic acid hexahydrate, sodium chloride, and sodium citrate were used as received from Sigma-Aldrich. Formic acid from Mallinckrodt Baker and compressed O_2 (industrial purity, 99.5%) from Airgas were also used as received. Deionized water (Milli-Q purification system, 18.2 MΩ·cm) was used for rinsing the membranes and preparation of the polyelectrolyte and formic acid solutions. The pH values of the polyelectrolyte solutions were adjusted with dilute solutions of HCl and NaOH.

A PS microfiltration hollow fiber membrane module containing 270 fibers was obtained from GE Lifesciences (Model # CFP-6-D-6A). Individual fibers were removed from the module and repotted in 15 cm lengths. Membranes have a stated maximum pore size of 650 nm, an inner diameter of 750 µm, and a wall thickness of 225 µm.

2.2.2 Synthesis of citrate-stabilized Pt nanoparticles

Synthesis of Pt nanoparticles followed a literature procedure that uses citrate to both reduce the Pt and prevent particle aggregation through charge repulsion.[54] Forty mg of platinic

acid dissolved in 255 mL of water was stirred and heated to reflux in a 500 mL round bottom flask before addition of 30 mL of a 1% (w/w) sodium citrate solution. The Pt solution slowly darkened from amber to brown and eventually to black over four hours of reflux. After cooling to room temperature over ice, the Pt colloid solution was stored in an amber glass bottle in a refrigerator. Immediately prior to deposition, the Pt colloids were diluted 12.5:1 with deionized water. Our previous transmission electron microscopy images of Pt nanoparticles prepared using this method showed a size distribution centered around 3 nm.[29]

2.2.3 Modification of hollow fiber membranes

Following a literature procedure, a 1.3 cm-diameter PVC tube housed the hollow fibers potted in epoxy resin (Loctite E-00NS Hysol Epoxy Adhesive).[55] Modules contained either one centered fiber or five fibers arranged in a "X" geometry with accessible fiber lengths of 15 cm between the epoxy resin at each end. Immediately prior to introduction into the module, all deposition solutions passed through a fresh filter (Ahlstrom grade 601 2.5 μm qualitative filter paper) to remove any particles that might block fiber pores. The polyelectrolyte solutions contained either 0.8 mM PSS or 0.8 mM PEI along with 20 mM NaCl. (Polymer concentrations are with respect to the repeating unit.) Initially, the PS hollow fibers were rinsed with distilled water for 30 min in a dead end setup with water flowing from shell to lumen. During polyelectrolyte and nanoparticle adsorption, solutions passed from the lumen to the shell side using lumen cross-flow under an applied pressure of 0.34 bar. A partially closed valve at the lumen exit forced most of the flow through the membrane pores (Figure 2.2). Modification

began by passage of 250 mL of PSS solution through the fiber to adsorb PSS via hydrophobic interactions with PS.[56,57] A deionized water rinse from shell through lumen (until the conductivity of the permeate was less than 10 µS, 100 to 800 mL of rinsing) removed excess polyelectrolyte from the membrane. Next, passage of 250 mL of PEI solution through the membrane, followed by rinsing, completed deposition of the first polyelectrolyte bilayer. Pt nanoparticles were subsequently adsorbed to the PEI layer during passage of 250 mL of the colloid solution (~0.02 mM in Pt atoms) prior to another rinse. Repetition of the PEI and Pt deposition process yielded additional bilayers. During the colloid adsorption, the fiber changed color from white to gray, indicating entrapment of Pt nanoparticles within the membrane.

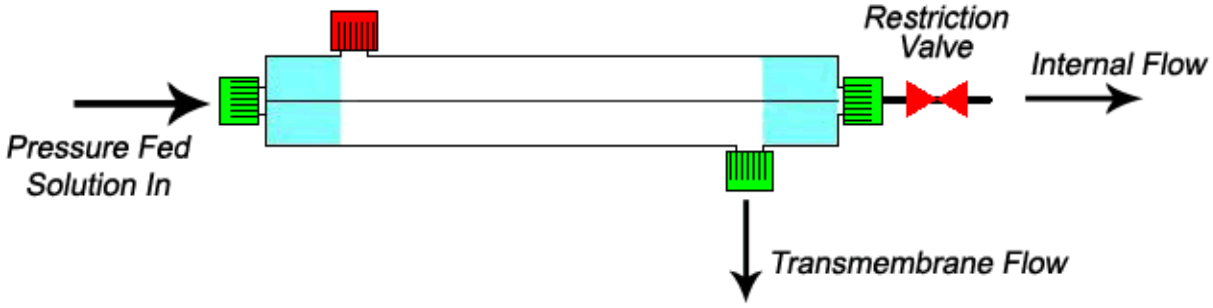

Figure 2.2: Apparatus for fiber modification with polyelectrolyte multilayers. Deposition solutions enter the fiber lumen before exiting under cross-flow. A valve located at the lumen exit creates backpressure to force most solution through the high surface area pores to the shell. Rinsing after depositions proceeds through passage of water from the shell side through the lumen in a dead-end setup. For interpretation of the references to color in this and all other figures, the reader is referred to the electronic version of this dissertation.

2.2.4 Membrane characterization

Scanning electron microscopy images of hollow fibers before and after modification were obtained using a Hitachi S-4700 II field-emission scanning electron microscope (SEM). Deposition of 8 nm of sputtered gold rendered the samples conductive for imaging. To prepare

membrane cross sections, the fiber segments were soaked in ethanol for two minutes to completely wet the fiber before fracturing in liquid nitrogen and mounting for imaging. Because the Pt nanoparticle size is below the resolution of the SEM, the Pt loading onto fibers was determined through analysis by inductively coupled plasma optical emission spectroscopy (ICP-OES). Fibers were cut into several pieces, sonicated in aqua regia for 10 min, and the resulting solutions were diluted 100-fold prior to analysis with a Varian 710-ES ICP-OES at 214.424 nm.

2.2.5 Catalytic reactions

Wet air oxidation of formic acid served as a model reaction for assessing the catalytic activity of PS hollow fibers. Initially, 250 mL of formic acid feed solution was pushed through the membrane using cross-flow at 0.34 bar to wet all pores. Again, a partially closed valve at the membrane outlet forced most of the flow from the lumen to the shell. Subsequently, a peristaltic pump pulled the formic acid solution through the fiber lumen at 0.1 mL/min while an O_2 or N_2 overpressure was applied to the shell side to prevent transmembrane flux. Four initial feed samples along with permeate samples at specified intervals were diluted and analyzed for formic acid using ion chromatography with a Dionex LC20 instrument equipped with an Ionpac AS16 column.

2.2.6 Modeling

The membrane reactor consists of a tubular fiber with solution introduced through the lumen, and the incoming formic acid reacts only in the fixed porous catalyst bed within the fiber walls. An overpressure on the shell side prevents liquid transmembrane flow but is not

sufficient to de-wet the pores. The model used for calculation couples the free fluid and porous media flow through the Navier-Stokes equations and Brinkman's extension of Darcy's law. Due to the symmetry of the system, only half of the fiber needs to be modeled using a two-dimensional axisymmetric geometry. The Navier-Stokes equation describes the fluid flow in the lumen according to equation 2.1, where $\nabla \cdot u = 0$.

$$\nabla \cdot (-\eta(\nabla u + (\nabla u)^T + pI) = -\rho(u \cdot \nabla)u \qquad (2.1)$$

Within the porous wall, the Brinkman equation describes the flow according to equation 2.2, where $\nabla \cdot u = 0$. In these equations, η denotes the viscosity of

$$\nabla \cdot (-\frac{\eta}{\xi_p}(\nabla u + (\nabla u)^T + pI) = -\frac{\eta}{k}u \qquad (2.2)$$

the fluid (Ns/m^2), ε_p is the dimensionless porosity, u is the velocity (m/s), ρ is the density (kg/m^3), p is the pressure (Pa), κ is the permeability (m^2), and I is the identity matrix.

A Fickian approach is suitable for formic acid diffusion, and equation 2.3 provides the mole balance for formic acid mass transport and reaction. In equation 2.3, c_A denotes the concentration of formic

$$\nabla \cdot (-D_A \nabla c_A + c_A u) = R_A \qquad (2.3)$$

acid (mol/m^3), D_A is the diffusivity (m^2/s), and R_A is the reaction rate for formic acid oxidation [mol/(m^3·s)]. We estimated D_A as 1.516 x 10^{-9} m^2/s.[58] The reaction only takes place in the porous walls, so the reaction term is zero in the lumen, and formic acid oxidation in the pores

occurs according to equation 2.4. Because the reaction rate did not vary significantly with external O_2 pressure within the range tested, we

$$\mathrm{HCOOH} + \frac{1}{2}\mathrm{O_2} \rightarrow \mathrm{CO_2} + \mathrm{H_2O} \tag{2.4}$$

assumed a first-order reaction rate, $R_A = -kc_a$, where k is the reaction rate constant.

Upon the solution's entry into the lumen, a fully developed laminar flow is assumed and equation 2.5 gives the velocities where n is the boundary normal vector and r is the distance from the

$$n \cdot u = u_{max}\left[1 - \left(\frac{r}{R}\right)^2\right] \tag{2.5}$$

center of the circular cross-section with a total radius R. At the fiber outlet, the boundary conditions for the Navier-Stokes equations are $t \cdot u = 0$ and $p = 0$ where t is any tangential vector to the boundary. The formic acid concentration at the inlet was fixed as $c_A(0) = c_{A0}$. At the outlet, convection dominates the formic acid mass transport yielding $n \cdot (-D_A \nabla c_A + c_A u) = n \cdot c_A u$. This implies the gradient of c_A in the direction perpendicular to the outlet boundary is negligible, a common assumption for tubular reactors with a high degree of transport by convection in the direction of the main reactor axis (Figure 2.3). Thus, this condition eliminates the need for specifying a concentration or a fixed value for the flux at the outlet boundary. At all other boundaries, insulation conditions apply as given by equation 2.6.

$$n \cdot (-D_A \nabla c_A + c_A u) = 0 \tag{2.6}$$

Equation 2.7 describes the formic acid conversion where c_A is the mixing cup concentration at the outlet determined from equation 2.8. All calculations were performed by Satish Muthu in the chemical engineering module of COMSOL Multiphysics 3.5a.

$$x_A = \left(\frac{c_{A0} - c_A}{c_{A0}}\right) \tag{2.7}$$

$$c_A = \frac{\int_0^R 2\pi r c_A u_z dr}{\int_0^R 2\pi u_z dr} \tag{2.8}$$

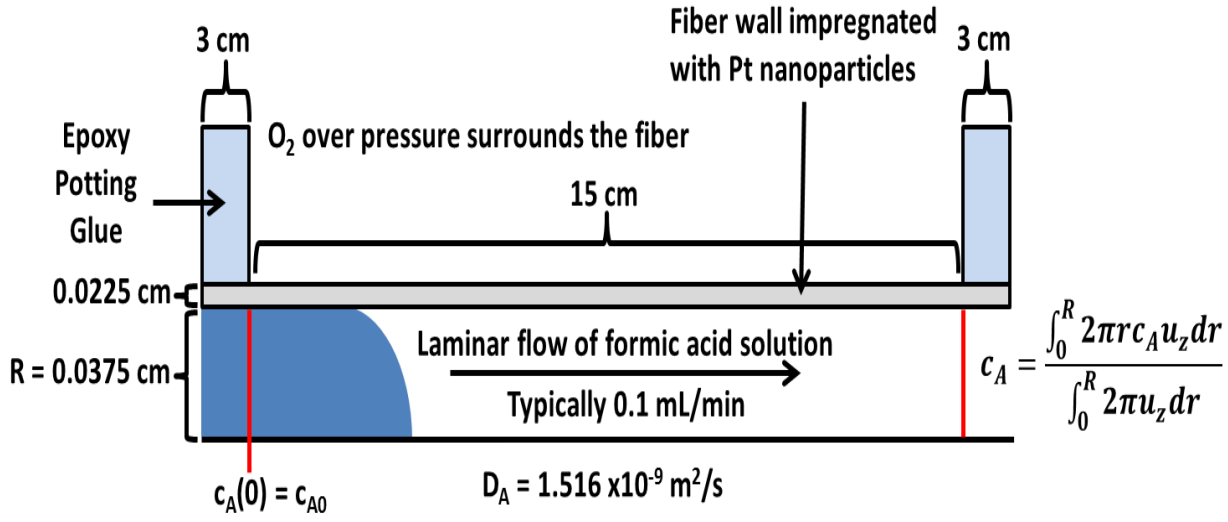

Figure 2.3: Modeled fiber system dimensions and boundary conditions for inlet and outlet formic acid concentrations showing only half of the lumen and a single wall.

2.3 Results and discussion

2.3.1 Membrane modification with Pt nanoparticles

Alternating adsorption of polyelectrolytes and Pt nanoparticles yields coated hollow fiber membranes with open pores. Adsorption occurs during permeation of polyelectrolyte or

nanoparticle solutions from the lumen to the shell, so films deposit throughout the membrane wall, and the membrane turns gray after nanoparticle deposition. The SEM images in Figure 2.4 (A,B) show no obvious changes in the membrane lumen pore sizes after deposition of a PSS/[PEI/Pt]$_2$ film, presumably because the thickness of the polyelectrolyte/nanoparticle films is less than 10 nm.[38,59] Meanwhile, the images of the smaller pores on the shell side (Figure 2.4 C,D) show some changes in the surface morphology after film deposition, but pores remain open. The absence of a cross-flow rinse on the shell side and solution dripping from this surface during modification likely leads to additional deposition on the shell compared to the lumen. When a cross-flow rinse was incorporated on the shell side during modification, no significant pore size reductions were visible in SEM images on either the lumen or shell surfaces. Overall, pore size reduction when depositing without cross-flow decreased O_2 permeability <20% at 0.2 bar, so the open pores on the shell surface will afford the gaseous reactant access to the catalyst-solution interface.

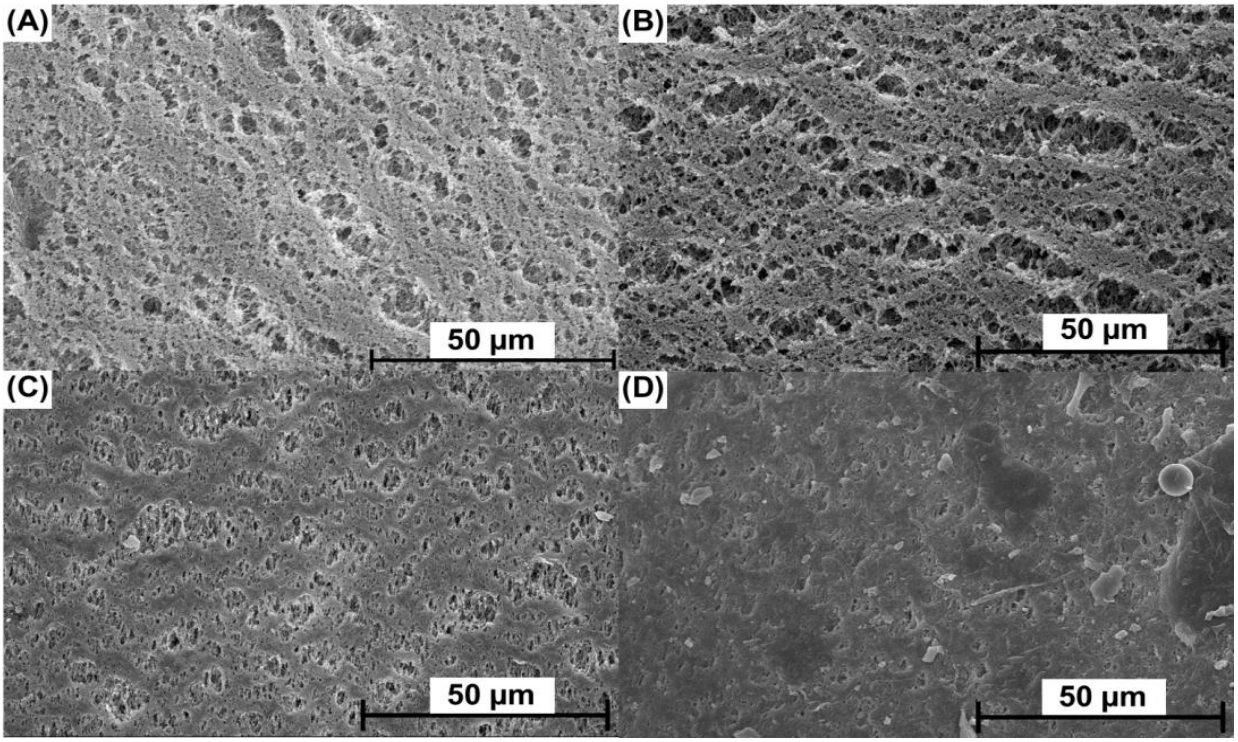

Figure 2.4: Representative SEM images of the lumen (A,B) and shell (C,D) surfaces of PS hollow fibers before (A, C) and after (B,D) adsorption of a PSS/[PEI/Pt nanoparticle]$_2$ film.

To examine the uniformity of Pt loading along the length of a PS fiber modified with a PSS[PEI/Pt]$_2$ film, we cut a 15 cm-long fiber into four 3.75 cm-long sections, dissolved the Pt in aqua regia, and analyzed the aqua regia solutions by ICP-OES. The relative standard deviation (RSD) in the Pt loading for the four segments (Table 2.1, row 1) was less than 10%. The uniform loading of Pt nanoparticles should ensure similar catalyst availability over the entire length of the fiber. We also simultaneously modified five fibers in a single module, cut each fiber into three 5 cm-long sections and determined the amount of Pt in each segment. In this case the relative standard deviation in the Pt content of the 15 segments was 17% (Table 2.1, rows 2 to 6). Overall, the loading/cm in the five-fiber module is about 60% of that in a single fiber. The

lower deposition solution cross-flow rate during adsorption in the five-fiber module might lead to lower loadings.

Table 2.1: Pt loading per length of fiber after LBL modification of a single-fiber module and a five-fiber module with PSS/$[PEI/Pt]_2$ films. Loadings were determined by dissolution of the Pt in aqua regia and analysis by ICP-OES. The segments were approximately 3.75 cm long for the single fiber and 5 cm long for the 5-fiber module.

	Loading (μg Pt/cm)				
Fiber	Segment 1	Segment 2	Segment 3	Segment 4	Average
Single	78.7 ± 3.5	76.8 ± 3.2	79 ± 2.0	80.9 ± 0.6	78.9 ± 2.6
Five Fiber Module					
Fiber 1	38.8 ± 1.0	53.4 ± 0.8	44.6 ± 1.2	n/a	45.6 ± 0.9
Fiber 2	41.8 ± 0.6	56.9 ± 2.5	48.3 ± 0.7	n/a	49.0 ± 1.3
Fiber 3	36.9 ± 0.5	51.3 ± 0.5	31.1 ± 0.4	n/a	39.8 ± 0.4
Fiber 4	53.5 ± 1.1	58.7 ± 1.4	54.6 ± 0.6	n/a	55.6 ± 0.9
Fiber 5	47.4 ± 1.0	58.3 ± 0.8	47.9 ± 1.9	n/a	51.2 ± 1.2

2.3.2 Catalytic performance of PS hollow fiber modules

2.3.2.1 CWAO of formic acid using a membrane contactor

Oxidation of formic acid is an ideal model reaction to test the catalytic activity of immobilized Pt nanoparticles because the only products are CO_2 and water, and Pt is a common catalyst for this reaction.[60-62] In a control experiment, we bubbled a 50 mM formic acid solution with O_2 and then passed this solution through the fiber lumen while applying a N_2 overpressure (0.69 bar) to the shell side of the membrane. One pass of the solution through a single, Pt-modified PS hollow fiber at 0.1 mL/min (membrane residence time of 40 s) resulted in oxidation of only 6 ± 3% of the formic acid (Figure 2.5**,** triangles). The low conversion stems

from the limited O_2 solubility in the feed solution. The room-temperature solubility of O_2 in water is ~ 1.25 mM at 1 atm of O_2,[29,63] and one molecule of O_2 can oxidize two molecules of formic acid. Thus, the O_2 in solution can oxidize a maximum of ~2.5 mM formic acid, which is similar to the observed reaction of 6 ± 3% of the 50 mM formic acid during passage through the membrane.

In contrast, application of an O_2 overpressure (0.69 bar) to the shell side of the hollow fiber resulted in steady-state oxidation of 63 ± 3% of the formic acid in a 50 mM feed solution during a single pass through the membrane lumen with a residence time of 40 s. (In this case, the solution was not saturated with O_2 prior to passing through the membrane.) As Figure 2.5 shows (diamonds), after changing the gas in the module from 0.69 bar N_2 overpressure to 0.69 bar O_2 overpressure with no prior O_2 saturation of the feed, the concentration of formic acid exiting the membrane decreased to the steady state value of 37% of the feed concentration after displacing the dead volume (~4 mL) at the exit of the hollow fiber module, demonstrating the O_2 dependence of the reaction. After 360 min of oxidation, we changed the shell gas from 0.69 bar O_2 to 0.69 bar N_2 (overpressure), and conversion declined again confirming the importance of the membrane contactor for delivering O_2 to enhance conversion.

To increase the fraction of formic acid oxidized without decreasing the overall volumetric flow rate, we increased the number of fibers in the module. Notably, with modules

containing 5 fibers operating at the same nominal flow rate, formic acid oxidation reaches 94 ± 3% in a single pass (Figure 2.5, squares) without saturating the solution with O_2 prior to passing it through the membrane. The increase in conversion results from the higher residence times (198 s) in modules with more fibers. Further increases in the number of fibers will allow even higher conversions or similar conversions at higher flow rates through the module.

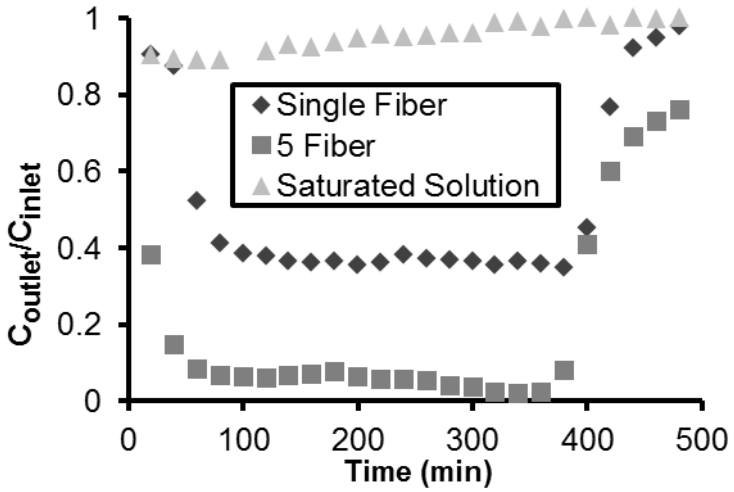

Figure 2.5: Ratio of the outlet to inlet concentrations of formic acid during CWAO in three different fiber modules coated with PSS/[PEI/Pt]$_2$ films. Triangles represent an O_2-saturated solution as the lone source of O_2 using a single Pt-coated PS fiber with N_2 (0.69 bar overpressure) on the shell side. Diamonds and squares represent a single and 5-fiber contactor reactor, respectively, where an O_2 overpressure (0.69 bar) was applied on the shell side at 0 min and subsequently replaced with a N_2 overpressure (0.69 bar) at 360 min. The solution flow rate was 0.1 mL/min in all cases.

2.3.2.2 Fiber longevity

The stability of modified fibers is a major concern because both oxidation of the polymer and shear stress may leach nanoparticles from the membrane. However, ten 8-hour replicates of CWAO (50 mM formic acid) with the same fiber show a RSD in formic acid oxidation of less than 20%, suggesting no continuous leaching of Pt from the system (Figure

2.6). While there is some spread in the net conversions in different experiments, the general trends remain the same in every trial. More importantly, after the first three trials, no clear trend of decreasing conversion with each subsequent trial occurred. The conversion decline after the first three trials does not appear to result from Pt leaching since the conversion did not decrease significantly during the trials. Instead, an inactivation of some catalyst sites may occur during drying of the fiber between experiments. The outlying data points from trial six are probably the result of IC instrument error rather than increased performance. Therefore, the fiber remained relatively stable during the eighty hours of testing in this experiment.

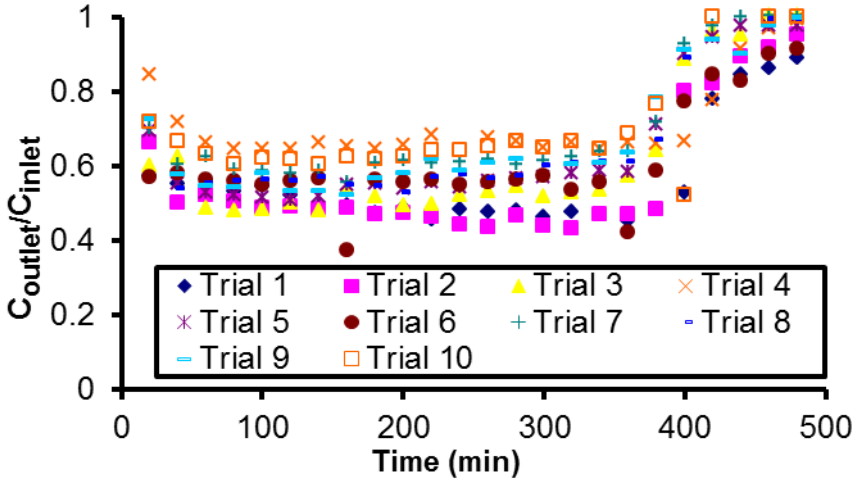

Figure 2.6: Ratio of the outlet to inlet concentrations of formic acid during CWAO for 10 trials of 8 hours using a single PS fiber module modified with a PSS/$[PEI/Pt]_2$ film. An O_2 overpressure of 0.69 bar was applied at 0 min on the shell side and replaced with N_2 at 360 min.

2.3.2.3 Dependence of oxidation rates on formic acid concentration and O_2 overpressure

To explore the factors limiting the rate of CWAO in hollow fiber membranes, we varied both the formic acid concentration and the O_2 overpressure during reactions. Figure 2.7 shows

the average concentration of formic acid oxidized (the difference between feed and outlet concentrations) as a function of the feed solution formic acid concentration passed through a single-fiber module. Error bars represent the standard deviation of the average oxidized formic acid concentration over a period of 5 hours for two replicate membranes with identical modification (n=2). At feed concentrations from 10 to 50 mM, the change in formic acid concentration upon passing through the membrane varies approximately linearly with the feed concentration. In contrast, the concentration of formic acid oxidized in a single pass through the membrane plateaus at 40 mM for feed concentrations from 80 to 150 mM. These data suggest that formic acid concentration limits the reaction rate at low feed concentrations (due to either diffusion or kinetic limitations), whereas either the availability of O_2 in the catalyst layer or the amount of catalyst limit the reaction at high formic acid feed concentrations.

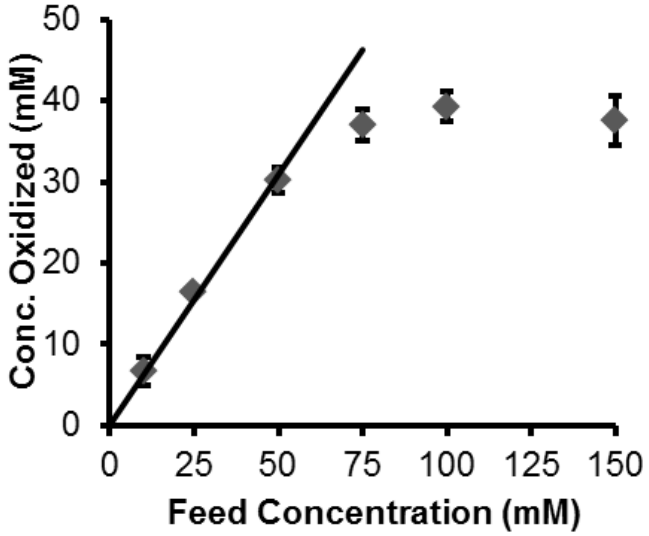

Figure 2.7: Concentration of formic acid oxidized (inlet - outlet concentration) in CWAO with a single-fiber module and an O_2 overpressure of 0.69 bar on the shell side of the membrane. The line represents a linear fit (forced through the origin, slope of 0.55) to the first three data points. Data are an average of two experiments with two modified single fibers.

Figure 2.8 shows the average concentration of formic acid oxidized when using a 50 mM formic acid feed and various O_2 overpressures on the shell side of single fiber modules. Within experimental error, the amount of formic acid oxidized is independent of the O_2 overpressure tested. The highest overpressure of ~1 bar represents the maximum recommended operating pressure from the manufacturer of this PS fiber. One concern in these experiments, however, is whether changing the overpressure alters the wetting of the pores. The Young-Laplace equation (2.9),

$$\Delta p = \frac{2\gamma\cos(\theta)}{r} \quad (2.9)$$

provides an estimate for the critical pressure, Δp, required to prevent pore wetting, where θ is the solution contact angle with the material, γ is the surface tension of the liquid, and r is the pore radius. Based on a water contact angle of 67° on polysulfone,[64] and a pore radius of 325 μm, this equation suggests that the pressure required to overcome capillary wetting would be around 1.7 bar for aqueous solutions. This is consistent with the fact that we observed no gas bubbles breaking through the membranes. If the pores are indeed wetted at all the pressures in these experiments, we would expect that increased O_2 solubility in water might enhance oxidation rates. The constant reaction rate at various O_2 pressures may stem from the fairly narrow range of total pressures (1.1-2 bar absolute pressure) and the fairly complicated kinetics of the formic acid oxidation. Harmsen et al. suggest that equation 2.10 describes the rate of formic acid oxidation, R.[65]

$$R = \frac{K[O_2]^{1/2}[HCOO^-]}{(1+K'[O_2]^{1/2}+K''[HCOO^-])^2} \quad (2.10)$$

In this expression, K, K' and K'' represent products of different equilibrium constants and surface site densities. At most, the reaction would show a square root dependence on the concentration of O_2 in solution.

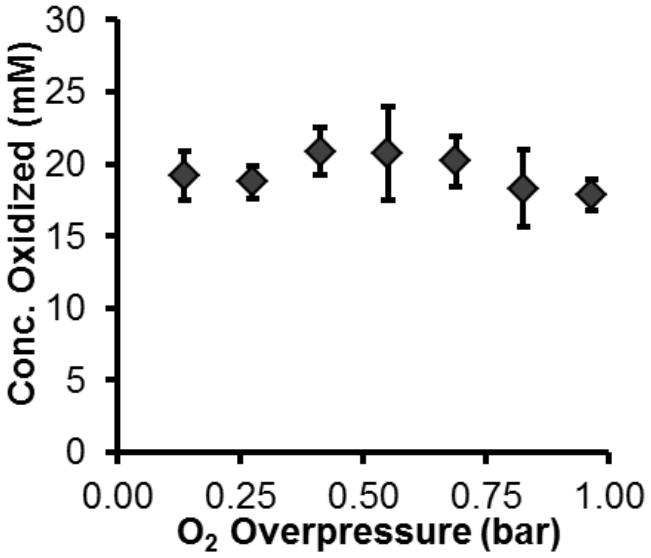

Figure 2.8: Concentration of formic acid oxidized during CWAO with single fiber modules at varying overpressures. Membranes were modified with PSS/$[PEI/Pt]_2$ films and the feed solution contained 50 mM formic acid. Data are an average of three replicate experiments on each of two different fibers.

2.3.2.4 Effect of Pt loading on conversion

Low Pt loading will limit the rate of formic acid oxidation when the catalyst is saturated with reactants. To examine the effect of catalyst loading on oxidation rate, we compared single-fiber membrane reactors modified with one and three PEI/ Pt bilayers atop a base layer of PSS. Analysis of Pt loading in these fibers using ICP-OES shows that adsorption of each PEI/Pt bilayer

adds approximately 500 µg Pt to the membrane. Figure 2.9 demonstrates that the amounts of formic acid oxidized in fibers containing 1 PEI/Pt bilayer (replicate fibers 1 and 3) are significantly less than in fibers containing 3 bilayers (replicate fibers 2 and 4) (p=0.99) for feed solutions containing 50 and 100 mM formic acid. At feed concentrations of 25 mM, the two types of membranes show similar conversions, presumably because the catalyst is not saturated with reactant. As in Figure 2.5, the concentration oxidized increases with the feed (inlet) concentration. The average ratios of the concentrations oxidized in membranes modified with 3 and 1 PEI/Pt bilayers were 1.14, 1.28, and 1.31 at feed concentrations of 25, 50, and 100 mM, respectively. Thus, although higher Pt loading enhances formic acid oxidation, the increase of ~1.30 in the amount oxidized is significantly less than the 3-fold increase in Pt loading. Perhaps Pt in the inner layers of the coating does not participate in oxidation due to slow formic acid diffusion into the coating.

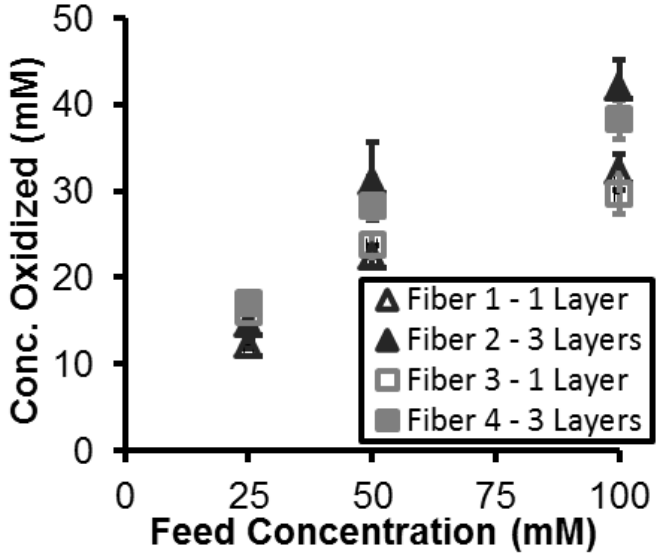

Figure 2.9: Concentration of formic acid oxidized (inlet - outlet concentration) in CWAO with a single-fiber module and various formic acid concentration in the inlet solutions. Fibers 1 and 3 were replicate fibers modified with PSS/PEI/Pt (1-Layer) films while fibers 2 and 4 were

modified with PSS[PEI/Pt]$_3$ (3-Layer) films. The error bars in the figure represent standard deviations with an n value of more than 40.

2.3.3 Calculated formic acid concentration profiles

We first calculated the diffusion-limited formic acid conversion. In this calculation, we assumed laminar flow throughout the fiber lumen and that formic acid oxidation occurs instantaneously upon encountering the fiber wall, i.e., the concentration of formic acid at the lumen wall is zero. Figure 2.10 shows the resulting concentration profile. For a 15 cm-long fiber and a flow rate of 0.1 mL/min, the mixing cup concentration exiting the fiber is only ~4% of the feed concentration (>96% oxidation of formic acid). Thus the reaction we observe in single fibers (40-60% oxidation) is significantly slower than the diffusion-limited case where reaction occurs instantaneously at the lumen wall. The diffusion-limited oxidation in the five-fiber module is even higher (>99.9%) because of the longer residence time, and this conversion is again much greater than the 94% we observed.

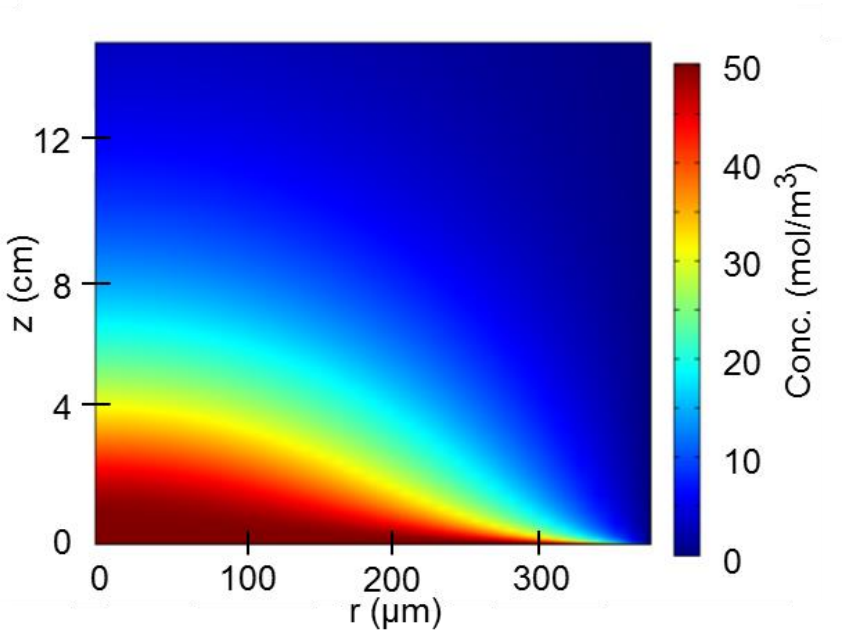

Figure 2.10: Diffusion-limited formic acid concentration profile in a single-fiber reactor as a function of the distances from the inlet (z,Y-axis) and the center of the fiber (r, X-axis). The fiber inner radius was 375 μm, and reaction was assumed to occur instantaneously at the fiber wall, where r=375 μm. The results predict 96% oxidation of the 50 mM formic acid by the time the solution reaches the outlet. The flow rate was 0.1 mL/min.

To more reasonably model the system, we allowed for diffusion to reaction sites within the membrane walls and varied the first-order rate constant for formic acid oxidation. We assumed fully developed laminar flow in the interior of the fiber and no convective flow in the membrane walls. Figure 2.11 shows the concentration profile in a single-fiber membrane reactor assuming a rate constant within the fiber walls of 0.01 s^{-1}. The vertical line indicates the lumen wall. In this case, a rate constant of 0.01 s^{-1} leads to a formic acid concentration profile very different from that in the diffusion-limited case. Reaction occurs throughout the wall, but is more prevalent near the lumen. The mixing cup outlet concentration is about half that of the feed concentration, which agrees well with the observed conversion. Note that we assumed a

first order rate constant because the O_2 pressure outside the fiber did not affect conversion, see Figure 2.7. In modeling the reaction in the five fiber module using the same rate constant, we also see agreement between experimental and observed conversion (94 ± 3 % experimental versus 97 % in the simulation). Additionally, we modeled O_2 concentration profiles for the polymeric fiber module at overpressures of 0.1, 0.69, and 1 bar, see Figure 2.12. As expected, the oxygen concentration decreases from the shell to the lumen, so a first-order reaction is an oversimplification. Near the lumen reaction rates will likely be lower than simulated, whereas near the shell wall they will be higher than simulated.

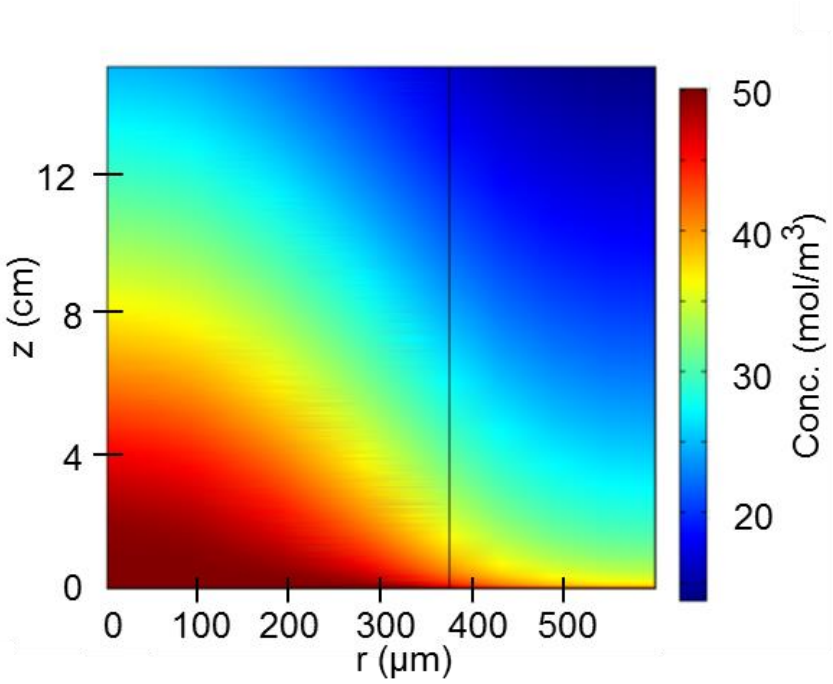

Figure 2.11: Calculated formic acid concentration profile during oxidation in a single-fiber reactor. The plot shows the concentration by color at any point along the length of the reactor (z, Y-axis) and at any radial distance between the center of the fiber to the outer wall (r, X-axis). The results predict ~52% oxidation of the formic acid by the time the solution reaches the outlet. The assumed first-order rate constant was 0.01 s^{-1}. The vertical line at r=375 μm represents the fiber wall.

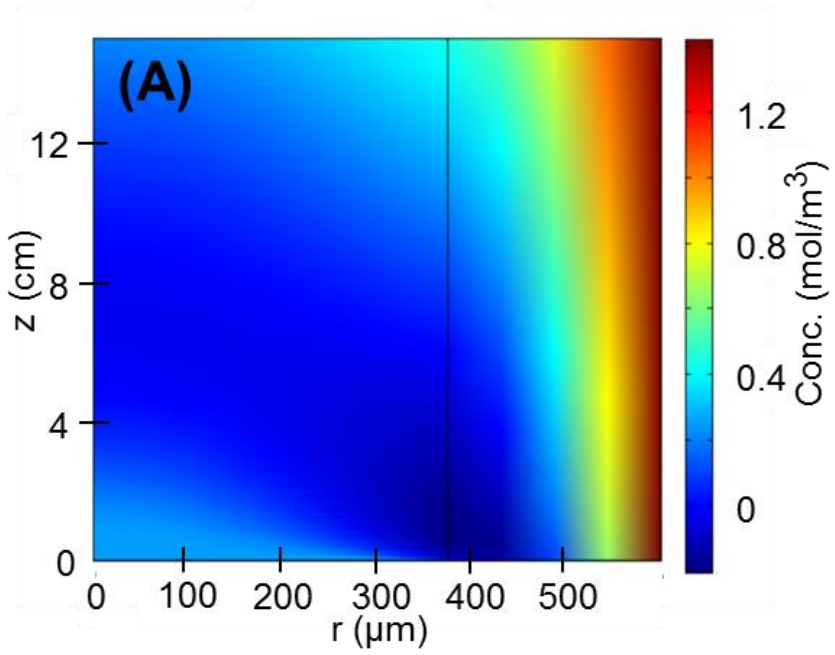

Figure 2.12: O_2 concentration profiles in a polymeric hollow fiber membrane as a function of the distances from the inlet (z,Y-axis) and the center of the membrane (r, X-axis). The simulation uses an O_2 diffusion coefficient of 1.96×10^{-9} m^2/s in solution. The inner fiber radius was 375 μm, and reaction was assumed to occur throughout the fiber wall with a first-order rate constant for formic acid oxidation of 0.01 s^{-1}. We assumed that the reaction (equation 2.4) is first order with respect to formic acid and zero order with respect to O_2. The formic acid solution enters the fiber lumen saturated with atmospheric O_2 (0.25 mM) while the shell of the fiber is exposed to (A) 0.1 bar O_2 overpressure (1.42 mM in solution), (B) 0.69 bar O_2 overpressure (2.18 mM in solution), and (C) 1.0 bar O_2 overpressure (2.58 mM in solution). Note than in Figure A there is a small region of negative concentration, showing that the assumption of zero-order reaction with respect to O_2 is an oversimplification.

Figure 2.12 (cont'd)

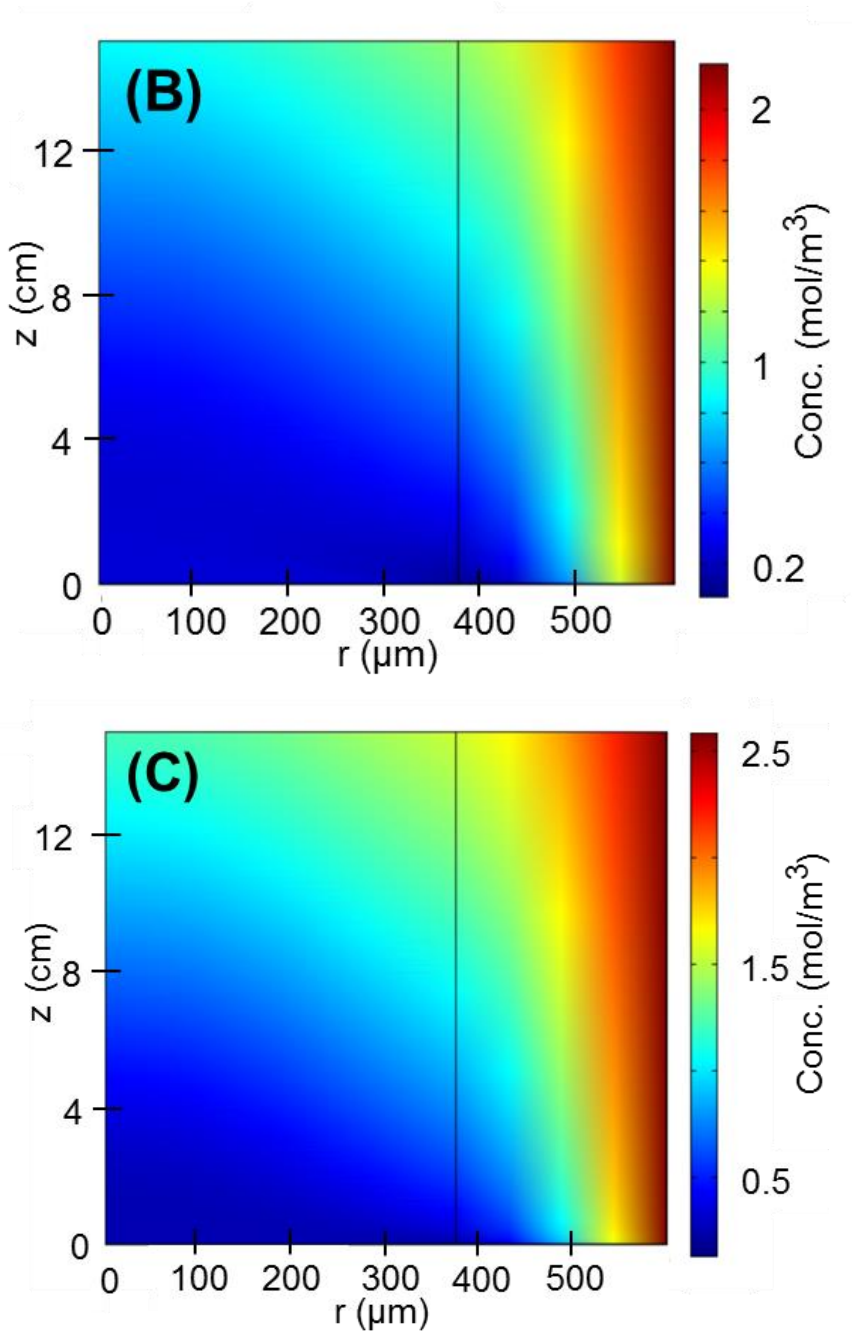

Figure 2.13 shows the predicted conversions for a single fiber module at a range of first-order rate constants from 0.001 to 1000 s^{-1}. At values above 1 s^{-1}, the reaction becomes

limited by diffusion of formic acid to the walls of the fiber, and the concentration near the lumen wall is nearly zero. Rate constants below 0.01 s^{-1} give much lower reaction than we observed. Conversion of the pseudo-homogeneous rate constant (k, 0.01 s^{-1}) to a heterogenous rate constant, k', requires normalization to the amount of Pt surface area, A, per solution volume, V, according to equation 2.11.

$$k' = \frac{kV}{A} \qquad (11)$$

Given the total Pt loading of 1 mg in a single fiber and assuming 3 nm-diameter particles, the value of k' is 8 x 10^{-7} cm/s.

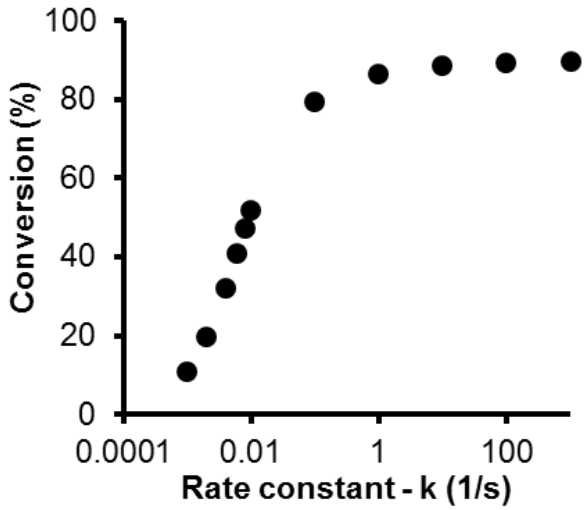

Figure 2.13: Simulated mixed cup conversion of formic acid for a single fiber reactor assuming first-order rate constants for formic acid wet air oxidation from .001 to 1000 (1/s).

Figure 2.14 shows the predicted effect of membrane wall thickness (over a range of 100-300 μm) on the extent of formic acid oxidation. We should note again that this calculation

neglects any effect the wall thickness may have on the availability of O_2 for the reaction. The results suggest that the thickness of the wall plays a modest role in the oxidation process, as the extent of formic acid oxidation only increases from 32% to 57% on increasing the wall thickness from 100 µm to 300 µm. Most of the reaction takes place within the first 100 µm of the lumen surface. The model assumes that the pores of the membrane are completely wetted, which, as mentioned above, is likely given the size of the pores and the water contact angle of the membrane.

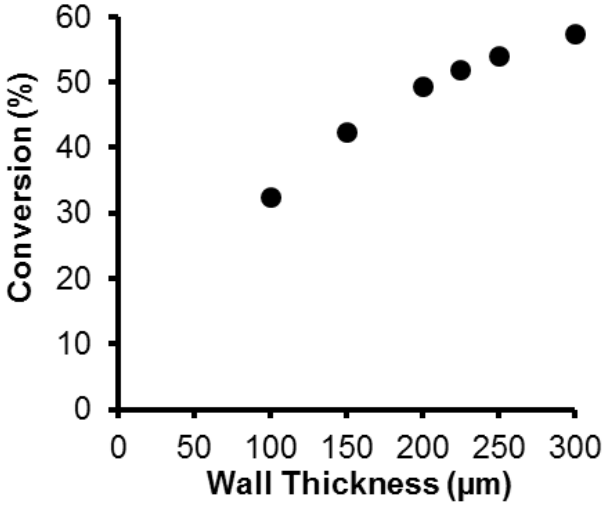

Figure 2.14: Simulated formic acid conversion in a single-fiber module with membranes having different wall thicknesses. The inner radius of the fiber was 375 µm, and the rate constant was 0.01 s^{-1}.

2.3.4 Comparison to previous work

The best tubular ceramic membranes for CWAO in Miachon's work catalyzed oxidation of about 10% of a 100 mM formic acid solution during a single pass at a flow rate between 7 and 10 mL/min (linear velocity of 0.43 cm/s, residence time of 58 s, membrane length of 25 cm).[49] Those membranes had a lumen diameter of 7 mm, and our simulation of diffusion-

limited oxidation in such large membranes gives a conversion of 13%, similar to the measured value (see Figure 2.15). The innermost 3 µm layer of the lumen wall in the ceramic membranes contained 20 nm pores which likely allow a high Pt loading near this wall, as determined by SEM-EDS mapping.[2] The high catalyst loading at the lumen wall may lead to a rate that is closer to the diffusion limit than in the case of the hollow fiber membranes.

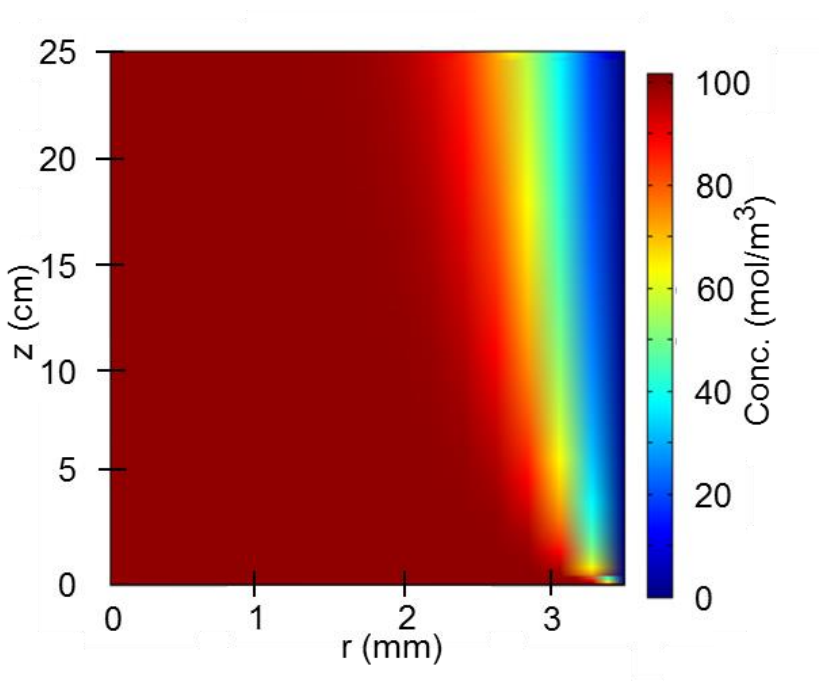

Figure 2.15: Diffusion-limited formic acid concentration profile in a tubular ceramic membrane as a function of the distances from the inlet (z,Y-axis) and the center of the membrane (r, X-axis). The inner radius was 3.5 mm, and reaction was assumed to occur instantaneously at the lumen wall, where r = 3.5 mm. The results predict 13% oxidation of the 100 mM formic acid by the time the solution reaches the outlet. The flow rate was 10 mL/min. The low conversion stems from high diffusion distance resulting from the large diameter of the ceramic membrane.

Nevertheless, at similar residence times, the polymer single fiber modules in this study give a higher single-pass conversion of formic acid than the previous ceramic hollow fibers, presumably because of the smaller average diffusion distances between the molecules in

solution and the polymer fiber. (For the large fiber, the depletion layer around the lumen never reaches the center of the fiber, Figure 2.15.) Use of ceramic membranes with smaller lumen diameters (3 mm) should also reduce formic acid diffusion distances and lead to somewhat higher single-pass conversions. However, the cost of the ceramic membranes may still limit their practicality. Additionally, while smaller ceramic fibers still contain larger pores on the shell surface than the lumen, they may lack the distinct multilayered wall composition that afforded high catalyst density near the lumen surface in the work of Miachon.[66]

Remarkably, the five-fiber PS modules in this study catalyzed oxidation of 94 % of the formic acid in a 50 mM feed solution in a single pass at a flow rate of 0.1 mL/min (linear velocity of 0.08 cm/s, residence time of 198 s, 15 cm fiber). Assuming performance remains the same with further scale up and the same linear velocity, a module containing 500 PS fibers would oxidize 94 % of the formic acid in a single pass, whereas a single 7 mm (inside diameter) ceramic fiber would oxidize only about 10 % of the formic acid at the same total flow rate. (The cost of a 500-fiber module is about the same as that of a ceramic fiber.)

One major disadvantage of the polymeric fibers, however, is the relatively low activity of the immobilized Pt. With a feed solution containing 100 mM formic acid, the modified PS fibers exhibited a normalized activity of 0.07 mmol formic acid/s·g Pt, whereas the best ceramic membranes showed an activity of 1.5 mmol formic acid/s·g Pt . The higher activity in the ceramic membranes likely stems from the 3 layer geometry of the fibers, and the high concentration of catalyst near the lumen. Moreover, because outer pores do not wet, nearly all of the catalyst resides near the liquid-air interface to provide readily accessible O_2 for

oxidation. In contrast, for the polymeric membrane Pt deposition and wetting occur throughout the fiber wall, so oxygen availability may significantly limit the reaction. Further refinement of catalyst deposition and wetting properties, probably using membranes with small pores at the lumen interface, should lead to increased activity in polymeric fiber reactors.

2.4. Conclusions

CWAO in single polymeric hollow fibers at room temperature leads to over 50% oxidation of the formic acid in 50 mM feed solutions during a single pass through a hollow fiber. Additionally, 94% oxidation occurs for a single pass through five parallel fibers at the same volumetric flow rate but lower linear velocity. The PS hollow fibers show significantly higher conversions than previous ceramic membranes because the small diameter of the hollow fibers decreases radial diffusion distances. Modeling the diffusion of formic acid within the lumen indicates the oxidation is significantly below the diffusion-limited rate. A simple first-order model of the reaction suggests an apparent rate constant of 0.01 s^{-1} and shows that reaction occurs throughout the fiber wall.

One major challenge to the use of the catalytic PS hollow fibers is the low catalyst activity caused by a disperse loading of Pt nanoparticles throughout the wall of the fibers instead of in a tightly concentrated region near the lumen surface. With increased nanoparticle deposition localized near the lumen walls and more controlled pore wetting, the activity might improve without decreasing conversion.

REFERENCES

REFERENCES

(1) Besson, M.; Descorme, C.; Bernardi, M.; Gallezot, P.; di Gregorio, F.; Grosjean, N.; Pham Minh, D.; Pintar, A. *Environmental Technology* **2010**, *31*, 1441.

(2) Vospernik, M.; Pintar, A.; Berčič, G.; Levec, J.; Walmsley, J. C.; Ræder, H.; Iojoiu, E. E.; Miachon, S.; Dalmon, J.-A. *Chemical Engineering Science* **2004**, *59*, 5363.

(3) Fritsch, D.; Bengtson, G. *Advanced Engineering Materials* **2006**, *8*, 386.

(4) Gabelman, A.; Hwang, S.-T. *Journal of Membrane Science* **1999**, *159*, 61.

(5) Miachon, S.; Perez, V.; Crehan, G.; Torp, E.; Ræder, H.; Bredesen, R.; Dalmon, J.-A. *Catalysis Today* **2003**, *82*, 75.

(6) Westermann, T.; Melin, T. *Chemical Engineering and Processing* **2009**, *48*, 17.

(7) Kleinert, A.; Feldhoff, A.; Schiestel, T.; Caro, J. *Catalysis Today* **2006**, *118*, 44.

(8) Peters, T. A.; Fontalvo, J.; Vorstman, M. A. G.; Keurentjes, J. T. F. *Chemical Engineering Research and Design* **2004**, *82*, 220.

(9) Wang, H.; Tablet, C.; Schiestel, T.; Caro, J. *Catalysis Communications* **2006**, *7*, 907.

(10) Mulder, M. *Basic Principles of Membrane Technology*; Kluwer Academic Publishers: Dordrecht, 1996.

(11) Ouyang, L.; Dotzauer, D. M.; Hogg, S. R.; Macanas, J.; Lahitte, J.; Bruening, M. *Catalysis Today* **2010**, *156*, 100.

(12) Wang, H.; Feldhoff, A.; Caro, J.; Schiestel, T.; Werth, S. *AIChE Journal* **2009**, *55*, 2657.

(13) Van der Vaart, R.; Lebedeva, V. I.; Petrova, I. V.; Plyasova, L. M.; Rudina, N. A.; Kochubey, G. F.; Tereshchenko, G. F.; Volkov, V. V.; van Erkel, J. *Journal of Membrane Science* **2007**, *299*, 38.

(14) Peirano, F.; Vincent, T.; Quignard, F.; Robitzer, M.; Guibal, E. *Journal of Membrane Science* **2009**, *329*, 30.

(15) Blondet, F. P.; Vincent, T.; Guibal, E. *International Journal of Biological Macromolecules* **2008**, *43*, 69.

(16) Israni, S. H.; Nair, B. K. R.; Harold, M. P. *Catalysis Today* **2009**, *139*, 299.

(17) Caro, J.; Caspary, K. J.; Hamel, C.; Hoting, B.; Kolsch, P.; Langanke, B.; Nassauer, K.; Schiestel, T.; Schmidt, A.; Schomacker, R.; Seidel-Morgenstern, A.; Tsotsas, E.; Voigt, I.; Wang, H.; Warsitz, R.; Werth, S.; Wolf, A. *Industrial & Engineering Chemistry Research* **2007**, *46*, 2286.

(18) Astruc, D.; Lu, F.; Aranzaes, J. R. *Angewandte Chemie, International Edition* **2005**, *44*, 7852.

(19) Pool, R. *Science* **1990**, *248*, 1186.

(20) Mei, Y.; Sharma, G.; Lu, Y.; Ballauff, M.; Drechsler, M.; Irrgang, T.; Kempe, R. *Langmuir* **2005**, *21*, 12229.

(21) Comotti, M.; Li, W. C.; Spliethoff, B.; Schüth, F. *Journal of the American Chemical Society* **2006**, *128*, 917.

(22) Jiang, Y.; Gao, Q. *Journal of the American Chemical Society* **2006**, *128*, 716.

(23) Meyer, D. E.; Bhattacharyya, D. *Journal of Physical Chemistry B* **2007**, *111*, 7142.

(24) Brandão, L.; Fritsch, D.; Mendes, A. M.; Madeira, L. M. *Industrial & Engineering Chemistry Research* **2007**, *46*, 5278.

(25) Valden, M.; Lai, X.; Goodman, D. W. *Science* **1998**, *281*, 1647.

(26) Park, K. H.; Jang, K.; Kim, H. J.; Son, S. U. *Angewandte Chemie, International Edition* **2007**, *46*, 1152.

(27) Pachón, L. D.; Rothenberg, G. *Applied Organometallic Chemistry* **2008**, *22*, 288.

(28) Bhattacharjee, S.; Dotzauer, D. M.; Bruening, M. L. *Journal of the American Chemical Society* **2009**, *131*, 3601.

(29) Dotzauer, D. M.; Abusaloua, A.; Miachon, S.; Dalmon, J.-A.; Bruening, M. L. *Applied Catalysis, B: Environmental* **2009**, *91*, 180.

(30) Perez, V.; Miachon, S.; Dalmon, J. A.; Bredesen, R.; Pettersen, G.; Ræder, H.; Simon, C. *Separation and Purification Technology* **2001**, *25*, 33.

(31) Zhong, L. S.; Hu, J. S.; Cui, Z. M.; Wan, L. J.; Song, W. G. *Chemistry of Materials* **2007**, *19*, 4557.

(32) Gates, B. C. *Chemical Reviews* **1995**, *95*, 511.

(33) Wolf, A.; Schüth, F. *Applied Catalysis, A: General* **2002**, *226*, 1.

(34) Zheng, N.; Stucky, G. D. *Journal of the American Chemical Society* **2006**, *128*, 14278.

(35) Dotzauer, D. M.; Bhattacharjee, S.; Wen, Y.; Bruening, M. L. *Langmuir* **2009**, *25*, 1865.

(36) Dotzauer, D. M.; Dai, J.; Sun, L.; Bruening, M. L. *Nano Letters* **2006**, *6*, 2268.

(37) Bhattacharjee, S.; Bruening, M. *Langmuir* **2008**, *24*, 2916.

(38) Kidambi, S.; Bruening, M. L. *Chemistry of Materials* **2005**, *17*, 301.

(39) Cho, J.; Caruso, F. *Chemistry of Materials* **2005**, *17*, 4547.

(40) Ostrander, J. W.; Mamedov, A. A.; Kotov, N. A. *Journal of the American Chemical Society* **2001**, *123*, 1101.

(41) Kidambi, S.; Dai, J.; Li, J.; Bruening, M. L. *Journal of the American Chemical Society* **2004**, *126*, 2658.

(42) Jiang, C.; Markutsya, S.; Tsukruk, V. V. *Langmuir* **2004**, *20*, 882.

(43) Joly, S.; Kane, R.; Radzilowski, L.; Wang, T.; Wu, A.; Cohen, R. E.; Thomas, E. L.; Rubner, M. F. *Langmuir* **2000**, *16*, 1354.

(44) Caruso, F.; Caruso, R. A.; Möhwald, H. *Science* **1998**, *282*, 1111.

(45) Datta, S.; Cecil, C.; Bhattacharyya, D. *Industrial & Engineering Chemistry Research* **2008**, *47*, 4586.

(46) Schönhoff, M. *Journal of Physics: Condensed Matter* **2003**, *15*, R1781.

(47) Gheith, M. K.; Sinani, V. A.; Wicksted, J. P.; Matts, R. L.; Kotov, N. A. *Advanced Materials* **2005**, *17*, 2663.

(48) Iojoiu, E. E.; Landrivon, E.; Ræder, H.; Torp, E. G.; Miachon, S.; Dalmon, J.-A. *Catalysis Today* **2006**, *118*, 246.

(49) Iojoiu, E. E.; Miachon, S.; Landrivon, E.; Walmsley, J. C.; Ræder, H.; Dalmon, J.-A. *Applied Catalysis, B: Environmental* **2007**, *69*, 196.

(50) Ræder, H.; Bredesen, R.; Crehan, G.; Miachon, S.; Dalmon, J.-A.; Pintar, A.; Levec, J.; Torp, E. *Separation and Purification Technology* **2003**, *32*, 349.

(51) Iojoiu, E. E.; Walmsley, J. C.; Ræder, H.; Miachon, S.; Dalmon, J.-A. *Catalysis Today* **2005**, *104*, 329.

(52) Iojoiu, E. E.; Miachon, S.; Dalmon, J.-A. *Topics in Catalysis* **2005**, *33*, 135.

(53) Dalmon, J.-A.; Cruz-Lopez, A.; Farrusseng, D.; Guilhaume, N.; Iojoiu, E. E.; Jalibert, J.-C.; Miachon, S.; Mirodatos, C.; Pantazidis, A.; Rebeilleau-Dassonneville, M.; Schuurman, Y.; van Veen, A. C. *Applied Catalysis, A: General* **2007**, *325*, 198.

(54) Brugger, P. A.; Cuendet, P.; Gratzel, M. *Journal of the American Chemical Society* **1981**, *103*, 2923.

(55) Rouaix, S. C., C.; Aimar, P. *Journal of Membrane Science* **2006**, *277*, 137.

(56) Malaisamy, R.; Bruening, M. L. *Langmuir* **2005**, *21*, 10587.

(57) Kotov, N. A. *Nanostructured Materials* **1999**, *12*, 789.

(58) Bidstrup, D. E.; Geankoplis, C. J. *Journal of Chemical and Engineering Data* **1963**, *8*, 170.

(59) Harris, J. J.; Bruening, M. L. *Langmuir* **2000**, *16*, 2006.

(60) Fein, D. E.; Wachs, I. E. *Journal of Catalysis* **2002**, *210*, 241.

(61) Palaikis, L.; Wieckowski, A. *Catalysis Letters* **1989**, *3*, 143.

(62) Fonseca, I.; Jiang, L.; Pletcher, D. *Journal of the Electrochemical Society* **1983**, *130*, 2187.

(63) *IUPAC Solubility Data Series Volume 7: Oxygen and Ozone*; Battino, R., Ed.; Pergamon Press Inc: New York, 1981; Vol. 7.

(64) Kim, K. S.; Lee, K. H.; Cho, K.; Park, C. E. *Journal of Membrane Science* **2002**, *199*, 135.

(65) Harmsen, J. M. A.; Jelemensky, L.; Van ANdel-Scheffer, P. J. M.; Kuster, B. F. M.; Marin, G. B. *Applied Catalysis, A: General* **1997**, *165*, 499.

(66) Dutczaka, S. M.; Luiten-Oliemanb, M. W. J.; Zwijnenbergc, H. J.; Bolhuis-Versteegd, L. A. M.; Winnubstb, L.; Hempeniuse, M. A.; Benesa, N. A.; Wessling, M.; Stamatialisd, D. *Journal of Membrane Science* **2011**, *372*, 182.

Chapter 3: Antifouling performance of a porous polypropylene coating in membrane distillation

3.1 Introduction

To address the rapidly growing worldwide water demands discussed in Chapter 1, MD provides an alternative to reverse osmosis for the purification of water from feeds containing non-volatile contaminants. Whereas reverse osmosis utilizes high pressures (> 25 bar) to selectively pass water through dense, non-porous polymeric films, direct contact membrane distillation (DCMD) relies on a vapor pressure difference between two liquid phases separated by a porous hydrophobic membrane.[1] The vapor pressure difference usually arises due to a temperature gradient across the membrane. Unlike traditional multistage flash distillation, MD does not require heating the feed stream until boiling occurs. Theoretically, complete rejection of non-volatile compounds occurs in MD because only water vapor passes through the unwetted membrane. Additionally, the low temperature requirements of MD allow for economic coupling to waste heat or solar energy. Through a combination of high separation efficiency and low operating temperatures and pressures, MD may provide a competitive option for water desalination and treatment.[2-6] MD is also attractive for dehydration of foods and beverages, where low processing temperatures may preserve flavor and avoid denaturation.

In all liquid-based membrane separations, and especially in MD, fouling control requires constant attention. Membranes for DCMD must be hydrophobic to adequately separate the aqueous feed and permeate streams and allow only vapor transport through the pores. The buildup of amphiphilic foulants within MD membranes leads to progressive wetting of pores and a crippling drop in solute rejection.[7,8] Several groups explored delaying humic acid fouling of microporous membranes through increasing the hydrophilicity of the membrane.[9-13] However, such treatments are incompatible with the need for hydrophobic membranes in MD. One previous study explored the addition of an oil- and water-repellant fluorocarbon polymer emulsion to poly(vinylidine difluoride) (PVDF) polyester composite membranes and found improved humic acid fouling resistance. Unfortunately, the water vapor flux values (0.08 g/m^2s) were too low for practical application.[14]

Fouling is an especially difficult challenge in food and beverage dehydration with MD. Despite the many studies on potential MD applications in food production,[15-19] only a few of these looked at dairy processes within the last decade, presumably because of fouling challenges.[20-22] For example, application of MD to dehydration of whey solutions will only be practical with improved resistance to fouling by the feed solution fats and amphiphilic whey proteins. The food and beverage industry formerly considered whey a waste product of cheese production, but now it is a common food additive and even contributes to ethanol production through lactose fermentation.[21] The recovery of whey proteins traditionally includes

concentration of dissolved solids to the osmotic limit using ultrafiltration, diafiltration to remove dissolved sugars and salts, and thermal evaporation and spray drying to reach a final whey protein product.[20] The development of a membrane coating that resists whey solution fouling could expand applications of MD in the dairy industry.

We hypothesize that superhydrophobic films on surfaces[23] and membranes[24] may afford some fouling resistance due to increased liquid slip[25-27] and decreased contact area with the membrane. Liquid slip increases due to air plastrons retained within the rough features of the coating (Figure 3.1). The air plastrons also reduce the membrane surface area available for foulant deposition.

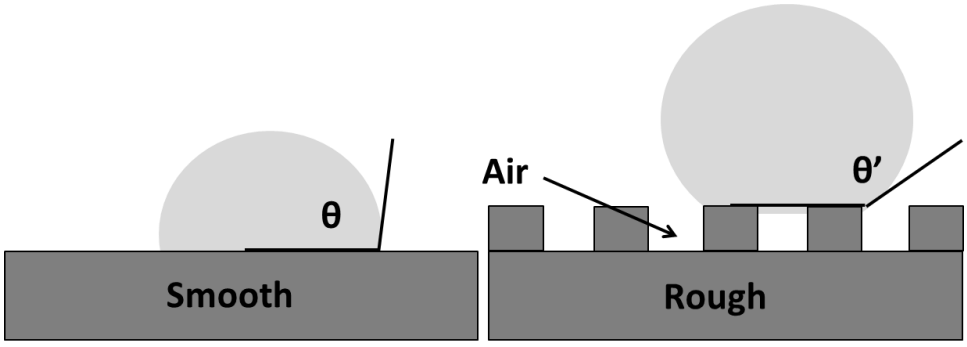

Figure 3.1: Illustration showing the increase of apparent water contact angle on a rough surface due to the presence of trapped air.

This chapter describes the application of rough PP films as superhydrophobic, fouling-reducing coatings on microporous PVDF membranes. We explore the effect of the thin porous PP coating on vapor flux and salt rejection during DCMD of a model humic acid fouling feed

solution and a dairy whey solution. The porous PP coatings demonstrate improved fouling resistance as they provide on average (n=3) >99% salt rejection after 20 hours of operation for humic acid solutions compared to untreated membranes which only reject 95% on average (n=5). These coatings also help prevent pore wetting by whey solutions. During whey filtration, the time required for fouling-induced pore wetting and salt breakthrough increases by an order of magnitude when using membranes coated with PP.

3.2 Experimental

3.2.1 Materials

Isotactic PP pellets (Mw=190,000 Mn=50,000), humic acid sodium salt, and calcium chloride dihydrate (99%) were obtained from Sigma-Aldrich. Sodium chloride (99%), hydrochloric acid (38%), and methylethylketone (MEK) (99%) were purchased from Columbus Chemical Industries, and p-xylene (99.6%) was obtained from Fisher Scientific. These reagents were used as received. Whey solution was obtained after removing casein from store-bought whole milk using dilute citric acid and calf rennet. Whey was filtered through Whatman #1 filter paper to remove suspended solids prior to use. HVHP PVDF membranes (25 mm diameter, 0.45 µm nominal pore size) were purchased from Millipore (#HVHP02500), and 25 mm diameter 0.2 µm nominal pore size anodized alumina membranes were obtained from Whatman (#6809-6022). Deionized water (Milli-Q purification system, 18.2 MΩ·cm) was used for rinsing the membranes and preparation of the fouling and permeate solutions. The pH of the humic acid solutions was adjusted with 1 N HCl.

3.2.2 Deposition of crystalline polypropylene films

Deposition of superhydrophobic PP films was based on literature procedures.[23,24,28] Isotactic PP (72 mg) was added to 4 mL of stirred p-xylene in a 25 mL round bottom flask. The flask was heated to 130 °C to dissolve the PP. Once the solution was homogeneous, 1.6 mL of warm MEK was added as a porogen. The MEK non-solvent induces PP crystal nucleation while also creating voids that lead to pores in cured films. Enough of the PP dispersion to evenly coat the membrane surface (~0.4 mL) was then deposited onto flat sheet membranes before spinning at 400 rpm for 30 s to remove excess solution. After the coating was deposited on the surface of the membrane, an ethanol rinse using approximately 10 mL sprayed from a wash bottle was sometimes used to remove excess PP from the membrane surface to create a thinner film. Finally, the deposited PP films were cured in a vacuum oven at 70 °C and 1 bar vacuum for 3 hours before further use.

3.2.3 Membrane characterization

Both treated and bare membranes were characterized by their liquid entry pressure as well as their apparent water contact angle. To assess the liquid entry pressures, each membrane was placed atop a porous stainless steel frit serving as a mechanical support within a modified Amicon 25 mm cell. The base of the Amicon cell was hollowed out to allow incorporation of a stainless steel frit to support the polymeric membrane under pressure. The cells were filled with water, and the pressure above the membranes was slowly increased until

water permeation was observed. Contact angles were determined with deionized water and a FTA200 Dynamic Contact Angle Analyzer system using an advancing droplet rate of 0.1 mL/min. SEM images of membranes before and after modification were obtained using a Hitachi S-4700 II field-emission scanning electron microscope (SEM) operated at an accelerating voltage of 15 keV. Deposition of 8 nm of sputtered gold rendered the samples conductive for imaging. Due to difficulties in obtaining a fracture suitable for cross-sectional imaging of PVDF membranes, PP coatings were also applied to alumina membranes that fracture with retention of pores. The film morphology is visually similar on PVDF and alumina membranes based on SEM images.

3.2.4 DCMD

Membranes were placed in a custom built holder that allows cross flow of both feed and permeate streams (Figure 3.2). The feed model for a brackish fouling solution contained 100 mg/L humic acid, 0.1 M NaCl, and 3.8 mM Ca^{2+} at pH 4. Previous studies showed that this solution rapidly fouls polymeric polyamide nanofiltration and PVDF MD membranes.[9,10,13] Calcium ions complex with humic molecules to cause aggregation that favors deposition on membrane surfaces. Additionally, the pKa of the carboxylic groups in humic acids is around 4, so the low feed pH reduces the humic acid charge state to increase fouling rates. The feed solution (2 L for humic acid, 500 mL for whey) was placed in a stainless steel tank and circulated through heat exchange coils within a warm water bath set to 70 °C (humic) or 50 °C (whey) for MD (Figure 3.3). The permeate reservoir, which initially contained distilled water (200 mL), was

placed on an analytical balance that was connected to a lab PC via LabView to record the increase in mass due to condensation of vapor flux through the membrane. The permeate solution was pumped through a chiller to cool the stream to 10 °C prior to passing over the membrane support and returning to the reservoir. Both the feed and permeate streams were recycled through their respective flow loops for at least one hour at approximately 30 mL/min prior to introduction to the membrane to ensure accurate temperature control. The temperatures of feed solutions entering and exiting the membrane were measured and found to differ by only 3 °C on average with a feed temperature of 70 °C.

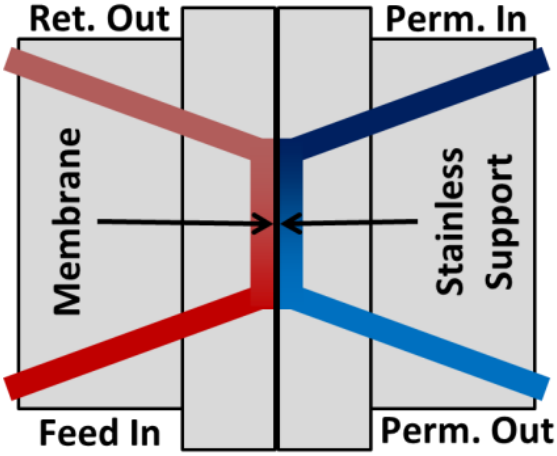

Figure 3.2: Cross-sectional diagram of the custom-built crossflow membrane holder. The membrane is sandwiched between the two halves of the holder and sits on a porous stainless steel frit that provides mechanical support. Warm feed solution enters the cell and travels across the skin of the membrane before exiting the module as retentate returning to the feed reservoir. Likewise, the cool permeate stream enters the other half of the module, passes along the stainless steel frit, and exits the module.

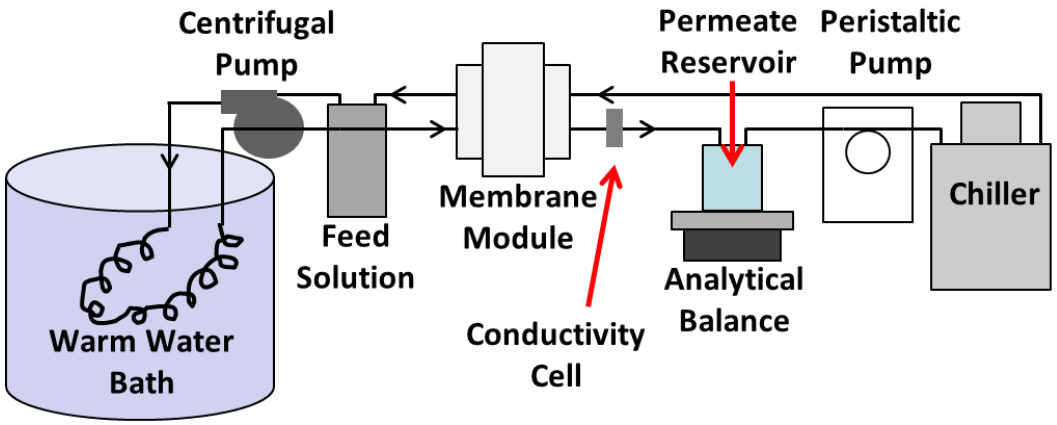

Figure 3.3: Diagram of the DCMD apparatus. Both feed and permeate streams pass through heat-exchange coils to achieve their desired temperatures prior to entry into the membrane module. The feed retentate is recycled to the feed reservoir, while water vapor diffuses through the membrane and condenses in the permeate stream. The analytical balance monitors increases in the mass in the permeate reservoir.

A home-built inline flow-through conductivity cell was also incorporated in the permeate stream immediately after the membrane module to monitor increases in conductivity due to solute passage using an Orion Model 115A+ conductivity meter. Real-time inline monitoring allows us to observe changes in conductivity with time to monitor membrane salt rejection. At the start of each trial, the permeate solution conductivity was negligible (< 5 µS/cm). Extracted feed samples from before and after MD were also analyzed through dilution of 1 mL aliquots with 6 mL of distilled water before vortex mixing. Conductivity values were measured in triplicate for each sample. To account for the nonzero permeate volume at the beginning of the DCMD experiments, a dilution factor (d) was calculated by dividing the initial volume of water by the volume of water which passed through the membrane during the trial. Utilizing the change in conductivity of the permeate solution from before and after each

distillation trial (ΔC_P), the conductivity of the feed solution (C_F) samples, and α, the rejection was calculated from the equation 3.1.

$$R = 1 - \left(\frac{\Delta C_P * \alpha}{C_F}\right) \quad (3.1)$$

3.3 Results and discussion

3.3.1 Membrane modification with polypropylene films

Deposition of PP films on 0.45 µm PVDF membranes causes no visually apparent changes. However, SEM images obtained before (Figure 3.4 A) and after modification (Figure 3.4 B,C) show the presence of PP in a beads-on-a-string morphology. For thicker films deposited without the ethanol rinse step (Figure 3.4 B), surface porosity decreases and the PP layer retains only minimal roughness. However, the films deposited with the ethanol rinse step (Figure 3.4 C) show minimally reduced porosity and high PP roughness, which should provide relatively open pores that can trap air plastrons. Films prepared without an ethanol rinse have a heterogeneous average thickness of 4.8 ± 1.8 µm with many peaks and valleys (Figure 3.5 A). Incorporation of the ethanol rinse reduced the average thickness to 1.8 ± 0.4 µm and improved homogeneity (Figure 3.5 B). Thinner, more uniform films are desirable to reduce fouling without greatly increasing mass-transport resistance in MD. All DCMD experiments with PP-modified membranes employed coatings prepared with the ethanol rinse step to minimize the reduction in flux due to the coating.

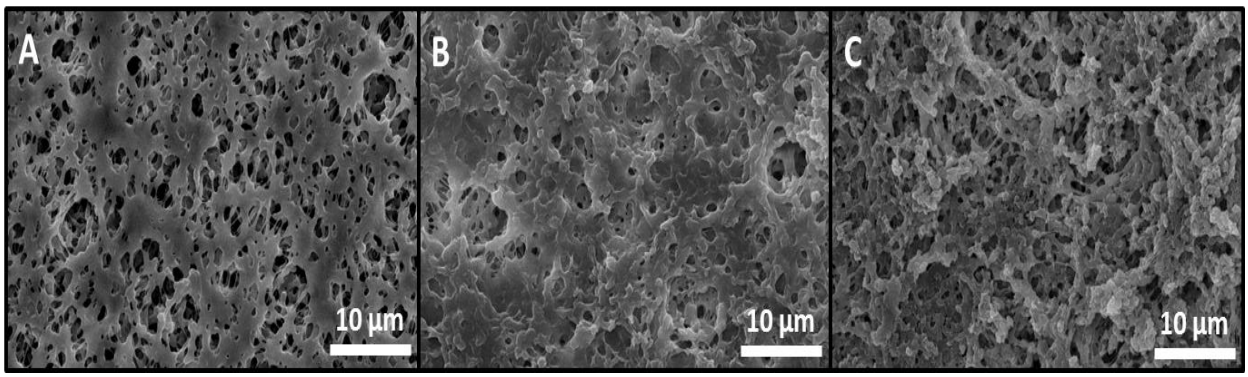

Figure 3.4: SEM images of 0.45 µm PVDF membranes before (A) and after (B,C) modification with porous PP. For the membrane in image (C), the coating was rinsed with ethanol prior to heating in vacuum.

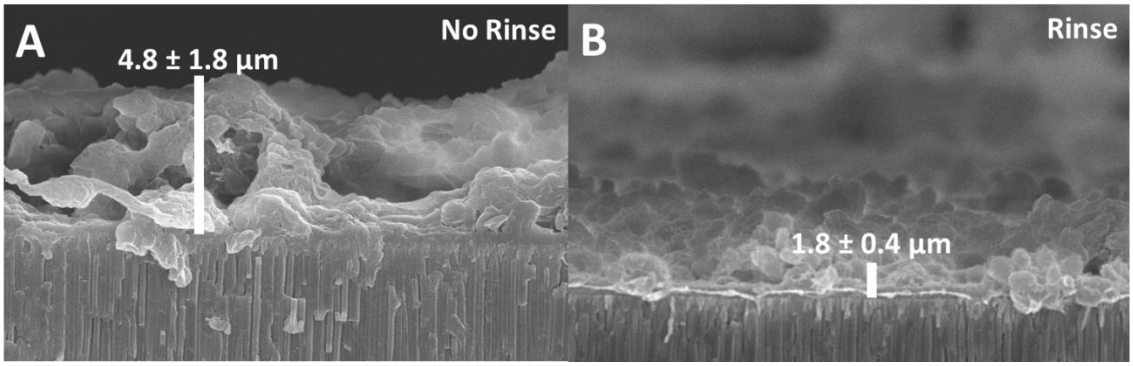

Figure 3.5: SEM images of cross-sections of 0.2 µm alumina membranes that were modified with thick or thin PP films. Image A shows the thick PP coating, which was prepared without an ethanol rinse, and image B shows the PP coating whose deposition included ethanol rinsing.

The advancing water contact angle increases from 124 ± 1° on the bare PVDF membranes to 154 ± 1° and 157 ± 3° for membranes coated with the thick and thin PP films, respectively. The increased roughness imparted by the film allows air entrapment at the surface to decrease the polymer-water contact area and increase contact angles. The liquid entry pressure of bare HVHP membranes was around 1.1 bar in accordance with previous studies.[29,30]

Addition of either the thin or thick PP coating increases the liquid entry pressure to ~2 bar. Equation 3.2 gives the theoretical expression for liquid entry pressure, ΔP, where γ is the surface tension of an air-water interface (72.8 mN/m at 25 °C), θ is the water contact angle with the membrane, and r is the membrane pore radius.

$$\Delta P = \frac{2\gamma \cos\theta}{r} \quad (3.2)$$

Based on this equation, an increase in contact angle from 120° to 160° without altering pore radius causes a nearly two-fold increase in the wetting pressure. The SEM images in Figure 3.4 suggest that pore size is approximately the same in coated and bare membranes, thus the two-fold increase in wetting pressure is consistent with contact angles and SEM images.

3.3.2 Humic acid DCMD

3.3.2.1 Bare PVDF membranes

Control experiments with PVDF membranes provide a baseline for examining whether PP-coated membranes increase fouling resistance. During filtration of feed solutions containing humic acid through bare membranes, increases in conductivity demonstrate substantial feed solution breakthrough within 200 minutes of operation (Figure 3.6 B) for two membranes. The buildup of hydrophilic humic acid deposits on the membrane likely allows progressive entrance of the feed solution into the pores and causes decreased solute rejection. In three other identical bare membranes tested, limited salt passage occurred (99.94 ± 0.05% average

rejection) but flux declined 31 ± 18% over 20 hours due to pore coverage by dissolved humic components. The differences in humic acid interactions with the bare membrane surface likely arise from the high complexity and compositional variability of humic acid.[31] Despite using a standard humic acid powder (Sigma-Aldrich), differences in humic solutions were visible and probably lead to the variable effects humic acid fouling on bare membranes. Nevertheless, both salt passage and flux decline are undesirable effects of fouling. For all five bare membranes, the average flux before breakthrough (as suggested by permeate conductivity increase) was 8.7 ± 0.9 g/m^2s, and the overall average rejection was 95.5 ± 6.3% based on conductivity measurements at the end of each distillation. The untreated, hydrophobic surface of PVDF provided a favorable location for foulant adsorption, which lead to rapid membrane failure by pore wetting (in the two membranes where breakthrough occurred) or cake layer formation. The initial flux was ~15% less than that through the same membrane with distilled water as the feed (~10 g/m^2s). The ~15% decrease is much greater than the < 1% that Raoult's Law would predict in reduced vapor pressure from salt addition. The extra flux decline likely arises from concentration polarization at the membrane surface. This concentration polarization not only will reduce the vapor pressure of water locally at the membrane surface, but may also lead to initial rapid fouling of the membrane skin to reduce mass transport.

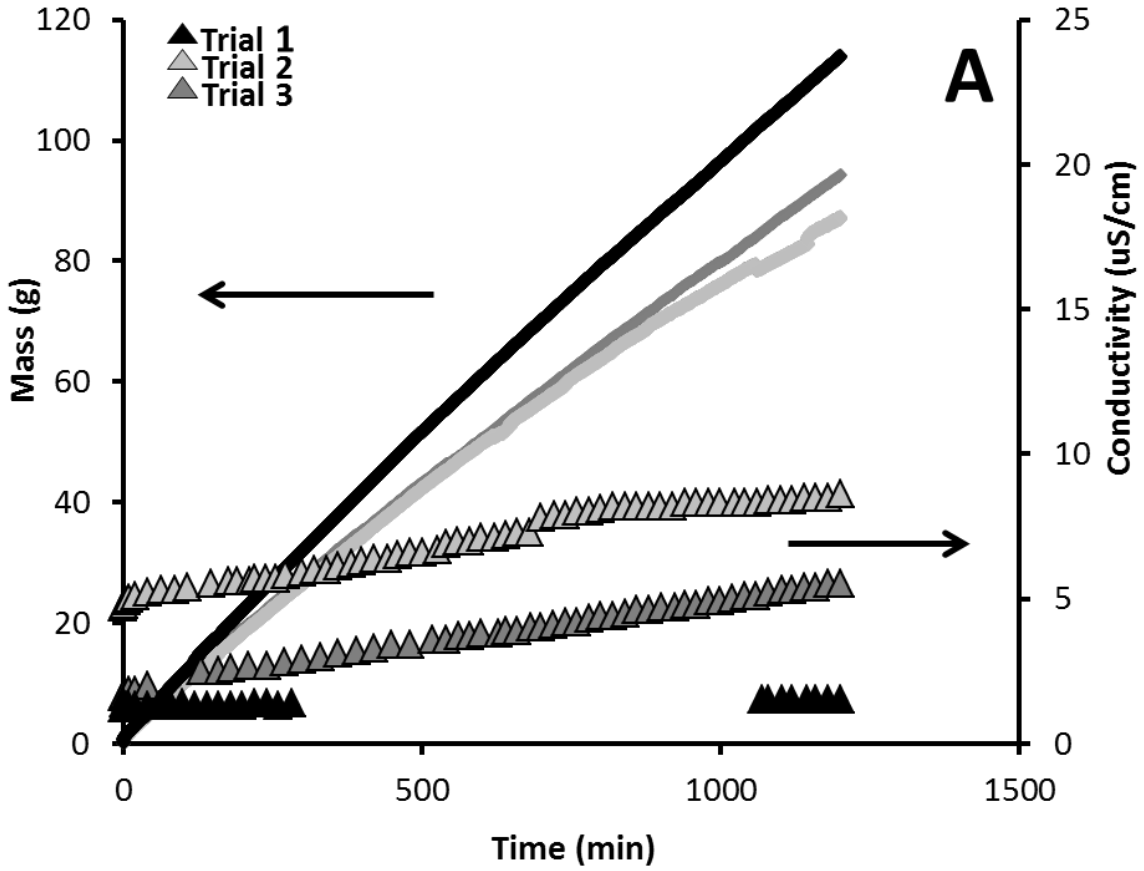

Figure 3.6: Change in permeate mass (lines) and conductivity (triangles) over time during DCMD of humic acid solutions through five bare PVDF membranes. (A) For three membranes, flux declines 31 ± 18% over 20 hours but salt rejection remains at 99.94 ±0.05%. (B) Two other membranes show significant increases in permeate conductivity after an initially stable region. The conductivity spike in (B) suggests entrance of the solution into some membranes pores within about 200 min of operation. The breakthrough leads to an overall 88.9 ± 2.0% salt rejection and negligible flux decline.

Figure 3.6 (cont'd)

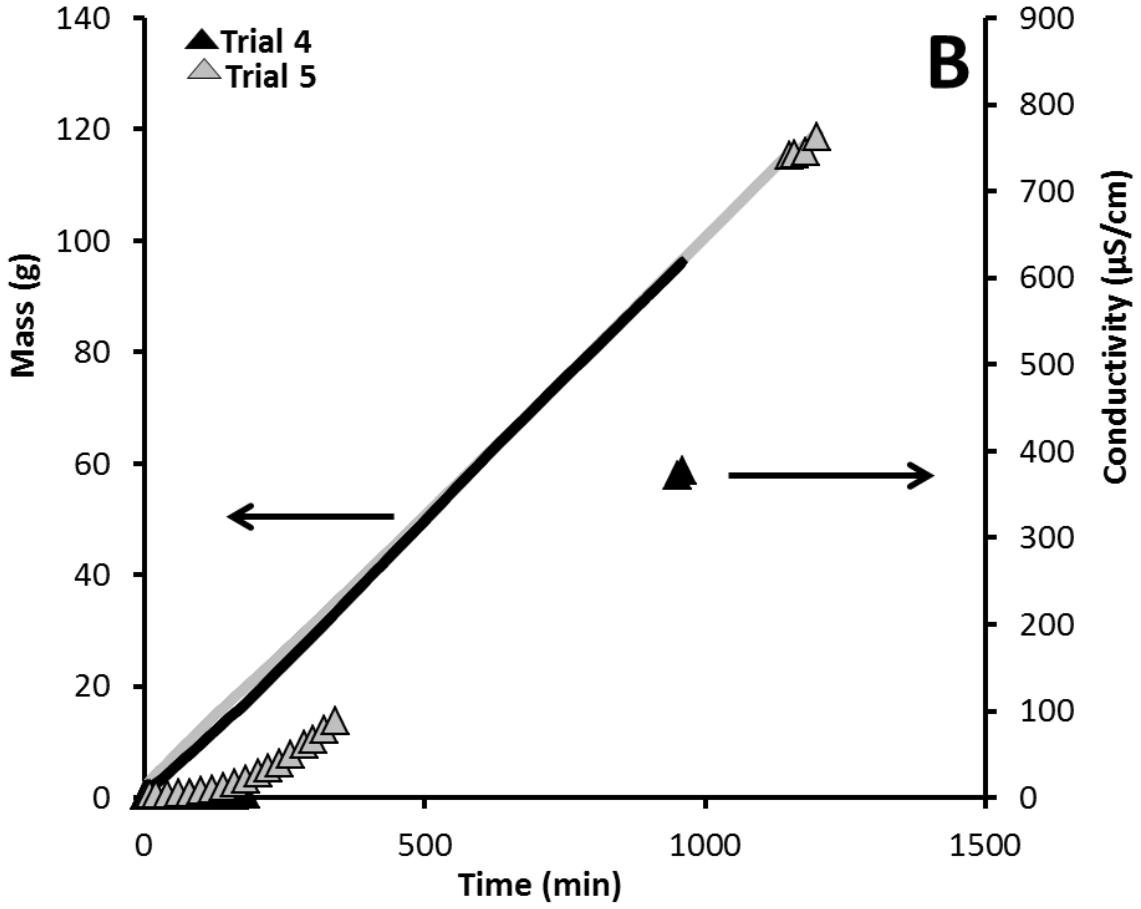

3.3.2.2 Membranes with thin PP coatings

We hypothesized that thin, porous PP coatings will resist fouling due to their superhydrophobicity (trapped air plastrons) without greatly decreasing flux relative to an untreated membrane. As Figure 3.7 shows, treated membranes showed essentially no increase in permeate conductivity for 20 h of filtration of a humic acid solution. The average flux over the first 100 minutes was 4.9 ± 1.8 g/m^{2}s, and the overall salt rejection based on conductivity measurements was 99.9 ± 0.01%. The slightly elevated (but constant) conductivity values in the

trial 3 resulted from traces of salt in the permeate solution at the start this experiment. Relative to bare membranes, the flux was ~45% lower for membranes with thin PP coatings, presumably due to blockage of PVDF membrane pores during PP film deposition. While lower flux is undesirable, the stable salt rejection and wetting resistance over 20 hours make PP-coated membranes attractive for MD with highly fouling solutions. Further reductions in the PP film thickness through increasing the rotation rate during spin coating may provide similar rejection while reducing the flux lost to modification.

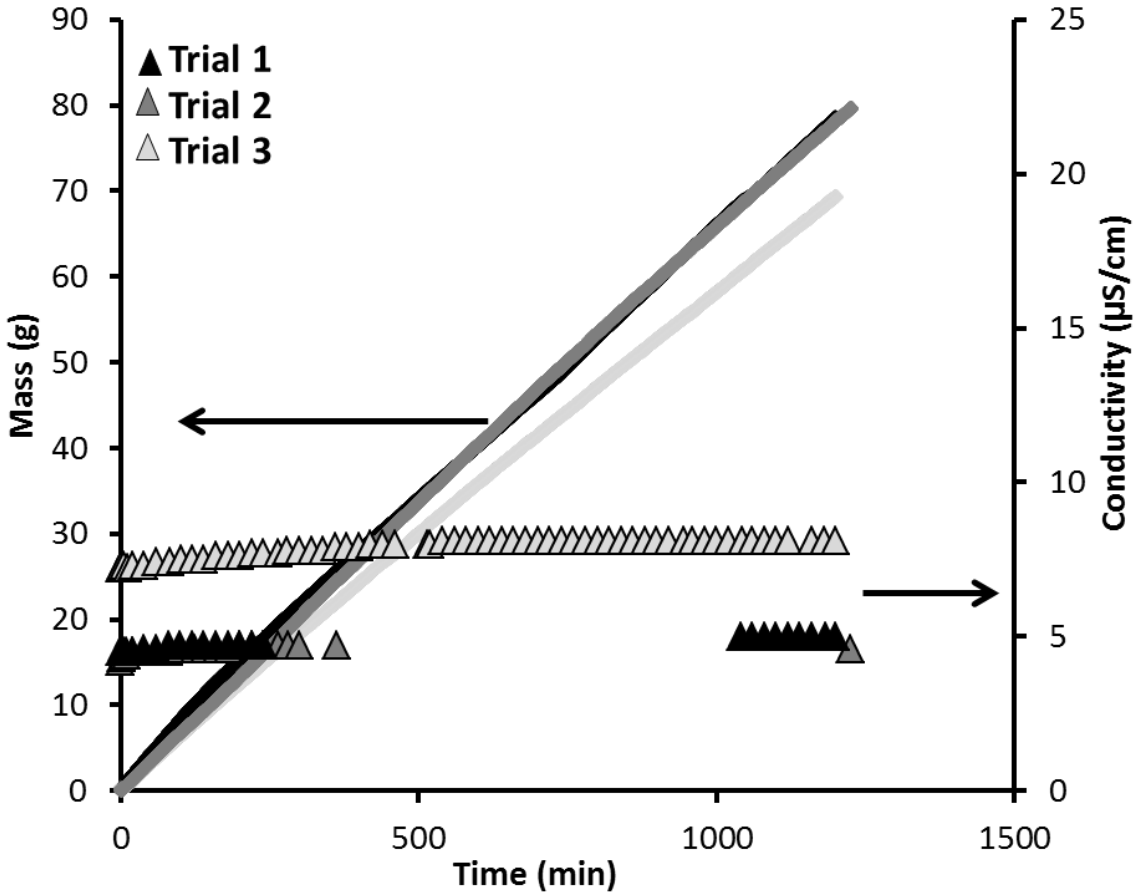

Figure 3.7: Change in permeate mass (lines) and conductivity (triangles) over time during DCMD of humic acid solutions through 3 PVDF membranes with thin PP coatings. The constant conductivity values indicate 99.9% salt rejection at a flux 45% lower than that through an untreated membrane.

3.3.3 Whey DCMD

3.3.3.1 Bare PVDF membranes

As with studies of humic acid fouling, in DCMD with whey solutions we first assessed the fouling properties of bare PVDF membranes. In whey solutions, these membranes demonstrated little resistance to fouling (Figure 3.8). Within 200 min, permeates from all three tested membranes showed increases in conductivity and mass flux through the membranes declined significantly. In fact, Figure 3.8 shows mass flux from the permeate to the feed after times as short as 150 min for two of the trials. Most likely, the pores wetted due to fouling and allowed osmotic water transport from the permeate to the feed. The eventual recovery of positive mass flux in the second membrane likely resulted from a decrease in osmotic pressure with time and thermally induced water transport from feed to permeate. In the case of a third membrane, osmotic flow mass flux always flowed from feed to permeate, but the permeate conductivity increased rapidly. Overall, bare membranes showed an average initial flux of 2.8 ± 0.8 g/m^2s for the first 100 minutes, but salt rejections cannot be calculated for the first two trials due to the presumed presence of both MD and osmotic flow preventing us from establishing a realistic dilution factor. However, the third trial showed only a ~40% salt rejection which is likely in line with the true value for the first two trials. Nonetheless, the bare membranes are clearly unsuitable for DCMD of whey solutions under the tested conditions. Visual inspection of bare membranes after whey MD revealed pore wetting from fats or proteins (Figure 3.9).

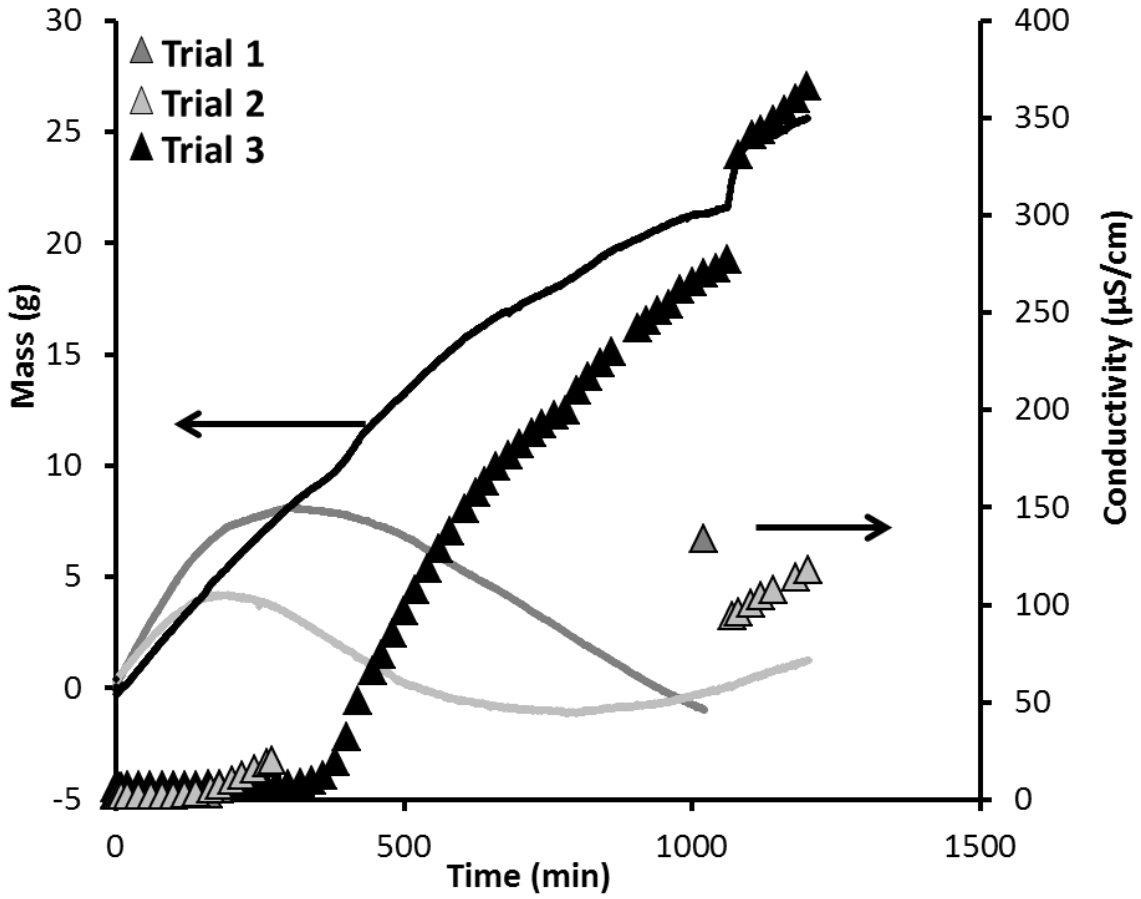

Figure 3.8: Change in permeate mass (lines) and conductivity (triangles) over time during whey DCMD through 3 bare PVDF membranes. All membranes show an increase in permeate conductivity within the first 400 min, suggesting pore wetting. The reversal of mass flow in two of the trials likely results from osmotic flow from permeate to feed through wetted pores.

Figure 3.9: Untreated PVDF membrane (feed surface) after DCMD of whey solution.

3.3.3.2 Membranes with thin PP coatings

Contrary to observations with bare PVDF membranes, DCMD of whey solutions using four membranes coated with thin PP films shows only minimal salt breakthrough over 20 hours (Figure 3.10). The average initial flux (100 minutes) was 2.5 ± 0.5 g/m^{2}s, and the average rejection over the entire experiment was 96.5 ± 4.6%. For two trials, the permeate conductivity increased negligibly (<3 µS/cm) over time, suggesting negligible pore wetting. Moreover, the flux through these membranes declined <55% over the 20-h filtration. In contrast, with two other replicate trials, significant surface fouling from whey components lead to a drastic (~ 99%) decline in flux. However, unlike bare membranes, despite the high amount of whey fouling, conductivity increased only mildly (<30 µS/cm). Additionally, the presence of the antifouling PP layer may allow for easier cleaning of adsorbed whey components to restore flux values. The initial flux is only 10% less than that through the untreated membrane, and the resistance to fouling and pore wetting over 20 h will allow for removal of more than an order of magnitude more water than DCMD with the bare membranes. Examination of the membrane feed surface after DCMD showed minimal signs of pore wetting, further supporting the notion that only a small amount of pores leaked during the trial (Figure 3.11). The improved whey fouling resistance to pore wetting provided by the PP coating may allow for further membrane use in the dairy industry for whey concentration. Nevertheless, the variable membrane performance observed through the four trials in this study likely demonstrates the need to improve whey pretreatment procedures to reduce deviation in the whey solution composition.

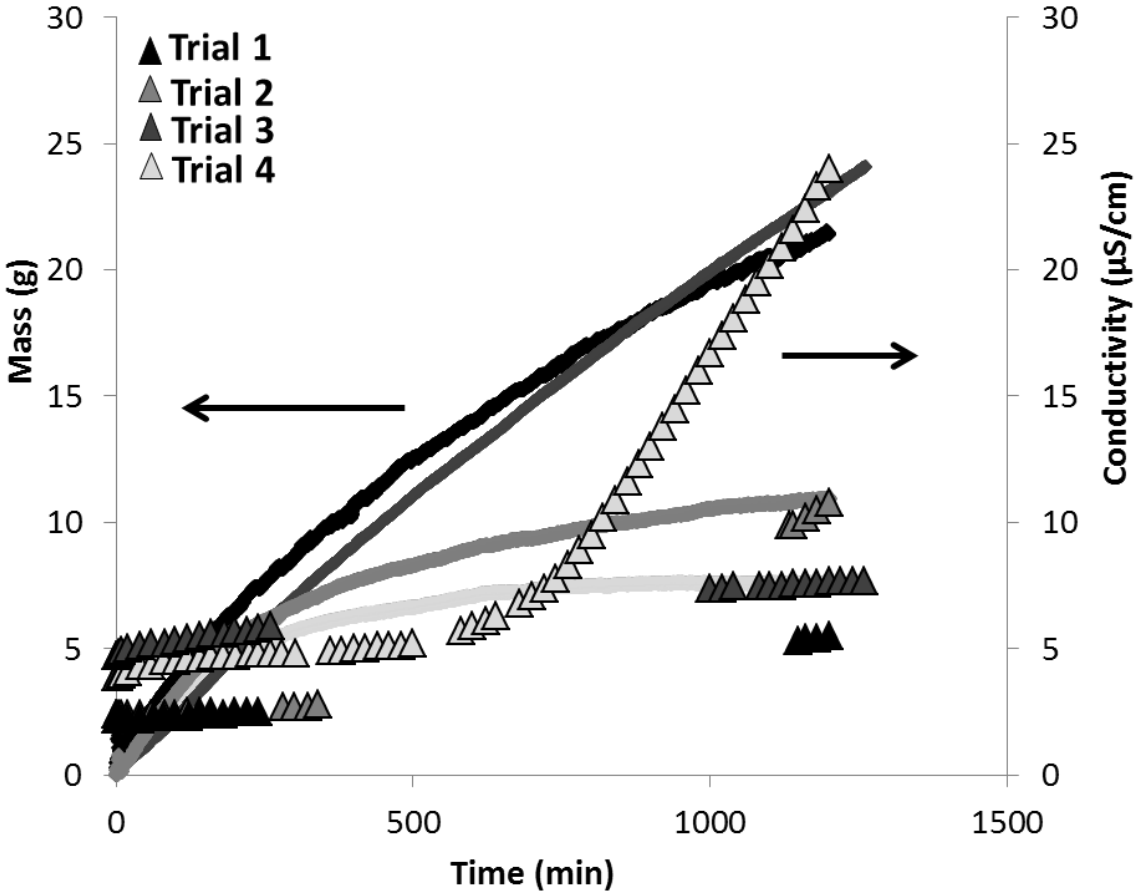

Figure 3.10: Change in permeate mass (lines) and conductivity (triangles) over time during DCMD of whey solutions through 4 PVDF membranes with thin PP coatings. High rejection (> 95%) results in all four trials with an initial flux (100 minutes) only 10% lower than through an untreated membrane.

Figure 3.11: PP coated PVDF membrane (feed surface) after DCMD of whey solution.

3.4 Conclusions

Deposition of porous PP coatings on PVDF membranes improves fouling resistance to avoid pore wetting during DCMD of humic acid and whey solutions. Both whey and humic acid solutions caused severe fouling of most untreated PVDF membranes within the first several hours of DCMD. Treated membranes resisted fouling to provide stable rejections for at least 20 hours. Due to fouling susceptibility, in two out of 5 cases bare membranes rejected only 88.9 ± 2.0% of feed salts from humic acid solutions and were unstable in whey solutions. Coating membranes with PP exhibited salt rejections of 99.9 ± 0.01% and 96.5 ± 4.6% for humic acid and whey solutions.

PP-treated membranes allowed fluxes 10-45% lower than those through bare membranes, presumably due to the additional mass transport resistance of the PP layer. While the PP coatings generally produce porous films with large (0.5-5 μm) pore diameters, the film morphology is spongy and likely blocks some PVDF membrane pores. Further optimization of PP deposition conditions may reduce the flux decline from coatings, but some decline will always occur. Even with the small flux decline, however, the greatly improved membrane performance in extreme environments makes these membranes attractive for some MD applications.

REFERENCES

REFERENCES

(1) Younos, T.; Tulou, K. E. *Journal of Contemporary Water Research and Education* **2005**, *132*, 10.

(2) Alkhudhiri, A.; Darwish, N.; Hilal, N. *Desalination* **2012**, *287*, 2.

(3) Pangarkar, B. L.; Sane, M. G.; Guddad, M. *ISRN Materials Science* **2011**, *2011*, 1.

(4) El-Bourawi, M. S.; Ding, Z.; Ma, R.; Khayet, M. *Journal of Membrane Science* **2006**, *285*, 4.

(5) Curcio, E.; Drioli, E. *Separation & Purification Reviews* **2005**, *34*, 35.

(6) Lawson, K. W.; Lloyd, D. R. *Journal of Membrane Science* **1997**, *124*, 1.

(7) Gryta, M. *Separation Science and Technology* **1996**, *41*, 1789.

(8) Tun, C. M.; Fane, A. G.; Matheickal, J. T.; Sheikholeslami, R. *Journal of Membrane Science* **2005**, *257*, 144.

(9) Hong, S.; Elimelech, M. *Journal of Membrane Science* **1997**, *132*, 159.

(10) Asatekin, A.; Kang, S.; Elimelech, M.; Mayes, A. M. *Journal of Membrane Science* **2007**, *298*, 136.

(11) Hamid, N. A. A.; Ismail, A. F.; Matsuura, T.; Zularisam, A. W.; Lau, W. J.; Yuliwati, E.; Abdullah, M. S. *Desalination* **2011**, *273*, 85.

(12) Abuhabib, A. A.; Mohammad, A. W.; Hilal, N.; Rahman, R. A.; Shafie, A. H. *Desalination* **2012**, *295*, 16.

(13) Srisurichan, S.; Jiraratananon, R.; Fane, A. *Journal of Membrane Science* **2006**, *277*, 186.

(14) Huo, R.; Gu, Z.; Zuo, K.; Zhao, G. *Journal of Applied Polymer Science* **2010**, n/a.

(15) Gunko, S.; Verbych, S.; Bryk, M.; Hilal, N. *Desalination* **2006**, *190*, 117.

(16) Madaeni, S. S.; Sasanihoma, A.; Zereshki, S. *Journal of Food Process Engineering* **2011**, *34*, 1535.

(17) Onsekizoglu, P.; Bahceci, K. S.; Acar, M. J. *Journal of Membrane Science* **2010**, *352*, 160.

(18) Bélafi-Bakó, K.; Koroknai, B. *Journal of Membrane Science* **2006**, *269*, 187.

(19) Cojocaru, C.; Khayet, M. *Separation and Purification Technology* **2011**, *81*, 12.

(20) Christensen, K.; Andresen, R.; Tandskov, I.; Norddahl, B.; du Preez, J. H. *Desalination* **2006**, *200*, 523.

(21) Tomaszewska, M.; Białończyk, L. *Desalination and Water Treatment* **2013**, *51*, 2362.

(22) Hausmann, A.; Sanciolo, P.; Vasiljevic, T.; Ponnampalam, E.; Quispe-Chavez, N.; Weeks, M.; Duke, M. *Membranes* **2011**, *1*, 48.

(23) Erbil, H. Y.; Demirel, A. L.; Avci, Y.; Mert, O. *Science* **2003**, *299*, 1377.

(24) Franco, J. A.; Kentish, S. E.; Perera, J. M.; Stevens, G. W. *Journal of Membrane Science* **2008**, *318*, 107.

(25) Aljallis, E.; Sarshar, M. A.; Datla, R.; Sikka, V.; Jones, A.; Choi, C.-H. *Physics of Fluids* **2013**, *25*, 025103/1.

(26) Lee, D. J.; Cho, K. Y.; Jang, S.; Song, Y. S.; Youn, J. R. *Langmuir* **2012**, *28*, 10488.

(27) McHale, G.; Newton, M. I.; Shirtcliffe, N. J. *Soft Matter* **2010**, *6*, 714.

(28) Lv, Y.; Yu, X.; Jia, J.; Tu, S.-T.; Yan, J.; Dahlquist, E. *Applied Energy* **2012**, *90*, 167.

(29) Khayet, M.; Matsuura, T. *Membrane Distillation: Principles and Applications*; Elsevier: Amsterdam, 2011.

(30) García-Payo, M. C.; Izquierdo-Gil, M. A.; Fernández-Pineda, C. *Journal of Colloid and Interface Science* **2000**, *230*, 420.

(31) Hayes, M. H. B.; Clapp, C. E. *Soil Science* **2001**, *166*, 723.

Chapter 4: Preliminary investigation of anionic polyelectrolyte multilayer films as coatings that resist fouling by negatively charged oil drops in oil-in-water emulsions

4.1 Introduction

Rising global energy demands are spawning new methods to extract previously unavailable natural resources. In particular, hydraulic fracturing is one of the most significant developments in energy production over the last 15 years. As discussed in Chapter 1, when coupled with horizontal drilling practices, hydraulic fracturing greatly improves oil and natural gas recovery from difficult formations.[1] However, hydraulic fracturing employs large quantities of water to crack rock formations and release oil. In fact, in 2007 88% of all liquid volumes collected at wells within the United States consisted of contaminated water, known as produced water. Additionally, the ratio of oil recovered to produced water declines with well age to such an extent that produced water increases up to 98% of all the collected volume near the end of a well's life.[2]

Although current industry practices include reusing recovered produced water to continue extracting oil, eventually the water accumulates too much contamination for further use. Some companies choose to pump the highly contaminated water back underground into non-producing formations for storage, but the potential risk for environmental contamination is high.[2] Hence, other companies attempt to decontaminate produced water through a complex multistep process to reduce possible environmental impacts. Generally, produced water

treatment first combines physical, chemical, and biological methods to de-oil the water before removing soluble organics and disinfecting. Subsequent treatment steps include removal of suspended solids, release of dissolved gasses, and finally desalination and water softening to remove excess salts and produce a water stream suitable for irrigation of crops, dust control, vehicle washing, power plant makeup water, and fire control systems.[3,4]

Current United States regulations govern the maximum offshore discharge of oil and grease at a daily maximum of 42 mg/L and a monthly average of less than 30 mg/L. Onshore regulations generally prohibit produced water discharge unless for direct agricultural or wildlife use with oil and grease levels below 35 mg/L and low salinity.[5] Regulations do not govern the salinity of offshore produced water discharge into the seas. Unfortunately, coagulation, flocculation, air flotation, gravity separation, and other common municipal water treatment procedures do not meet these discharge limits for produced water.[6] Membranes have emerged as an attractive treatment option in a number of studies[7-10] because they produce high quality water and require minimal space.[11] However, direct membrane exposure to produced water generally causes rapid flux declines due to surface and pore fouling by rejected oil and grease components. Furthermore, despite the wide range of treatment options currently available, the removal of small (< 10 μm), well dispersed oil droplets remains limited.[4]

To reduce oil fouling of membranes, many groups explored new membrane coatings and formulations aimed to increase hydrophilicity.[2,10,12-14] Water adsorption resulting from

increased hydrophilicity restricts oil interactions with the wetted surface (Figure 4.1). The incorporation of polyethylene glycol polymer chains alone or among copolymer blends represents a common method to increase hydrophilicity. High chain density combined with film swelling upon exposure to water leads to the innate antifouling ability of polyethylene glycol.[15,16] In a less common method, Tuteja and coworkers reduced the surface energy on membranes through addition of fluorinated polyhedral oligomeric silsequioxane features combined with a unique surface reentrant geometry tailored to generate omniphobic surfaces by producing a metastable Cassie-Baxter state even for liquids with low surface tensions such as oils.[7,17,18] While increasing hydrophilicity may reduce membrane fouling in produced water treatment, unless pore sizes are small such membrane will still not reject small oil particles. Omniphobic membranes that allow water passage while preventing oil transport are attractive but current systems have limited throughput and only function under precisely controlled conditions (<0.07 bar feed pressure).

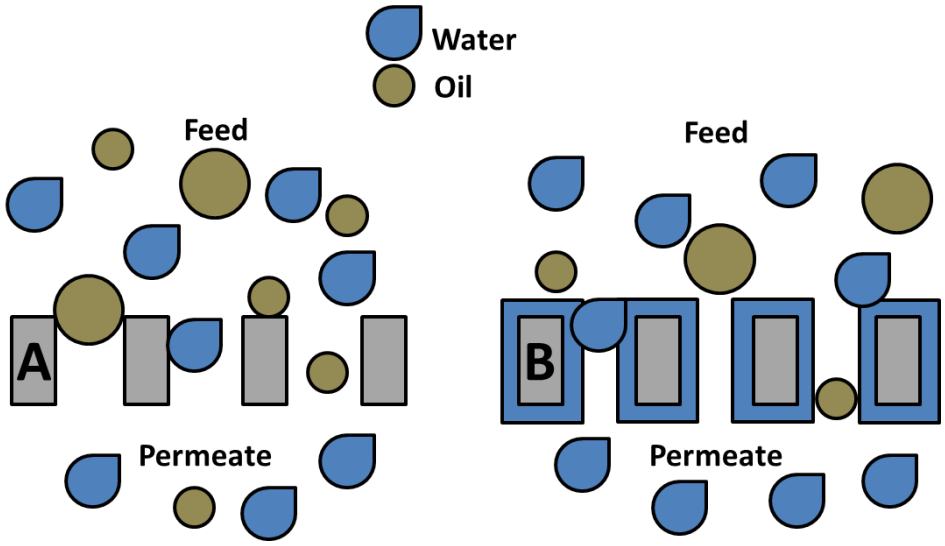

Figure 4.1: Membrane fouling without (A) and with (B) hydrophilic modifications.

Improved membrane filtration of oil-in-water emulsions will require a simple, cost effective surface modification or new membrane material. We propose exploiting the antifouling abilities of hydrophilic surfaces formed through adsorption of highly charged polyelectrolyte multilayers (PEMs). Counterintuitive to current procedures, we also propose the addition of either anionic or cationic surfactants to feed solutions. Naturally, the inclusion of surfactants will reduce the interfacial energy between oil and water to stabilize droplets and reduce coalescence. Traditionally, rejection of oil in membrane processes relies on size-based exclusion of oil droplets at the membrane surface, which leads to a local increase in oil concentration. As the droplets become more concentrated at the membrane surface, coalescence occurs and the average droplet size increases (Figure 4.2A). In our method, the surface charge of the PEM deposited on the membrane will match the charge of the surfactant used to stabilize the oil. The similar charge on droplets and the membrane surface should lead

to electrostatic repulsion of the droplets to help prevent them from reaching the membrane (Figure 4.2B). Furthermore, in contrast to traditional methods, oil droplets with diameters smaller than membrane pores may still undergo rejection due to electrostatic exclusion. We think the combination of this electrostatic rejection with the antifouling abilities of extremely hydrophilic surfaces will lead to coatings with superior performance for removal of oil from water during water polishing steps. This chapter focuses on the deposition of polyanion-terminated PEMs to rejection anionic emulsion droplets. Simultaneous work in our laboratory is examining polycation-terminated PEMs and cationic emulsions.

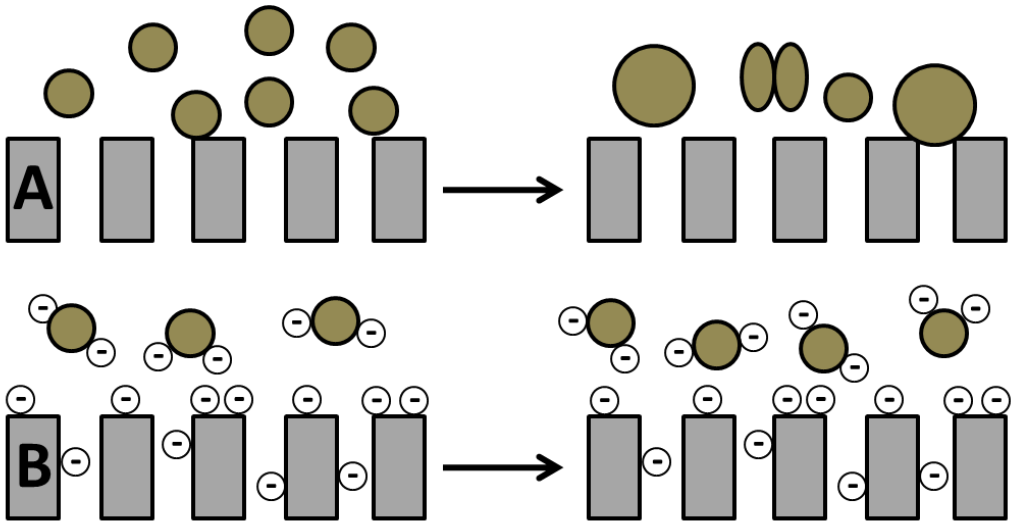

Figure 4.2: Oil-membrane interactions in traditional size exclusion (A) and the proposed electrostatic exclusion (B) systems.

4.2 Experimental

4.2.1 Materials

Poly(sodium 4-styrenesulfonate) (PSS, Mw = 70,000 Da), poly(allylamine hydrochloride) (PAH, Mw = 56,000 Da), hexadecane, cetrimonium bromide (CTAB), sodium dodecyl sulfate (SDS), and Triton X-100 (Triton) were used as received from Sigma-Aldrich. Sodium chloride (99%, CCI), manganese chloride dihydrate (Alfa Aesar), sodium bromide (Jade Scientific), dichloromethane (DCM, Mallinckrodt), decane (Alfa Aesar), phosphoric acid (JT Baker), and formaldehyde (CCI) were also used as received. Deionized water (Milli-Q purification system, 18.2 MΩ·cm) was used for rinsing the membranes and preparation of the polyelectrolyte solutions and oil-in-water emulsions. The pH values of the polyelectrolyte solutions were adjusted with dilute solutions of HCl and NaOH. Nylon microfiltration membranes with a nominal pore size of 5.0 µm and a diameter of 25 mm were obtained from GE Osmonics (#R50SP02500) and Sterlitech (#NY5025100). Nylon microfiltration membranes with a nominal pore size of 0.45 µm and a diameter of 25 mm were also obtained from Millipore (#HNWP02500).

4.2.2 Modification of nylon membranes

Nylon membranes were immersed in a solution containing phosphoric acid in a formalin solution (50 mL formaldehyde and 1 mL 85% phosphoric acid) at 60 °C to introduce hydroxyl and anionic surface groups.[19] During modification with PEMs, the membranes were

placed in a dead-end holder similar to an Amicon cell. First, a 10 mL solution containing 0.2 M PAH, 0.5 M NaBr at pH 2.3 was circulated through the membrane pores using a peristaltic pump at 3 mL/min for 5 minutes. Next the membrane was rinsed thoroughly with water at 5 mL/min to remove and unbound or weakly bound PAH. PSS adsorption then occurred during circulation of 10 mL of 0.2 M PSS, 0.5 M MnCl2 at pH 2.1 for two minutes at 3 mL/min followed by subsequent rinsing again at 5 mL/min. Additional bilayers were adsorbed in the same way to obtain films with 4, 6, or 8 PAH/PSS layers. Based on our prior work, polyelectrolyte supporting salts and deposition pH values were selected to produce charged surfaces.[20]

4.2.3 Membrane characterization

SEM images of nylon membranes before and after modification with 4, 6, or 8 PAH/PSS bilayers were obtained using a Hitachi S-4700 II field-emission scanning electron microscope. Deposition of 8 nm of sputtered gold using a Pelco SC-7 auto sputter coater rendered the samples conductive for imaging at 15 keV. Additionally, the water permeability of each membrane was tested at a range of pressures (0-1.4 bar) before and after LbL deposition to qualitatively observe polymer film growth.

4.2.4 Emulsion preparation

Three different emulsion solutions were prepared to produce droplets with cationic, anionic, or neutral charge, depending on the surfactant used to stabilize the droplets. In all

cases, a 10% (v/v) solution of hexadecane in 0.01 M NaCl was prepared with the appropriate surfactant at 5 mM. Hexadecane was first saturated with Oil-Red-O dye (Sigma-Aldrich) by adding several milligrams of dye to 50 mL of hexadecane until no more could be dissolved. To disperse the oil, each solution was sonicated using a Misonix ultrasonic liquid processor (3000 Series) with active sonication for a total of 2 minutes consisting of four 30 s periods at power level 8.0 separated by three 10 s periods without sonication. The droplet size distribution was determined with dynamic light scattering using a Malvern Mastersizer (Hydro 2000SM) to ensure that the majority of droplets were below 5.0 µm in diameter. Additionally, droplet charge was measured using a Brookhaven Instruments ZetaPals Electro Kinetic Analyzer system.

4.2.5 Electrostatic oil rejection from large pores

Wet membranes containing 0, 4, 6, or 8 polyelectrolyte bilayers were first placed inside a Kimwipe to remove excess surface moisture while still leaving the film hydrated. The membranes were then placed into a holder (similar to an Amicon cell) equipped with a suspended magnetic stir bar to ensure feed solution homogeneity. Emulsion solutions were shaken immediately prior to use just like before particle size determination to redistribute any settled of oil drops. One mL of the feed solution was removed and stored in a test tube for later analysis by gas chromatography (GC). Next, 5 mL of the oil emulsion was added to the stirred membrane holder. The pressure was then increased to 0.68 bar in a dead-end mode and the permeate was collected. Permeate collection continued for 10 minutes or until all the feed solution passed through the membrane. Any remaining solution in the membrane holder was

then collected and stored for GC analysis. After each dead-end filtration, membranes were rinsed with isopropanol (to remove any adsorbed oil films) followed by water. Furthermore, membranes were stored immersed in water to maintain hydration between trials. The same procedure was followed to assess the rejection of 20-fold diluted oil emulsions to determine whether oil concentration influenced droplet rejection.

Analysis of feed, permeate, and retentate aliquots included oil extraction and GC. One mL of each sample (feed, permeate, or retentate if present) was placed into a small test tube, and 10 drops of 1 M HCl were added to Triton- and SDS-stabilized emulsions. Due to the enhanced stability provided by charged surfactants, 1 mL of NaCl saturated brine was added to the SDS emulsions to break the emulsion through screening the surfactant charge. All solutions were then briefly (~10 s) vortex mixed to ensure incorporation of salt and acid throughout the sample. Next, 1 mL of DCM was added to each sample before vortex mixing an additional 30 seconds to extract hexadecane into the organic layer. The layers separated within 1 minute, and 0.5 mL of each DCM layer was removed and placed in a GC vial along with 10 µL of decane (internal standard). Samples were then analyzed with a Shimadzu GC-17a gas chromatograph using the parameters from Table 4.1.

Table 4.1: GC analysis parameters.

Parameter	Setting
Column	Restek RTX-5 (15 m)
Initial Temperature	70 ◦C for 1 minute
Ramp Rate	35 ◦C/min
Final Temperature	310 ◦C
Injection Volume	1 µL
Injection	Splitless

Areas were obtained for all hexadecane peaks and normalized by dividing by the area of each decane peak to remove variations in sample injection and detection. Rejections, R, were determined based on the normalized hexadecane peak areas from the permeate (A_P) and feed (A_F) solutions (equation 4.1).

$$R = 1 - \frac{A_P}{A_F} \tag{4.1}$$

Similarly, hexadecane enrichment, *E*, in retentate solutions was calculated based on the normalized hexadecane peak areas from the retentate (A_R) and feed (A_F) solutions (equation 4.2).

$$E = \frac{A_R}{A_F} - 1 \tag{4.2}$$

4.2.6 Microfiltration flux decline assessment

Similar to oil rejection experiments, the surfaces of wet membranes were dried with Kimwipes before placing the membrane in a custom built cross-flow holder (Figure 4.3). Next, 10 mL of the 10% hexadecane emulsion with 5 mM SDS was added to 500 mL of water and vigorously stirred to create a feed solution. The feed solution was placed into a feed tank connected to a centrifugal pump (Figure 4.4). A 500-mL Erlenmeyer flask aligned to receive the permeate was placed on top of an analytical balance connected to a computer via LabView software to capture mass values every 5 seconds. Once mass collection began, the feed solution was pumped across the membrane surface at 80 mL/min under an applied pressure of 2 bar, and flux was recorded over a period of 2 or more hours.

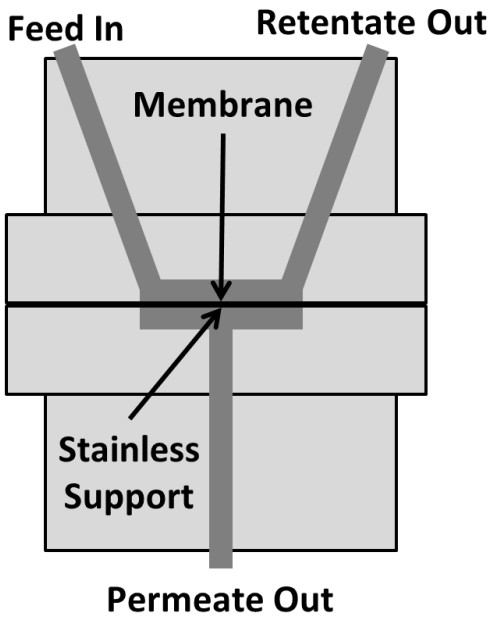

Figure 4.3: Diagram of the cross-section of a custom built cross-flow membrane holder. The membrane is sandwiched between the two halves of the holder atop a porous stainless steel frit that serves as a mechanical support.

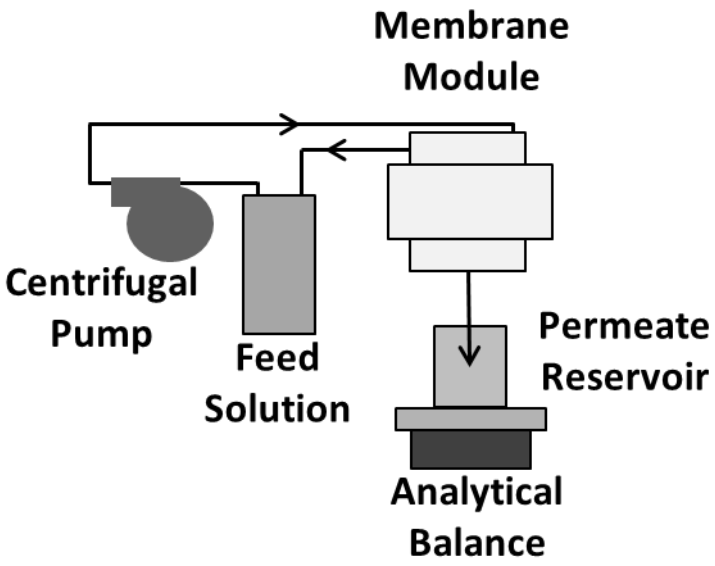

Figure 4.4: Scheme of the microfiltration apparatus.

4.3 Results and discussion

4.3.1 Membrane modification with PSS and PAH films

Adsorption of highly swollen PAH/PSS films in membrane pores significantly reduces membrane permeability. With a constant transmembrane pressure, flux declines after modification are 22 ± 14%, 58 ± 16% and 73 ± 18% after adsorption of 4, 6, and 8 PAH/PSS bilayers (uncertainties are standard deviation and n = 4). This decline in flux suggests pore blockage or restriction by the deposited polyelectrolyte films. For the proposed study, pores need to remain large (~ 5.0 μm) to assess the membrane's ability to reject small oil droplets (<5.0 μm) electrostatically without size exclusion. Hence, film growth should ideally not constrict pore size. Previous ellipsometric measurements and SEM measurements of similar 4.5 bilayers PSS/PAH films deposited on gold wafers and alumina membranes showed a film

thickness of only 20 nm.[20] Thus, the large flux decline observed for the 6 and 8 bilayer modified membranes was unexpected. Flow through the membrane may trap some polyelectrolyte to give thicker films.

SEM images of the 5.0 μm nylon membranes coated with 0, 4, 6, and 8 PAH/PSS bilayers (Figure 4.5) show no obvious blocking or coverage of membrane pores after film deposition. Film swelling could lead to a reduction in pore size, but previous studies showed that [PSS/PAH] films barely swell (at most by ~120%) upon exposure to salt solutions.[21] Therefore, the high flux decline most likely results from blocking of small pores within the heterogeneous interior of the spongy membrane.

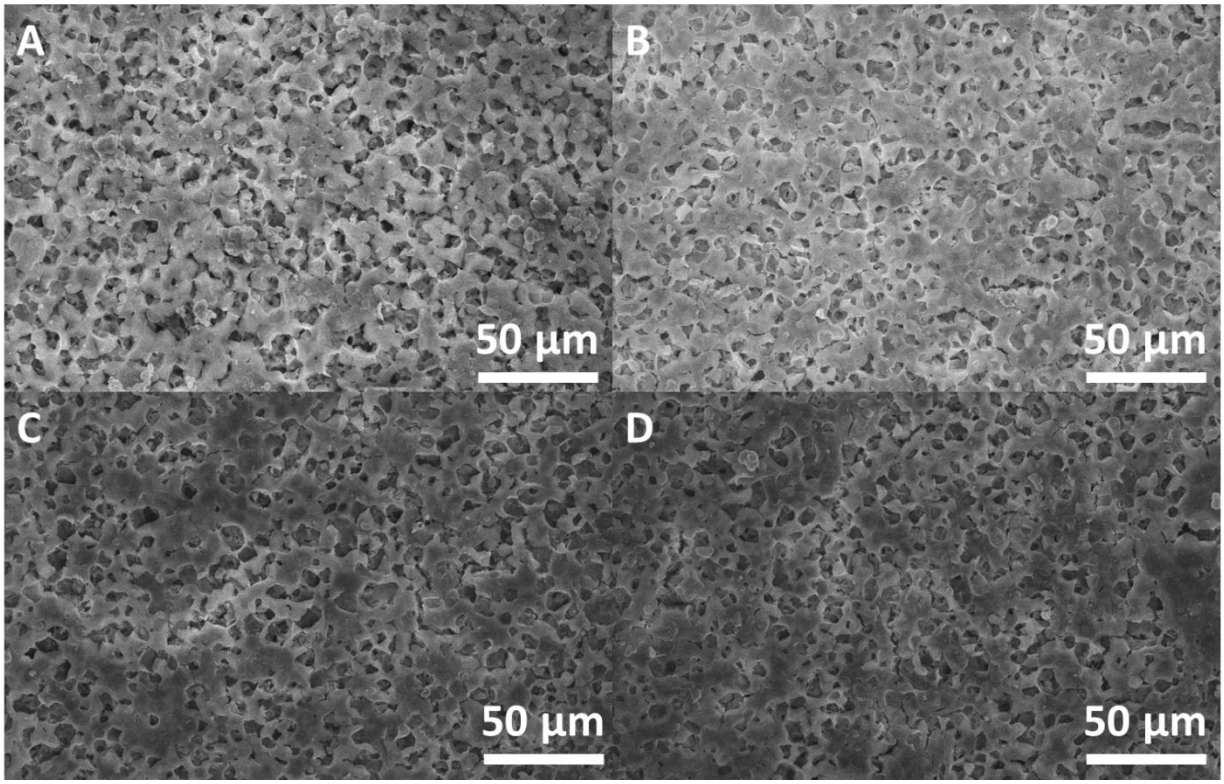

Figure 4.5: SEM images of the top face of 5.0 µm nylon membranes before (A), and after coating with $[PAH/PSS]_4$ (B), $[PAH/PSS]_6$ (C), and $[PAH/PSS]_8$ (D) films. The images show no obvious signs of pore blockage from film deposition.

4.3.2 Formation of oil emulsions using sonication

Upon sonication, dispersion of oil into water results in a transition from two transparent fractions to a single opaque layer. Examination of the droplet size distribution after sonication reveals the relative stability of the emulsion. Large droplets quickly coalesce due to inherent instability, whereas small droplets (<5 µm) persist for longer periods of time (days). Dynamic light scattering revealed that within 2 min of sonication, some large (> 10 µm) droplets were present in the emulsion as seen by the peaks corresponding to large droplets in the size distributions (Figure 4.6). However, after 20 minutes light scattering did not detect any

remaining large droplets in emulsions prepared with three different surfactants (Figure 4.7). Large droplets likely coalesced due to instability and floated to the surface of the emulsion away from the sampled region near the bottom of the container. Light-scattering measurements showed no evidence for droplet coalescence in these three well-dispersed emulsions for 10 days. However, the feed solution droplet size distribution was always assessed before and after any rejection experiments to rule out changes in droplet exclusion due to coalescence. These stable emulsions with droplet sizes less than 10 μm allow us to study oil/water separations with solutions that typically show low oil rejection in microfiltration.

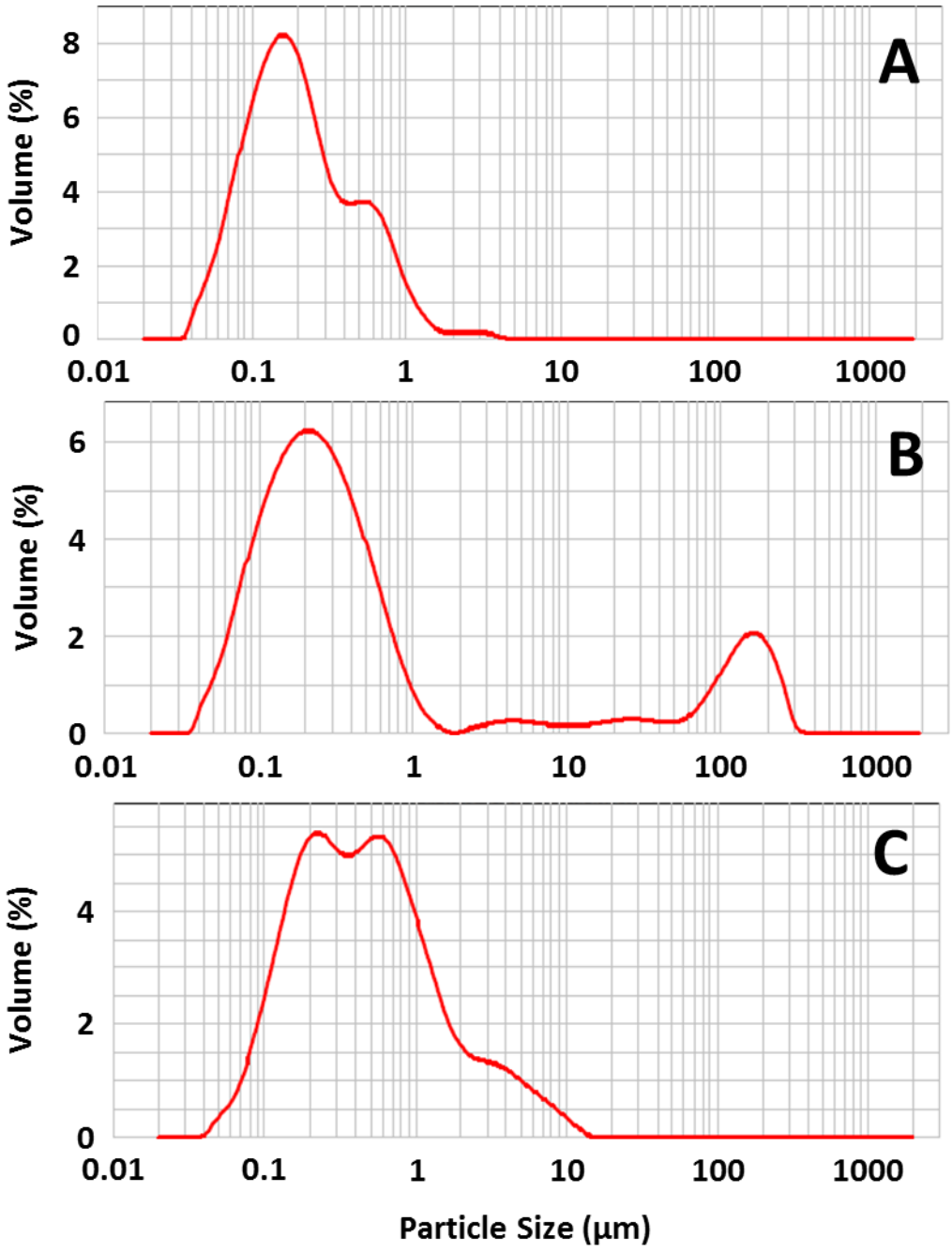

Figure 4.6: Oil droplet size distributions obtained within 2 min of sonication of 10% hexadecane in water. Emulsions were stabilized with SDS (A), CTAB (B), and Triton (C).

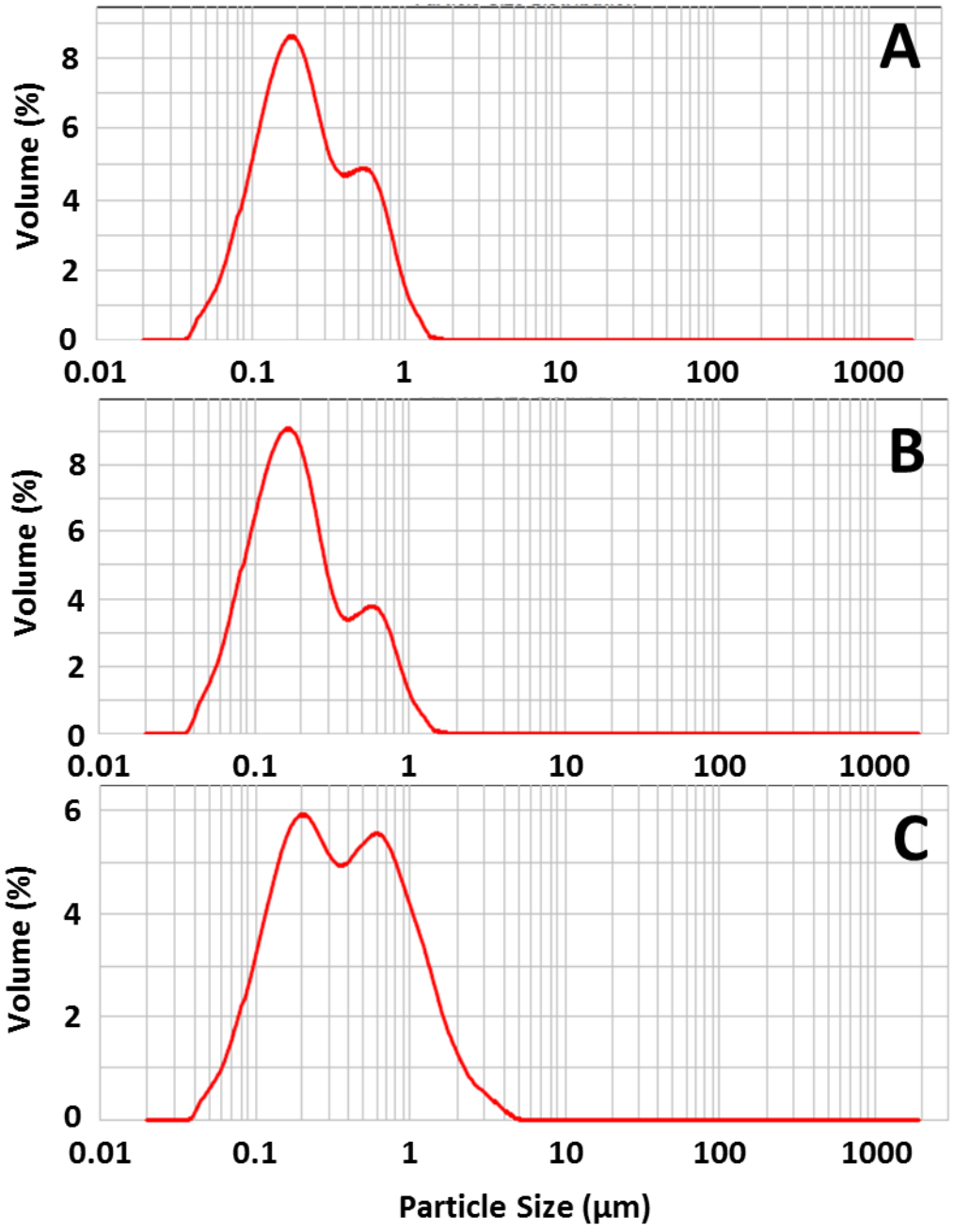

Figure 4.7: Oil droplet size distributions obtained 20 min after sonication of 10% hexadecane in water. Emulsions were stabilized with SDS (A), CTAB (B), and Triton (C).

Zeta potential measurements with each of the three emulsions give an indication of the charge present on oil droplets. The cationic CTAB emulsions have particles with an approximate zeta potential of 67 mV, whereas the anionic SDS emulsions contain particles with zeta potential of -58 mV. Triton emulsions, which contain a neutral surfactant showed a zeta potential of only -8 mV. While the zeta potentials for SDS- and CTAB-stabilized emulsion may seem high, the zeta potential for the SDS emulsion is consistent with a literature value (-60 mV).[22] Therefore, the droplets in SDS- and CTAB-stabilized emulsions are highly charged so electrostatic repulsion from charged membrane coatings may be effective.

4.3.3 Oil rejection by membranes with large pores

Filtration using membranes with nominal pore sizes greater than the average oil droplet diameter allows us to examine whether electrostatic exclusion can contribute to rejection of charged droplets. Unmodified control membranes with minimal surface charge should allow complete oil passage, regardless of the droplet charge (Figure 4.8). In contrast, modified membranes should electrostatically exclude only droplets whose charge has the same sign as the charge on the membrane surface.

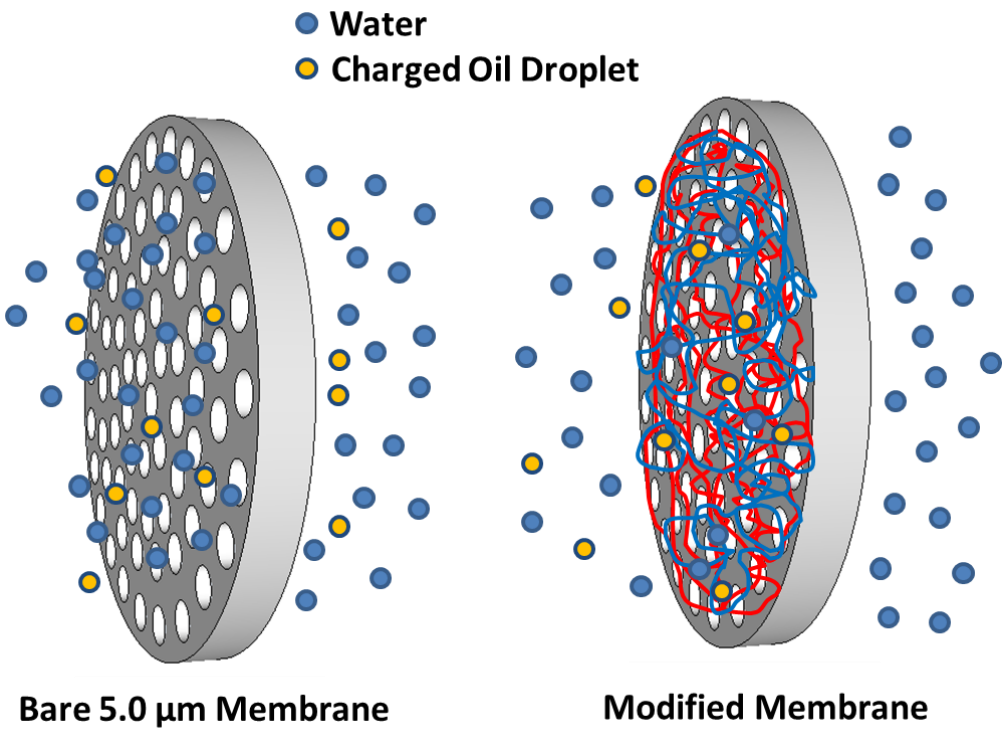

Figure 4.8: Control experiment design showing no oil rejection through large, unmodified pores and electrostatic exclusion with membranes coated with PEMs.

Initial results for three repeated passes of new neutral and anionic 10% hexadecane emulsions through the same membrane modified with [PAH/PSS] bilayers show encouraging results (Figure 4.9). The bare membrane shows no neutral oil rejection and only ~5% anionic oil rejection. The membrane likely has a small negative native charge, so a low percentage of anionic oil rejection is not surprising. Importantly, rejection of the neutral (triton-stabilized) emulsion remains zero for membranes coated with 4 and 6 PAH/PSS bilayers. After adsorption of 8 PAH/PSS bilayers the oil rejection for the triton-stabilized emulsion increases to ~24%. Meanwhile, anionic oil rejection increases to ~45%, ~60%, and ~95% upon increasing from 4 to 6 to 8 PAH/PSS bilayers in a membrane, respectively. Although the 95% rejection observed for

the membrane modified with 8 PAH/PSS bilayers is remarkable, the partial rejection of neutral oil through this particular membrane suggests some size exclusion contributes to rejection. Unfortunately, we cannot easily determine what mechanism is responsible for oil rejection in this case. However, the 60% oil rejection with the SDS-stabilized (anionic) emulsion and the membrane coated with the $[PAH/PSS]_6$ film is equally impressive due to the lack of neutral oil (triton-stabilized) rejection. This promising result suggests proper matching of surfactant and membrane charge may prevent oil accumulation at the membrane surface and lead to higher oil rejections with reduced fouling.

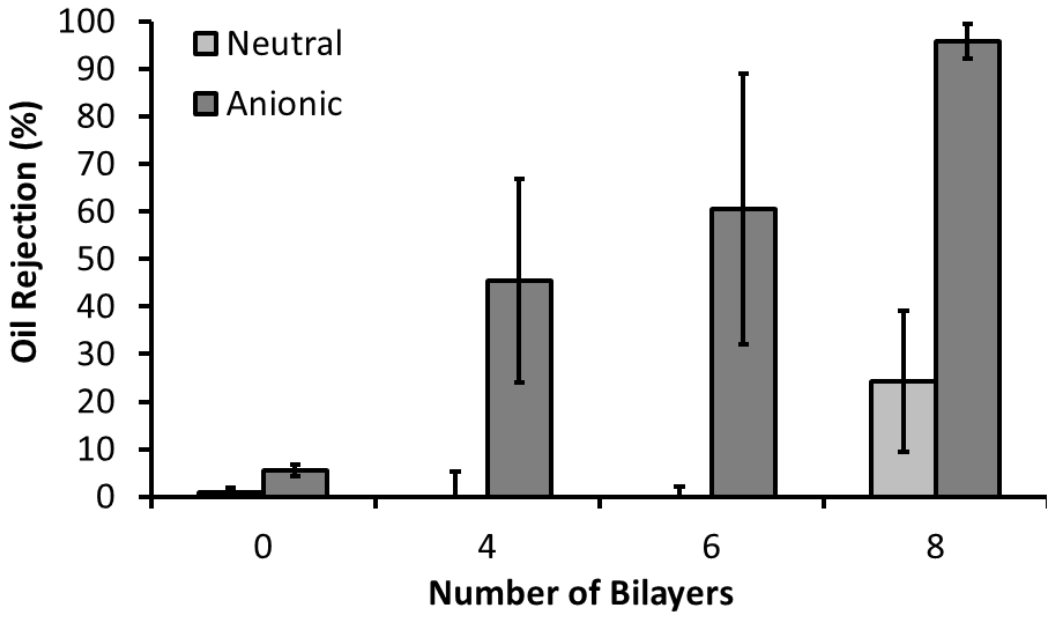

Figure 4.9: Oil rejections in the first replicate of dead-end filtration of a 10% hexadecane-in-water emulsion through 5 μm nylon membranes modified with 0, 4, 6, and 8 PAH/PSS bilayers. Emulsions were stabilized with either SDS (anionic droplets) or Triton (neutral droplets). Error bars represent the standard deviation of average oil rejection in three replicate trials using the same membrane.

Figure 4.10 shows oil rejections from a second batch of membranes used for dead-end filtration of the 10% hexadecane emulsions. Although the general trend of increasing SDS emulsion rejection with increasing film thickness remains, the oil rejections for the neutral Triton emulsions are nearly as high as those for the anionic emulsion. Rejection of the ~neutral droplets rose from a negligible value for a $[PAH/PSS]_6$-coated membrane in the first replicate to ~27% in the second replicate. Likewise, the rejection of neutral droplets by the $[PAH/PSS]_4$-coated membrane was essentially equal to oil rejection with the anionic rejection. The increased triton rejection in this second replication may result from the emergence of a second small peak in the droplet size distribution centered at 30 μm. The presence of oil droplets larger than the membrane pores might lead to increased neutral oil rejection and help explain differences between the two trials. Additionally, the first trial used membranes from Millipore while the second trial employed membranes from Sterlitech. However, LbL deposition should be possible for a wide variety of substrates. Regardless, further is needed on the reproducibility of concentrated oil rejections with treated membranes.

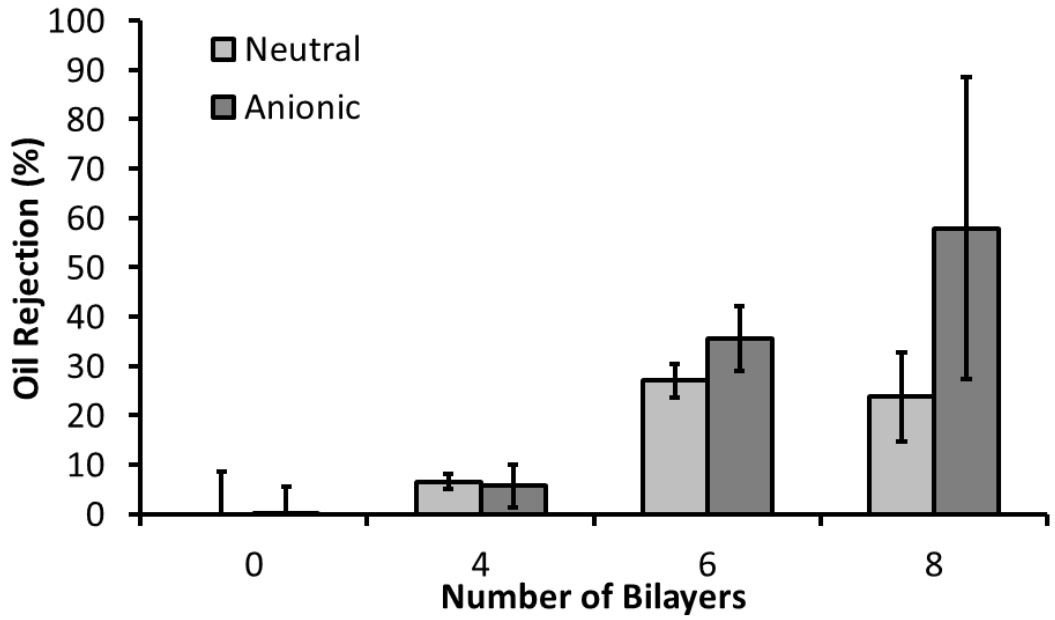

Figure 4.10: Oil rejections in the second batch of membranes prepared for dead-end filtration of a 10% hexadecane-in-water emulsion through 5 μm nylon membranes modified with 0, 4, 6, and 8 PAH/PSS bilayers. Emulsions were stabilized with either SDS (anionic droplets) or Triton (neutral droplets). Error bars represent the standard deviation of average oil rejection in three replicate trials using the same membrane.

We also assessed rejection of oil droplets prepared by a 20-fold dilution of the stock 10% hexadecane-in-water emulsions to explore the role oil concentration plays in this rejection mechanism. Dead-end filtration of these dilute solutions through the same membranes used for replicate 2 did not show increased rejection of anionic oil droplets (Figure 4.11). Both neutral and anionic emulsions show noticeable oil rejection even with bare membranes. By diluting the stock solution 20 fold, the SDS concentration decreases to only 0.25 mM, well below the critical micelle concentration of 8 mM.[23] At concentrations below the critical micelle concentration, the SDS may not stabilize oil droplets and coalescence may occur. Studying the average droplet size over time by dynamic light scattering for these dilute SDS solutions should

provide us with information about the droplet stability. However, the critical micelle concentration for Triton is only 0.25 mM so dilution should not destabilize Triton solutions as much as SDS.[24] Nonetheless, rejection still results for both anionic and ~neutral emulsions.

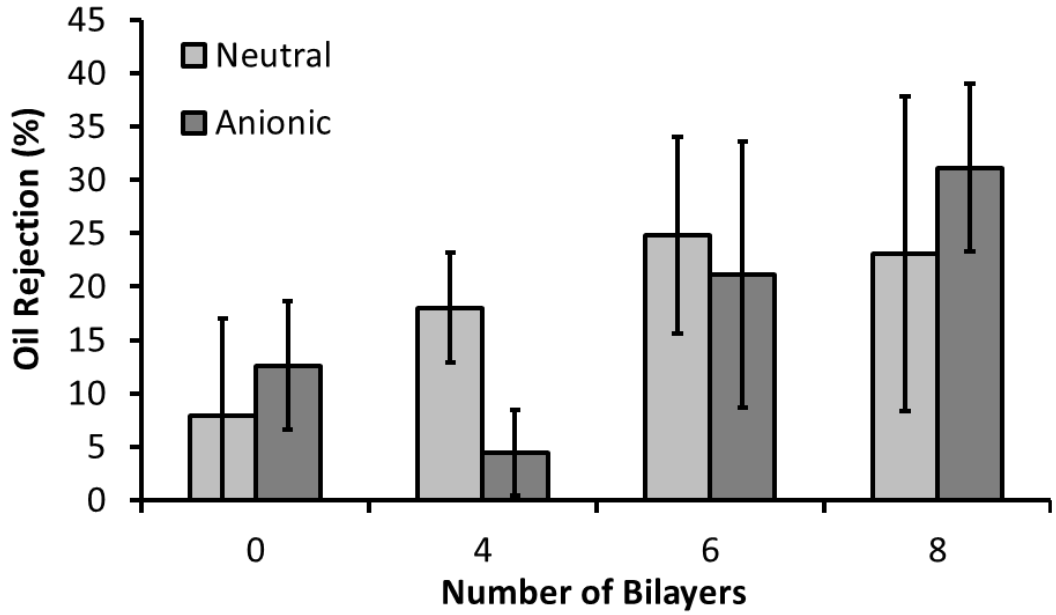

Figure 4.11: Oil rejections in the first replicate of dead-end filtration of a 0.5% hexadecane-in-water emulsion through 5 μm nylon membranes modified with 0, 4, 6, and 8 PAH/PSS bilayers. Emulsions were stabilized with either SDS (anionic droplets) or Triton (neutral droplets). Error bars represent the standard deviation of average oil rejection in three replicate trials using the same membrane.

4.3.4 Flux decline during microfiltration of oil emulsions

Although the preliminary results in section 4.3.3 are not conclusive, Figure 4.9 suggests that electrostatic repulsion of charged oil droplets using PEMs occurs. However, filtration through polyelectrolyte-coated membranes with extremely large pores (5 μm) is not intended as a practical method for removal of dispersed oil and grease components. Instead, these

studies attempt to demonstrate the concept of enhanced rejection through tailored electrostatic repulsion. For more practical applications, deposition of [PAH/PSS] films in membranes with smaller pores may reduce fouling arising from oil adsorption onto membrane surfaces and pores.

We propose that both the hydrophilicity of the PEM and the surface charge contribute to antifouling behavior. The use of two complimentary methods for fouling reduction should better stabilize flux compared to other hydrophilic antifouling treatments. The water treatment industry already doses organic and inorganic additives into water streams during coagulation and flocculation processes. Therefore, addition of surfactants or polyelectrolytes to increase oil droplet charge is a foreseeable fouling prevention paradigm.

PEM layers were adsorbed on nylon membranes with nominal 0.45 μm pore sizes to compare flux declines in cross-flow filtration of oil-in-water emulsions. The plot of permeate mass versus time in Figure 4.12 shows a decline in water passage over time for both bare membranes and membranes coated with $[PAH/PSS]_4$ films. The second PEM modified membrane and the bare membrane have a similar initial flux but the bare membrane fouls more extensively as demonstrated by the plateau in permeate mass. The first membrane coated with a $[PAH/PSS]_4$ films showed a smaller initial flux, but a relatively small flux decline. Figure 4.13 shows the ratios of flux to initial flux for each of the membranes. The membranes with polyelectrolyte coatings clearly foul less extensively. However, this comparison is most valid for membranes with similar initial fluxes, because the permeate flow brings foulants to the membrane.

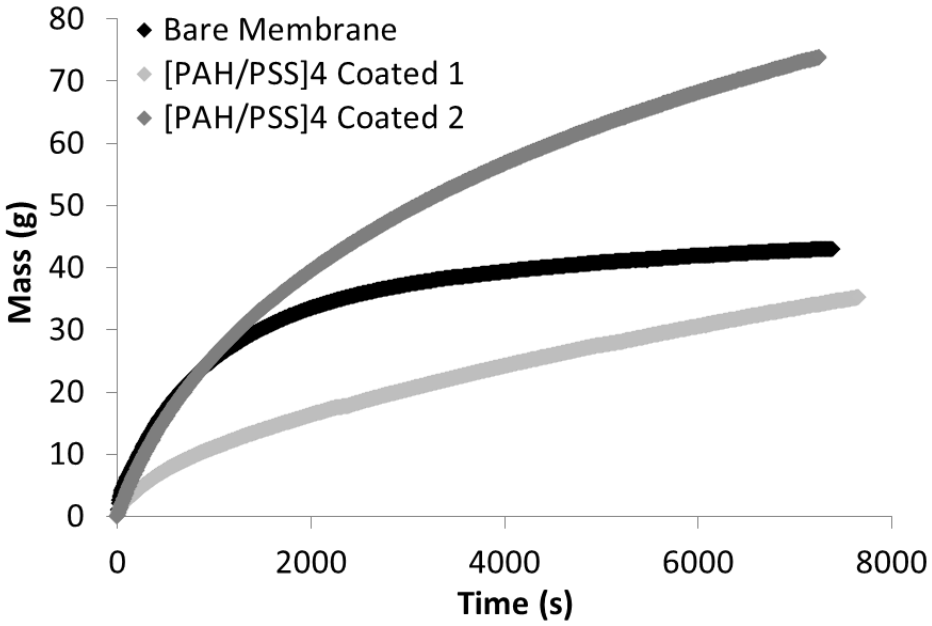

Figure 4.12: Permeate mass as a function of time during cross-flow filtration of a 0.2 % (v/v) hexadecane emulsion through a bare and and two different membranes modified with $[PAH/PSS]_4$ films. The emulsions were stabilized with 0.1 mM SDS in 0.2 mM NaCl.

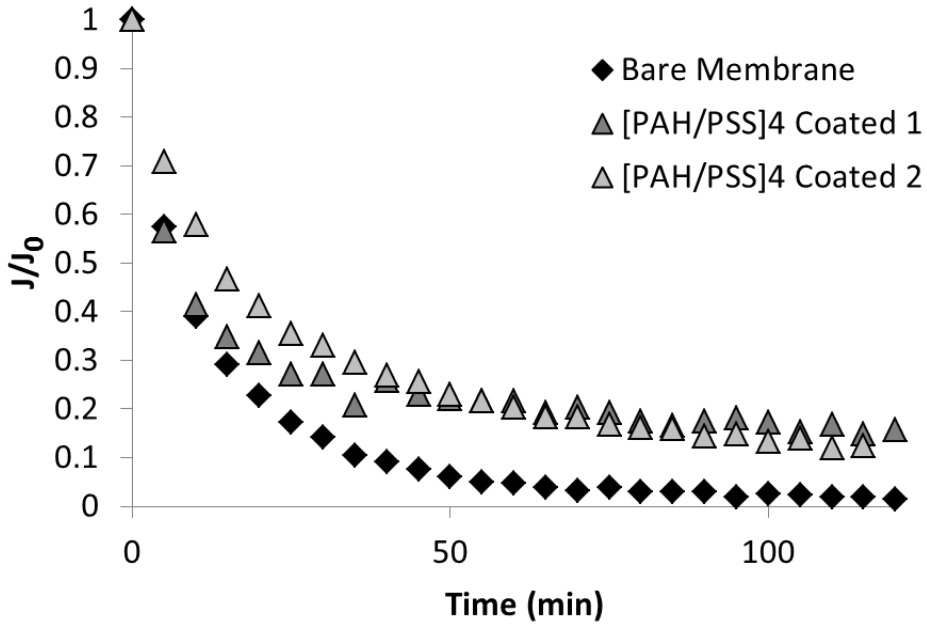

Figure 4.13: Relative flux values over time for a bare and two trials of PEM modified membranes during cross-flow filtration of a 0.2 % (v/v) hexadecane emulsion in a 0.1 mM SDS 0.2 mM NaCl solution.

In addition to the flux decline differences observed between bare and PEM modified membranes during filtration of dilute oil emulsions, hydrophobic dye adsorption readily occurs on bare membranes whereas treated membranes remain relatively unchanged after each trial (Figure 4.14). Unfortunately, subsequent attempts to reproduce flux decline behavior with bare membranes have yet to produce a steady flux value. In each case, unstable flux values have resulted which lack noticeable trends. Current work is ongoing to discover the cause of this irreproducibility. Nevertheless, despite the unusual flux values, rejection for three different bare membranes was consistent with an average hexadecane rejection of 45 ± 13% (n=3). Addition of PEM multilayers increases the average oil rejection to 84 ± 15% (n=2) while also reducing flux decline and demonstrating the benefits of our proposed antifouling scheme. After searching the literature, no papers have been discovered detailing the use of polyelectrolyte multilayers to repel charged oil droplets to date.

Figure 4.14: Comparison of irreversible membrane staining from uncharged, hydrophobic oil-soluble dye for bare and PEM modified membranes after oil emulsion cross-flow filtration at 80 mL/min and an applied transmembrane pressure of 2 bar.

4.4 Conclusions

Deposition of highly charged $[PAH/PSS]_n$ films on porous membranes produces hydrophilic surfaces that may have innate antifouling properties. Meanwhile, additions of charged surfactants to feed solutions increase the surface charge of dispersed oil droplets. The preliminary combination of hydrophilic, charged polyelectrolyte multilayer and charged oil droplets promises as a new strategy for crafting fouling resistant membranes for oil-in-water filtration. When using membranes with pores much larger than oil droplets (~15 x), membranes treated with anionic terminated PEM layers appear to show enhanced rejection of anionic emulsions compared to similarly sized neutral oil droplets. The enhanced rejection demonstrates the possibility of adding charged surfactants or polymers to feed solutions as a pretreatment step to aid water recovery by reducing membrane fouling. Similarly, the inclusion of the same [PAH/PSS] PEMs as a surface treatment for cross-flow microfiltration membranes does not appear to reduce flux significantly and appears to resist surface fouling to mitigate flux decline.

While still preliminary in nature, the results presented in this chapter encourage further exploration of the abilities and limitations of our proposed fouling mitigation scheme. The low cost and high availability of many charged surfactants and polyelectrolytes suitable for addition to feed solutions suggests that such a technique might by industrially practicable for removing oil-in-water emulsions from aqueous streams. Notably, the application of promising antifouling properties of hydrophilic films combined with our concept to match dispersed particle charge

with membrane surface charge represents an exciting opportunity for advancement of membrane treatment technology.

REFERENCES

REFERENCES

(1) United States Environmental Protection Agency, *Hydraulic Fracturing Research Study Fact Sheet*, Washington, D.C., 2010, http://www.epa.gov/safewater/uic/pdfs/hfresearchstudyfs.pdf (accessed 03/09/2013).

(2) Wandera, D.; Wickramasinghe, S. R.; Husson, S. M. *Journal of Membrane Science* **2011**, *373*, 178.

(3) *Technical Summary of Oil and Gas Produced water Treatment Technologies*, Tulsa, OK, 2005, http://w.all-llc.com/publicdownloads/ALLConsulting-WaterTreatmentOptionsReport.pdf (accessed 04/05/2013).

(4) Ahmadun, F. l.-R.; Pendashteh, A.; Abdullah, L. C.; Biak, D. R. A.; Madaeni, S. S.; Abidin, Z. Z. *Journal of Hazardous Materials* **2009**, *170*, 530.

(5) National Energy Technology Laboratory. Produced Water Management Technology Descriptions: Fact Sheet - Discharge. http://www.netl.doe.gov/technologies/pwmis/techdesc/discharge/ (accessed 04/01/2013).

(6) Cheryan, M.; Rajagopalan, N. *Journal of Membrane Science* **1998**, *151*, 13.

(7) Kota, A. K.; Kwon, G.; Choi, W.; Mabry, J. M.; Tuteja, A. *Nature communications* **2012**, *3*, 1025.

(8) Sagle, A. C.; Van wagner, E. M.; Ju, H.; McCloskey, B. D.; Freeman, B. D.; Sharma, M. M. *Journal of Membrane Science* **2009**, *340*, 92.

(9) Xu, P.; Drewes, J. E. *Separation and Purification Technology* **2006**, *52*, 67.

(10) Yi, X. S.; Yu, S. L.; Shi, W. X.; Sun, N.; Jin, L. M.; Wang, S.; Zhang, B.; Ma, C.; Sun, L. P. *Desalination* **2011**, *281*, 179.

(11) Xu, P.; Drewes, J. E.; Heil, D. *Desalination* **2008**, *225*, 139.

(12) Faibish, R. S.; Cohen, Y. *Journal of Membrane Science* **2001**, *185*, 129.

(13) Xu, Z.-L.; Chung, T.-S.; Loh, K.-C.; Lim, B. C. *Journal of Membrane Science* **1999**, *158*, 41.

(14) Chakrabarty, B.; Ghoshal, A. K.; Purkait, M. K. *Journal of Membrane Science* **2008**, *325*, 427.

(15) McPherson, T.; Kidane, A.; Szleifer, I.; Park, K. *Langmuir* **1998**, *14*, 176.

(16) Hamming, L. M.; Messersmith, P. B. *Material Matters* **2008**, *3*, 52.

(17) Tuteja, A.; Choi, W.; Mabry, J. M.; McKinley, G. H.; Cohen, R. E. *Proceedings of the National Academy of Sciences* **2008**, *105*, 18200.

(18) Kobaku, S. P. R.; Kota, A. K.; Lee, D. H.; Mabry, J. M.; Tuteja, A. *Angewandte Chemie* **2012**, *51*, 10109.

(19) Xu, F. J.; Zhao, J. P.; Kang, E. T.; Neoh, K. G.; Li, J. *Langmuir* **2007**, *23*, 8585.

(20) Stanton, B. W.; Harris, J. J.; Miller, M. D.; Bruening, M. L. *Langmuir* **2003**, *19*, 7038.

(21) Dubas, S. T.; Schlenoff, J. B. *Langmuir* **2001**, *17*, 7725.

(22) Tucker, I. M.; Petkov, J. T.; Jones, C.; Penfold, J.; Thomas, R. K.; Rogers, S. E.; Terry, A. E.; Heenan, R. K.; Grillo, I. *Langmuir* **2012**, *28*, 14974.

(23) Domínguez, A.; Fernández, A.; González, N.; Iglesias, E.; Montenegro, L. *Journal of Chemical Education* **1997**, *74*, 1227.

(24) SigmaAldrich, *Sigma Product Information: Triton X100*, http://www.snowpure.com/docs/triton-x-100-sigma.pdf (accessed 04/17/2013).

Chapter 5: Conclusions and future work

5.1 Conclusions

This dissertation focused on developing coatings that can potentially improve the performance of membranes in remediation of industrial wastewater, desalination of brackish or seawater, and removal of oil from oil-in-water emulsions. As the demand for water continues to increase to sustain agricultural, residential, and industrial needs, new methods for producing high quality water must improve to keep pace. Future directions in water treatment need to focus on the decontamination and sanitization of toxic or otherwise challenging sources. Rapid developments in membrane technology over the last half century have greatly increased our ability to produce safe water. In fact, Singapore, which has very limited sources of fresh water, has developed a large-scale wastewater reclamation project to produce drinking water through use of advanced membrane technology.[1] Realization of a cost effective method to quickly and reliably treat challenging water sources would greatly reduce global water stress in the coming years.

Chapter 2 focused on the application of PEMs containing Pt nanoparticles as polymer membrane coatings for CWAO of industrial waste. Several other groups demonstrated potential benefits of the CWAO process using membranes as interfacial contactors.[2-4] These studies employed ceramic membranes due to their temperature and chemical resistance. However, ceramic membranes are generally an order of magnitude more expensive than polymeric

options. Our work utilized inexpensive polymeric hollow fibers with inner diameters several times smaller than what is currently available with practical ceramic membranes.

Remarkably, we observed over 50% oxidation of formic acid during a single pass through polysulfone (PS) membranes modified with PEMs containing Pt nanoparticles. Using modules with five fibers resulted in over 90% formic acid oxidation in a single pass due to a longer residence time in the membrane. Modeling of the reaction suggested that the membrane was operating well below the diffusion-limited rate with an apparent reaction rate constant of 0.01 s^{-1}. Despite these positive observations, the PEM-modified polymeric membranes have low Pt catalytic activity compared to similarly modified ceramic membranes. The low Pt activity in the polymeric membranes likely results from the loading of Pt throughout the entire wall thickness rather than in a concentrated region near the air-water interface.

Chapter 3 described porous PP coatings that decrease fouling and prevent pore wetting during MD of humic acid and whey solutions. As an attractive, low-temperature water desalination technique, MD may couple with solar energy or waste heat to economically provide safe water in underdeveloped or water-stressed regions. To reduce the number of people lacking access to safe drinking water by 2015 as proposed in the Millennium Development Goals, freshwater production must increase in underdeveloped and remote areas despite significant infrastructural deficiencies.[5] A portable MD system capable of low-maintenance operation may be an ideal method for meeting such goals.

In studies using humic acid solutions that simulate brackish water samples with high fouling capability, unmodified PVDF membranes rapidly fouled and wetted to allow salt passage and an average rejection of only 32 ± 12% after 20 hours. In contrast, despite a 20-30% drop in flux relative to unmodified membranes, porous PP-modified PVDF membranes maintained a steady flux while resisting pore wetting to give 99.9 ± 0.1% salt rejection over 20 hours. The operational stability of the PP-treated membranes more than compensates for the slight flux decline resulting from the increased mass transport resistance of the added PP. Similarly, when using dairy whey as a feed solution, bare PVDF membranes did not resist surface and pore fouling by the proteins and oils present in whey. The conductivity in the permeate rose ~150 μS/cm during MD, and the flux actually reversed for bare membranes with pure water moving backwards through membrane pores under osmotic flow. Porous PP films deposited on the PVDF membranes, on the other hand, prevented pore wetting, and the modified membranes gave 97 ± 0.5% salt rejection over a 20 hour period. Although the porous PP coating resisted humic acid and dairy whey fouling, the coating was not effective in the presence of surfactants, so the composition of feed solutions should be well-characterized before using PP-modified membranes.

Finally, chapter 4 discussed preliminary work on a new strategy for removing oil from oil-in-water emulsions. The goal was to modify membranes with PEM films and create charged hydrophilic surfaces that resist adsorption of oil droplets with the same surface charge as the PEM. Addition of charged surfactants to create charged oil droplets should increase rejection and decrease fouling due to electrostatic repulsion of the droplets. Many membranes consist of hydrophobic polymers that rapidly adsorb oil to cause fouling during filtration of oil-in-water

emulsions. In the case of PEM-modified membranes, the combination of a tightly held water boundary layer and electrostatic repulsion of charged oil droplets may provide a new paradigm for fouling management during oil removal from water.

Initial work using large membrane pores generally incapable of rejecting small oil droplets demonstrates the ability of negatively charged PEMs to electrostatically repel similarly charged oil droplets. While further work remains to better define differences in rejection based on the number of PEMs deposited, rejections of anionic oil droplets generally exceed those of neutral droplets when oil emulsions pass through anionically terminated PEMs. Additionally, we presented promising initial results that are consistent with our hypothesis of reduced fouling with hydrophilic coatings that electrostatically repel oil droplets. During two h of cross-flow filtration of a 0.2% hexadecane-in-water emulsion, 2 $[PAH/PSS]_4$-coated membranes showed an 80% decline in flux, but flux through a bare PVDF membrane declined more than 90%. Additionally, PEM-treated membranes resisted dye staining during the two hours of filtration while showing nearly 2-fold higher oil rejection than bare membranes.

5.2 Future work

5.2.1 Polypropylene hollow fibers for CWAO

As the most expensive component of our CWAO system, Pt must be used efficiently for practical applications. In an effort to overcome the low catalyst activity in our PS hollow fiber membranes, we propose the use of similarly sized polypropylene membranes that will maintain

high single pass conversions while increasing catalytic activity due to increased control over Pt location. PS membranes are hydrophilic so PEM and nanoparticle deposition solutions fill the entire pore volume to deposit nanoparticles throughout the membrane wall (Figure 5.1, top). However, the high catalytic activity of previous ceramic membranes arose from the ability to focus the gas-liquid interface to the innermost region of the membranes where all the catalyst was loaded at high density. The diffuse loading of catalyst throughout our fiber walls precluded our ability to localize the reaction to catalyst rich areas. Additionally the hydrophilicity of PS resulted in complete wetting of membrane pores at all available oxygen overpressures.

The hydrophobicity of polypropylene fiber membranes could prevent pore wetting and limit polyelectrolyte and nanoparticle adsorption to regions near the inner wall of the membrane (Figure 5.1, bottom). However, adsorption of PEMs to PP surfaces is difficult due to the hydrophobicity and lack of functional groups that interact with PEMs. Therefore, localized polyelectrolyte adsorption requires a way to increase the hydrophilicity of the PP surface near the inner wall of the membrane. Plasma and photo-irradiation techniques are not suitable since neither will modify the lumen surface effectively. However, flow of chemical oxidants, such as ammonium persulfate, through the membrane lumen may increase the hydrophilicity of PP membranes only near the lumen surface.[6] Short oxidant residence times should prevent modification inside the pores. The localization of PEM and nanoparticles adsorption in this region may allow Pt loading only at the gas-liquid interface to achieve superior catalyst activity (Figure 5.1)

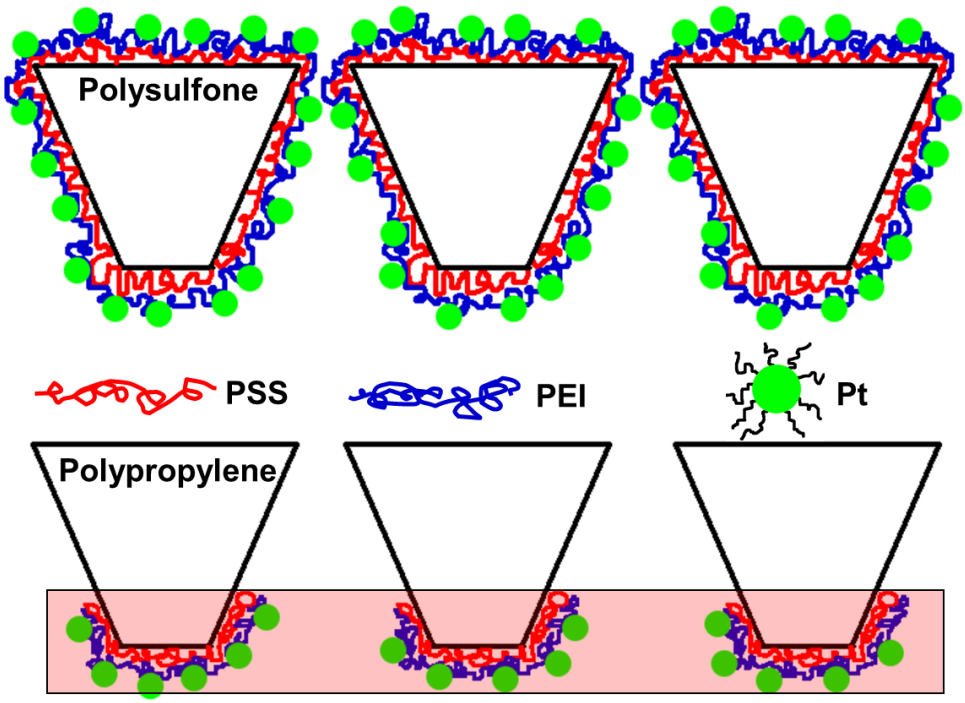

.

Figure 5.1: Cartoon of the potential catalyst locations resulting from adsorption of [PSS/PEI/Pt] coatings in hydrophilic PS membranes and chemically treated polypropylene membranes.

The fabrication of polymeric membranes with high activity for CWAO at low temperatures and pressures could increase the feasibility of CWAO for industrial waste treatment. Polymeric membranes are much less expensive than ceramic membranes. Additionally, the small fiber diameters reduce the diffusion distance for pollutants to give high single-pass conversions at short residence times and hopefully avoid the need to recycle feed solutions through membranes multiple times for high conversion. Similarly, the small fiber size allows for high packing density within membrane modules to increase throughput while maintaining a small footprint.

5.2.2 Antifouling MD membranes for the food and beverage industry

MD is principally used for either the production of high quality water or the concentration of non-volatile aqueous solutions. The dairy industry is well suited to use both functions of MD operation simultaneously. In this way, the distillation of whey solutions produces both fresh water for use in other areas and concentrated whey solutions suitable for further drying before sale. Obtaining value from whey solutions, at one point considered a waste product requiring disposal costs, improves dairy industry profitability.

While we demonstrated improved whey fouling resistance using porous PP coatings, further studies should examine the duration of resistance to pore wetting in partnership with a local dairy industry representative. For superhydrophobic films to maintain antifouling properties, they must retain air trapped within surface roughness features. Long-term studies, should also explore air back-flushing steps at specified intervals as a simple cleaning procedure. If short periods of air exposure help maintain air entrapment within surface roughness features, duration of the PP antifouling properties should increase. Additional MD applications within the food and beverage industry include other Michigan products such as apple juice and wine. Apple juice primarily consists of carbohydrate sugars and apple oils extracted during the juicing process. The removal of water from apple juice allows for the formation of juice concentrate for shipment in larger quantities and lower prices to markets by removing a majority of the water and allowing consumers to replace the water later. The use of porous PP coatings may also reduce fouling from apple solutions, which would increase plant productivity and reduce membrane treatment costs. When excess alcohol is present in wines, winemakers need to

remove it MD may be effective in selective removal of ethanol over water due to ethanol's higher vapor pressure.

5.2.3 Polishing of oil-in-water emulsions using membrane filtration

Membranes provide many advantages over alternative techniques for the removal of small, well dispersed oil droplets from aqueous solutions. However, oils rapidly foul membrane surfaces to reduce fluxes and require frequent cleaning procedures. Based on our preliminary investigation in Chapter 4, the surprising addition of charged surfactant to oil emulsions leads to higher oil rejections by charged membranes despite also stabilizing oil droplets from coalescence. The next logical step for this project would be the inclusion of these films on nanofiltration or other membranes with small pores capable of rejecting many sizes of oil droplets.

The ability to reduce fouling over time during oil filtration experiments while increasing oil rejection due to electrostatic influences could significantly impact oil removal operations. Additionally, the use of inexpensive polyelectrolytes and surfactants should avoid high treatment costs for membranes. Moreover, if PEMs are used to increase the hydrophilicity of a chemically resistant membrane, such as a ceramic one, the coatings can be considered sacrificial. Over time as their performance possibly degrades due to oil buildup on treated films, the PEMs can be eluted from the membrane using acidic or basic conditions.[7] The coatings

could then be reapplied within a matter of minutes (depending on the number of bilayers) to reestablish antifouling properties and high oil rejections.

5.3 Summary

In summary, the use of inexpensive PEMs and thin porous PP films can positively alter the properties of membrane substrates. PEMs can incorporate catalytically active nanoparticles within membranes, with tunable catalyst loading for industrial waste remediation using CWAO. Porous PP films deposited on substrates in a controlled environment rapidly produce a reliably superhydrophobic surface that prevents humic acid and whey protein fouling during MD. Finally, the incorporation of PEMs on membranes while dosing charged surfactants to feed solutions leads to improved fouling resistance and oil droplet rejection when compared to untreated membranes. In total, this dissertation covers three avenues in which thin, polymeric coatings may assist in developing technologies for the next generation of water treatment and production facilities.

REFERENCES

REFERENCES

(1) Siemens Water Technologies. Membrane Filtration System Improves Water Sustainability at NEWater Plant in Changi, Singapore. http://www.water.siemens.com/en/about_us/corporate%20information/Pages/default.aspx (accessed 04/17/2013).

(2) Iojoiu, E. E.; Landrivon, E.; Raeder, H.; Torp, E. G.; Miachon, S.; Dalmon, J.-A. *Catalysis Today* **2006**, *118*, 246.

(3) Miachon, S.; Perez, V.; Crehan, G.; Torp, E.; Ræder, H.; Bredesen, R.; Dalmon, J. A. *Catalysis Today* **2003**, *82*, 75.

(4) Dotzauer, D. M.; Abusaloua, A.; Miachon, S.; Dalmon, J.-A.; Bruening, M. L. *Applied Catalysis, B: Environmental* **2009**, *91*, 180.

(5) United Nations. Millenium Development Goals: Environmental Sustainability. http://www.un.org/millenniumgoals/environ.shtml (accessed 03/09/2013).

(6) Piletsky, S.; Piletska, E.; Bossi, A.; Turner, N.; Turner, A. *Biotechnology and Bioengineering* **2003**, *82*, 86.

(7) Shan, W. Q.; Bacchin, P.; Aimar, P.; Bruening, M. L.; Tarabara, V. V. *Journal of Membrane Science* **2010**, *349*, 268.